Fundamental Investigation on Nano-precision Surface Finishing Using MCF (Magnetic Compound Fluid) Slurry

（MCF(磁気混合流体)スラリーを用いた
ナノレベル超平滑研磨の基礎研究）

By

Huiru Guo

郭　会茹

Submitted in Partial Fulfillment
of the
Requirements for the Degree
Doctor of Philosophy

Supervised by

Professor Yongbo Wu

Graduate School of
Systems Science and Technology

Akita Prefectural University
Akita, Japan

September 2014

Abstract

Magnetic field-assisted polishing techniques using magnetic fluids (MFs) or magnetorheological (MR) fluids have been successfully utilized to nano-precision surface finishing of optics in the last four decades. Finishing processes, namely magnetorheological finishing (MRF), magnetorheological abrasive flow finishing (MRAFF) and fixed-charge MRF (wheel-type), have been developed. In these techniques, the behaviour of the abrasive particles contained in the fluid is controlled by an applied magnetic field. The fluid generally changes from nearly Newtonian to Bingham plastic in the presence of magnetic field. The material removal behaviour potentially strongly relates to the shearing action during finishing.

The work presented concentrates on nano-precision surface finishing using magnetic compound fluid (MCF) slurry. An MCF is developed by mixing an MF and an MR fluid. MCFs exhibit higher magnetic pressure and apparent viscosity than MFs and a more stable distribution of particles than MR fluids under a magnetic field. Two kinds of constructed experimental approaches and MCF slurry are introduced first. Investigations on work life of MCF slurry through spot tests follow. We are pleased that both stable material removal rate (*MRR*) and smooth surfaces inside spots over a relative long spot polishing period were attained through polishing with MCF slurry (namely MCF polishing).

Behaviours of the MCF slurry strongly relates to the *MRR* and surface finish. In our experiments, a rotary magnetic field was adopted. The magnetic flux density is constant but the magnetic lines of force constantly revolve around the magnet holder axis. The MCF slurry manifests dynamic behaviours and was distributed in a clear-cut terminal shape under the rotary magnetic field, which significantly enhances particle dispersity and shape restoring ability. The mechanical characteristics of MCF slurry were investigated by measuring normal and shear forces simultaneously under a rotary

magnetic field. Besides, the structure of MCF slurry was observed to clarify why a better surface finish is obtained under a rotary magnetic field than under a static one.

Following the clarification of behaviours of MCF slurry, nano-precision polishing of polymethyl methacrylate (PMMA) was performed with a novel zirconia (ZrO_2)-coated carbonyl-iron-particle (CIP) based MCF slurry as conventional CIP has little ability against corrosion in a common water-based carrier. A surface roughness less than 1 nm R_a has been obtained for PMMA. ZrO_2-coated CIP based MCF slurry also extends its application in ultrafine finishing of soft magnetic materials, such as nickel-phosphorus plated mold, while conventional HQ CIP based MCF slurry frequently results in scratches and CIP embedding on the Ni-P plating layer. It is noted that a certain scanning path help enhance both the surface roughness and flatness.

To complete the development of MCF polishing technique, material removal behaviour in polishing of optical glass were studied through the investigation on the relationship between pressure/shear stress and *MRR*, and the characteristics of the removal function, namely the polishing spot. An *MRR* model for MCF polishing was proposed. According to the model, material removal is governed more by shear stress than pressure. The removal function is strongly related to the magnetic field distribution and the geometry of internal structure of MCF slurry.

According to the above results, the rotary magnetic field assisted polishing with MCF slurry is a promising technique for nano-precision finishing of optics.

Acknowledgements

This thesis work is a result of three and a half years of hard work. It would be impossible to accomplish this work without the kindhearted help and full-hearted support of many people. I am very pleased to give my gratitude to those people who have continuously supported me over the past several years.

First and foremost I express my sincere appreciation to my advisor, Prof. Yongbo Wu who has supported me through the path of this thesis work with his patience, knowledge and guidance which are the best gifts I have ever received. I have learned a lot about polishing process with magnetic compound fluid (MCF) slurry from my countless discussions and daily work with him. His rigorous attitude towards scientific research will guide me for the rest of my life and future research work. I couldn't thank him more for his help in finishing this thesis work.

I am very grateful to Prof. Kunio Shimada of Fukushima University, Prof. Mamoru Mizuno and Prof. Teruo Bitoh of Akita Prefectural University for their willingness to serve as members of my thesis defense committee.

I would like to acknowledge Prof. Stephen Jacobs and Mrs. Sivan Salzman of University of Rochester for their invaluable advice and suggestions on my work, providing the ZrO_2-coated CIPs, and sharing me with their knowledge about magnetorheological finishing (MRF). The communications with them have always inspired me a lot and will be memorized forever.

My cordial thanks are extended to Prof. Mitsuyoshi Nomura, Dr. Masakazu Fujimoto and Mr. Seiichi Kimura for their kind help, advice and assistance in my work. The discussions with them always enlighten my thoughts and make things easier to deal with.

I would like to express sincere thanks to the JFE 21st Century Foundation for their financial support to my work and the Olympus Corporation for supplying the Ni-P plating

molds.

I would like to express my sincere gratitude to my advisor of master's course, Prof. Xuyue Wang of Dalian University of Technology, for his continuing encouragement and support in my study and life in Japan. Thanks to his kindhearted recommendation and help, I am fortunate to have such a precious opportunity to study under guidance of Prof. Wu. Prof. Lessons learned from Prof. Wang over master's course have greatly helped me in pursing the doctoral degree.

I must express many thanks to Ms. Aki Asada for her kindhearted help, advice and assistance in my stay in Japan.

I would like to thank my roommates: Prof. Li Jiao and Prof. Dong Lu for their invaluable suggestions in my research and life and kindly sharing me with their constructive and inspiring thoughts. The friendship with them is precious gift to me.

I feel fortunate for working with a lot of excellent people: Dr. Weixing Xu, Dr. Yaguo Li, Mr. Jianguo Cao, Mr. Jinkui Ma, Mr. Youliang Wang, Mr. Tailin Zhu, Prof. Weiping Yang, Dr. Wenqing Song, Mr. Jingti Niu, Mr. Sisi Li, Prof. Huijin Fan, Prof. Xiongbo Wan, Prof. Ye Li, Prof. Yinghuai Dong, Mr. Ryutaro Mori, Mr. Kosuke Sasaki and Mr. Nobuto Oura. Thank you very much for sharing your valuable experiences with me and unselfish help in my work and life.

I had so many great memories in Japan thanks to the following excellent people: Dr. Yang Zhao, Prof. Yang Yu, Dr. Lin Lei, Dr. Xueli Wu, Dr. Dongxiao Jiang, Mr. Paipai Pan, Mr. Xingguo Zhang, Mr. Wei Wang, Mr. Xiaofeng Li, Miss Daiyan Yao, Miss Wenjuan Zhang, Mrs. Limin Zang, Prof. Chao Yang, Mrs. Lijun Wang, Miss Fei Ding, Miss Jingyan Huang, Dr. Guan Gui and his family, Dr. Jian Shi, Miss Baiyi Chen, Mr. Liqiang Gu and Mr. Bin Wang.

I would like to acknowledge the financial support of several kind Japanese groups to my study and living in Japan.

I would like to thank my Japanese teachers: Mrs. Nobuko Sakamoto, Mrs. Izumi Takeda and Mrs. Ibuki Aiba for sharing me with interesting knowledge about Japanese

patiently.

Special gratitude goes to my friends and relatives back in China and/or here in Japan. Sorry not to list all the names here owing to the limited space. You are always being there to encourage and support me. The friendship with you is cherished forever.

I was so fortunate to be able to have my husband Zhiyong Feng in my life. He is not only the love of my life, but also my best friend. Thank you for all of your love and support. I also feel so lucky to have diligent and good-natured mother-in-law and father-in-law.

Finally, I would like to express my heartiest appreciation to my parents for their unconditional support and encouragement of my education at universities. Throughout my entire life I have always been given love and encouragement. I thank my sister and brother-in-law, my brother and sister-in-law for their love and support. I owe them a lot and appreciate their generous dedication to my family. The love my family gives to me always lightens up the path I walk through over the years.

Contents

List of Tables

List of Figures

Nomenclature

α	index of pressure in the *MRR* model proposed for MCF polishing
A_i	pressure/shear stress measurement area at step *i* (mm^2)
b	scanning path interval (mm)
β	index of shear stress in the *MRR* model proposed for MCF polishing
C_p	coefficient in Preston's equation in conventional polishing processes
C_{pmcf}	coefficient in the *MRR* model proposed for MCF polishing
d	distance from the spot centre (mm)
$d_{\max}$	radial position where maximal material removal occurs (mm)
dR	depth removal (μm)
$dR_{\max}$	maximal depth removal (μm)
dRR	depth removal rate (μm/min)
$dRR_{\max}$	maximal depth removal rate (μm/min)
Δ	working gap between the MCF slurry carrier and the workpiece (mm)
δ	clearance between the MCF slurry carrier and the magnet (mm)
F_n	normal force (N)
$F_{n,i}$	normal force at step *i* (N)
$f_{n,i}$	normal force increment at step *i* (N)
F_t	shear force (N)
$F_{t,i}$	shear force at step *i* (N)
$f_{t,i}$	shear force increment at step *i* (N)
F_{tx}	shear force along x-axis (N)
F_{ty}	shear force along y-axis (N)
h	carrier shifting interval (mm)
H	magnetic field strength (KGs)
$h_{\max}$	maximum length of the slurry terminal shape along its diameter direction

	(mm)
H_{max}	maximum length of the slurry terminal shape at the mountaintop (mm)
H_x	magnetic field strength along x-axis (KGs)
H_z	magnetic field strength along z-axis (KGs)
i	pressure/shear stress measurement step number
j, k, l	number of position d
MR_d	material removal at radial position d (μm)
MR_{max}	maximal material removal (μm)
MRR	material removal rate (μm/min)
MRR_{cal_d}	calculated material removal rate at radial position d (μm/min)
MRR_d	material removal rate at radial position d (μm/min)
n_c	MCF slurry carrier rotational speed (rpm)
n_m	magnet revolution speed (rpm)
P	pressure (MPa)
P_i	pressure at step i (MPa)
P_d	pressure at radial position d (MPa)
r	magnet eccentricity (mm)
R	radius of the removal function (mm)
R_a	arithmetic roughness average (nm)
rms	root mean square (nm)
S_x	scanning distance along x-axis (mm)
S_y	scanning distance along y-axis (mm)
t	slurry shape formation measurement time (s)
T	time required for researching the slurry terminal shape (s)
τ	shear stress (MPa)
τ_i	shear stress at step i (MPa)
τ_d	shear stress at radial position d (MPa)
v	supplied MCF slurry volume (mL)

V	relative velocity between the polishing tool and the workpiece (mm/min)
V_d	relative velocity between the polishing tool and the workpiece at radial position d (mm/min)
V_f	relative speed during scanning polishing (mm/min)
VR	volumetric removal (mm^3)
VRR	volumetric removal rate (mm^3/min)
W	diameter of the slurry terminal shape (mm)

Chapter I
Introduction

1.1 Optical materials

Optical materials, such as glasses and polymers, possess excellent mechanical, chemical and physical properties and have been extensively used as the construction material in the detection and control of radiation, including visible light, gamma rays, X-rays, ultraviolet and infrared. Optical materials have found a wide spectrum of applications in scientific and industrial fields, including laser system, astronomical telescopes, microscopes, semiconductor industry, etc. (Fig. 1.1).

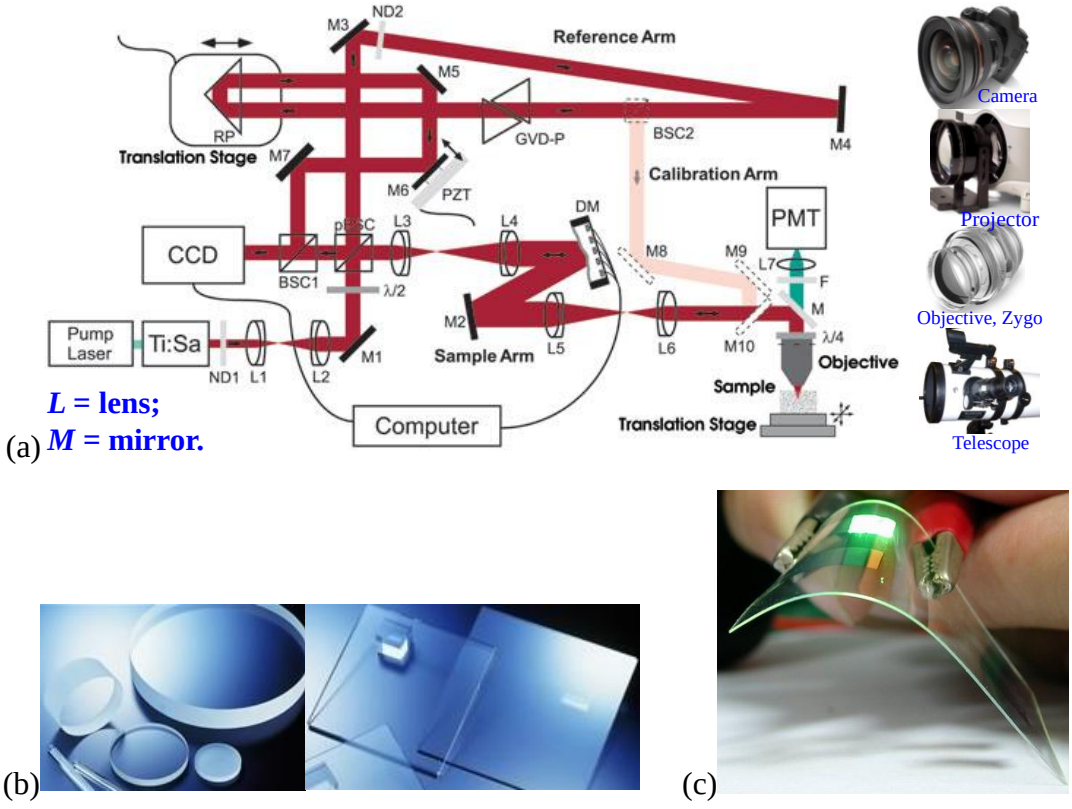

(a)

(b)

(c)

Fig. 1.1 Optical materials used in different systems: (a) Lens used in a laser system, camera, projector and objective, (b) Glasses for integrated circuit and photomask and (c) Polymer light-emitting diodes

To meet the required performance, the surfaces of these devices must be finished to nano-level roughness with no sub-surface damage. Therefore, during the manufacturing of optical devices, the construction material is generally subjected to nano-precision polishing as the final process after machining (e.g. cutting and grinding). Nano-precision polishing not only reduces the surface roughness but also eliminates breaks, cracks and damaged layers on the work surface caused by previous processes such as ultra-fine grinding. Conventionally, nano-precision polishing is accomplished by freshly feeding loose abrasive slurry in the polishing zone between a pitch lap or polyurethane pad and the workpiece. To achieve the desired surface quality, this technique requires a long processing time and a continuous plentiful supply of slurry [1]. Li et al. [2] polished optics with a polyurethane pad and eliminated surface damage several hours later, thereby mitigating subsurface damage and achieving surface roughness of approximately 1 nm. Consequently, traditional nano-polishing is a costly and time consuming process. Maintaining the required quantity of active abrasive slurry and ensuring that abrasive particles are uniformly distributed within the polishing zone are among the main difficulties. Therefore, novel polishing methods that supply large amounts of uniformly-distributed abrasive particles in the polishing zone are of high priority.

1.2 Review of magnetic field-assisted polishing processes

1.2.1 Behaviours of fluids

Magnetic field-assisted polishing using magnetic fluids (MFs) or magnetorheological (MR) fluids is a promising advanced finishing technique. In this technique, the behaviour of the abrasive particles is controlled by an applied magnetic field to achieve a nano-precision-polished surface with no surface and/or sub-surface damage. Tani et al. [3] developed a polishing method based on magnetohydrodynamic behaviour of MFs. They blended SiC grains into an MF and achieved an appreciable stock removal rate greater than 2 μm/min and surface roughness less than R_{max} = 0.04

μm for finishing of acrylic resin. Umehara and Kalpakjian [1] developed a polishing technique known as magnetic fluid grinding that uses controlled low level force during polishing. The process was found to produce more accurate surfaces at significantly less time than conventional polishing. Umehara et al. [4] studied the behaviour of abrasives in an MF during polishing and reported that the number of abrasives on the work surface could be controlled by a magnetic field. Prokhorov and Kordonski [5] proposed a novel magnetorheological finishing (MRF) technique in which the MR fluid contained magnetic carbonyl-iron-particle (CIP), abrasive grains, carrier fluid and stabilizers. An MRF machine usually consists of an MR fluid nozzle, electromagnet, a wheel for carrying MR fluid, workpiece fixture and a fluid delivery system. Kordonski and Jacobs [6] revealed that the MR fluid becomes viscous and morphs into a kind of Bingham fluid under an applied magnetic field. Jha and Jain [7] developed a new magnetorheological abrasive flow finishing (MRAFF) process. The MRAFF setup consists of MR fluid cylinders with pistons, workpiece fixture, electromagnet, hydraulic drive and controls, and supporting frame. The rheological behaviour of MR fluid changes from nearly Newtonian to Bingham plastic in the presence of magnetic field. They demonstrated that the roughness reduces gradually with the increase of magnetic field strength and validated the role of rheological behaviour of MR fluid in exerting finishing action. From the rheological experiments in MRAFF process, Das et al. [8] concluded that the viscosity of the fluid increases in a third-order logarithmic function with an increase in the magnetic field for the same applied pressure a larger plug flow region of the flowing fluid is obtained with higher magnetic field due to the formation of strong structure of CIP chains with increased magnetic field. Das et al. [9] experimentally characterised rheological properties of MR fluid in MRAFF process. They described that the MR fluid in MRF, MRAFF and similar other processes is a suspension of micron-sized magnetisable particles such as CIPs and non-magnetic abrasive particles dispersed in either an aqueous or non-aqueous carrier fluid like paraffin oil, silicone oil, mineral oil, or water and stabilizing additives. They observed

that magnetic field has the highest contribution on the yield stress and viscosity of MR fluid than the volume concentrations of CIPs, abrasive particles and grease.

1.2.2 Polishing of optical materials

Jacobs et al. [10] described that MRF machine deterministically polished out the workpiece by removing microns of subsurface damage, smoothing the surface to a microroughness of 10 angstroms *rms*, and correcting surface figure errors to less than 0.1 micrometers p-v. Spheres and aspheres can be processed with the same machine set-up using the appropriate machine program. Golini et al. [11] commercialized the MRF technique for optical fabrication and reported that this technique eliminates subsurface damage, smoothes root mean square (*rms*) microroughness to less than 1 nm, and corrects PV surface figure errors to λ/20 in minutes. DeGroote et al. [12] successfully smoothed a diamond turned polymethyl methacrylate (PMMA) part to 0.5 nm in *rms* with MRF. Kim et al. [13] proposed a surface-finishing method for three-dimensional microchannel structures utilizing magnetorheological fluid mixed with abrasives as a polishing tool and demonstrated that the proposed method was effective in finishing of microstructures. Jha and Jain [7] developed the MRAFF process for complex internal geometries using MR fluid. Seok et al. [14] proposed a finishing process for curved surfaces using MR fluid and performed the fabrication of circular surfaces on silicon-based millistructures, in which the edge effect is actively utilized. The finishing tool assembly was composed of a cylindrically shaped permanent magnet and a rim. Cheng et al. [15] polished aspherical optical components with fixed-charge MRF, namely using a 2-axis wheel-shaped tool supporting dual magnetic fields, improved the surface roughness from 3.8 nm to 1.2 nm after 10 min of pre-polishing and corrected form errors from an *rms* value of 2.27 μm to 0.36 μm after 60 more minutes of fine polishing. Singh et al. [16, 17] proposed a nano-finishing process using a ball end MRF tool and applied it to flat and 3D ferromagnetic work surfaces, thus verifying that the newly developed method was effective in finishing typical 3D ferromagnetic work surfaces.

1.2.3 Material removal mechanism

For conventional polishing processes, Preston's equation $MRR = C_p PV$ states that, for a conventional polishing process, material removal rate is proportional to normal force or pressure [18]. Kordonski and Jacobs [6] considered the mechanism of material removal in the polishing zone in MRF as a process governed by the particularities of the Bingham flow. They predicted the existence of a thin layer of high shear in contact with the optic where polishing occurs and obtained the shear stress distribution from the experimental measurements of the pressure distribution in the polishing spot. Shorey et al. [19] proposed an *MRR* model which contains a term for the coefficient of friction, or drag force equal to the coefficient of friction multiplied by the normal force. They justified the proposed *MRR* model by stating that there is not only a linear relation between the material removal rate (*MRR*) and the drag force in MRF but also no material removal when there is no drag force. DeGroote et al. [20] introduced a new *MRR* model for the MRF of glass, which contained terms for the near surface mechanical properties of glass, drag force, polishing abrasive size and concentration, chemical durability of the glass, MR fluid pH and the glass composition. They found that increasing the drag force or shear stress in the modified *MRR* model produced higher material removal rate for each glass type with increasing nanodiamond concentration. Miao et al. [21] demonstrated how the calculated shear stress governs the material removal in MRF of optical glasses based on their mechanical properties and incorporated the shear stress and material mechanical properties into a modified Preston's equation. Miao et al. [22] also investigated the effect of process parameters (nanodiamond concentration, penetration depth, the relative velocity between the part and the MR fluid, and magnetic field strength) on *MRR* in MRF of borosilicate glass (BK7). They found that shear stress is independent of the process parameters. The volumetric removal rate (*VRR*) is only insensitive to the magnetic field strength. Thereby, the *MRR* model for MRF was expanded by including nanodiamond concentration and penetration depth. Das et al. [8] performed the theoretical

investigations into the mechanism of MRAFF process and concluded that shearing action takes place during finishing when the shear force acting on the abrasive particles is greater than the reaction force due to the strength of the workpiece material opposing material removal. By analyzing MRF processes, Dai et al. [23] established a calibrated predictive model of material removal function by introducing an efficiency coefficient, thereby improving finishing determinacy and model applicability. Seok et al. [24] studied the tribological properties of an MR fluid in a wheel-type MRF process. They concluded that the dominant MR finishing wear mechanism is abrasion supported by the fact that the MRR increases with the increase of the slip of particles. They also emphasized that it is technically difficult to separate the effects of the frictional shear force from those of the interfacial slip of particles. Sidpara and Jain [25] measured the normal and tangential forces in MRF. They concluded that maximum contribution is made by a working gap on the forces developed on the workpiece surface followed by CIPs concentration, whereas minimum contribution is noted by the wheel speed.

1.3 Polishing process with magnetic compound fluid (MCF) slurry

In a magnetic field, magnetic pressure and apparent viscosity of an MF are smaller than that of an MR fluid, whereas the particles are more stably distributed in the former than in the latter. To overcome the disadvantages and exploit the advantages of MFs and MR fluids, Shimada et al. [26] developed a magnetic compound fluid (MCF) by mixing an MF and an MR fluid with the same base solvent. Hence, MCF includes not only μm-sized iron particles but also nm-sized magnetite particles whereas there are no nm-sized magnetite particles within MR fluid. They confirmed that MCFs exhibit higher magnetic pressure and apparent viscosity than MFs and a more stable distribution of particles than MR fluids under a magnetic field, while maintaining a fluid-like behaviour. As an engineering application of MCFs, Shimada et al. [27] proposed an MCF slurry, a novel magnetic polishing liquid in which abrasive particles and α-cellulose fibre are blended into the MCF. The slurry showed strong performance

in constant contact-force polishing under a static magnetic field. As mentioned above, constant contact-force polishing with MCF slurry frequently does not remove the micro-groove, ribs and other three-dimensional (3D) surface defects, and frequently scratches or cracks the work surfaces. To resolve these problems, Shimada et al. [28] employed MCF slurry in a contact-free surface finishing method for work surfaces with micro 3D structures, and thereby successfully performed mirror surface finishing of a brass specimen with rib-shaped grooves. They confirmed that there are needle-like magnetic clusters in MCF [29] and found smaller clearance enhances the polishing effect and shortens the time necessary, and magnetic field strength dominates the distributions of the abrasives, i.e. inside or between the magnetic clusters, greatly influencing the polishing effect [28]. Shimada et al. [30] demonstrated that shear force in the contact-free finishing process is strength by adding α-cellulose into MCF and the polishing effect of MCF depends on the shear stress along the rotation direction of the polishing tool as the normal stress is nearly zero during polishing. Following the work by Shimada et al., Furuya et al. [31] and Wu et al. [32] experimentally investigated the fundamental characteristics of contact-free MCF polishing in the flat surface finishing of stainless steel and acrylic resin, respectively, and optimized the respective process parameters, including the composition of the MCF slurry. Jiao et al. [33] employed MCF slurry in a semi-fixed-abrasive, ultra-fine finishing, i.e. MCF wheel and investigated the performance of the wheel by spot polishing of fused silica glass. They found that a better work surface and greater material removal were obtained with a smaller working clearance and a higher wheel rotational speed probably because both the normal and tangential polishing forces increase. They also observed that a higher *MRR* occurs near the edge of the magnet where the magnetic field is stronger because of the edge effect, resulting in a thicker MCF layer, a higher distribution density of abrasive particles and a higher polishing pressure.

However, under a static magnetic field in which the magnetic flux density and the spatial distribution of magnetic lines of force are retained constant, the geometrical

shape/size and distribution of the magnetic clusters generated within the MCF slurry are governed by the external conditions. These behaviours disfavour surface finishing because the abrasive particles within the MCF slurry are magnetically clustered, which hinders their uniform distribution. Indeed, the shape restoring ability of MCF slurry is extremely low. To overcome this weakness, Sato et al. [34] replaced the static field applied to the MCF slurry with a rotary magnetic field.

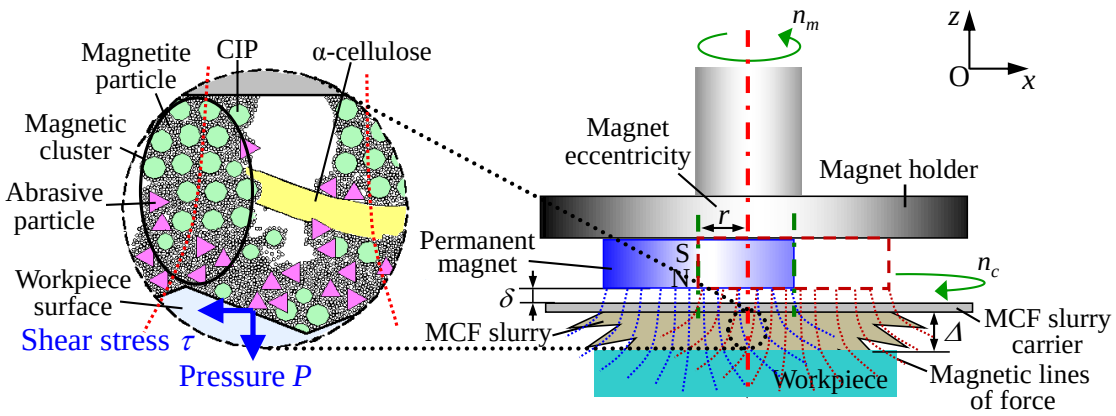

Fig. 1.2 Principle of MCF polishing under a rotary magnetic field

The principle of MCF polishing under a rotary magnetic field is illustrated in Fig. 1.2. A disk-shaped permanent magnet is attached to the lower end face of its holder with an eccentricity r, and a non-magnetic carrier, such as an aluminium plate, is positioned between the magnet and a workpiece at distance δ from the magnet. When the magnet holder is rotated at a speed n_m, the magnet revolves around the axis of the holder, thereby generating a rotary magnetic field. The magnetic flux density is constant but the magnetic lines of force constantly revolve around the magnet holder axis. Once the working gap Δ between the carrier and the workpiece has received a certain volume of MCF slurry, as shown in the left side of Fig. 1.2, chain-shaped magnetic clusters composed of nm-sized magnetite particles and μm-sized CIPs are formed along the magnetic line of force immediately; non-magnetic abrasive particles are entrapped into the clusters or distributed between clusters and α-cellulose fibres have interwoven with the clusters if the fibres are employed. Kim et al. [13] defined

magnetic levitation as forces exerted on nonmagnetic bodies by a magnetic functional fluid. Therefore, under magnetic levitation and gravitational forces, a majority of nonmagnetic abrasive particles within the MCF slurry move downward towards the workpiece surface. In addition, all of the clusters are collected forcibly by the magnetic attraction force and they are gathered in the area where the magnetic field is stronger. This leads to the generation of a pressure P (i.e. normal force F_n divided by the interacting area between the MCF slurry and the workpiece) acting on the workpiece. When the magnet holder and the carrier are rotated at their respective rotational speeds of n_m and n_c, a shear stress τ (i.e. shear force F_t divided by the interacting area between the MCF slurry and the workpiece) is imposed on the workpiece owing to the n_m/n_c-induced friction between the particles and the workpiece and the micro-cutting action of abrasive particles that remove unwanted materials.

Sato et al. [35] adopted the rotary magnetic field in an improved MCF polishing process for 3D metal components. Under the rotary magnetic field, the polishing performance of the MCF slurry was much higher than under the static magnetic field, confirming that MCF polishing is applicable to 3D-structured surface finishing. Complete development should begin by thoroughly clarifying the fundamental characteristics of the MCF slurry under the rotary magnetic field, including its dynamic behaviour, the polishing forces during polishing and the function that describes material removal.

1.4 Overview of thesis

The objectives of this thesis research work are to clarify dynamic behaviour of MCF slurry under a rotary magnetic field, to smooth optical materials to nano-level surface roughness with MCF slurry and to elucidate material removal behaviours during MCF polishing.

Chapter I first briefly reviews magnetic field-assisted polishing processes from

aspects of behaviours of fluids, polishing of optical materials and material removal mechanism. Popular techniques for achieving nano-precision surface finishing are outlined. Then, the development of polishing with MCF slurry is introduced.

Chapter II describes experimental approaches and all the instrumentations used for this thesis work, followed by the components of MCF slurry and the work life of MCF slurry.

Chapter III first investigates the variation process of external MCF slurry shape under a rotary magnetic field and how various process parameters, namely magnet eccentricity r, magnet revolution speed n_m, MCF slurry carrier rotational speed n_c and supplied MCF slurry volume v affect the formed slurry terminal shape and the formation time. Then, effects of magnet revolution speed n_m, MCF slurry carrier rotational speed n_c and working gap Δ on the normal and shearing forces are discussed. Finally, the structure of MCF slurry is analyzed to make clear why a better surface finish is obtained under a rotary magnetic field than a static one.

Chapter IV reports the nano-precision polishing of polymethyl methacrylate (PMMA) with a zirconia (ZrO_2)-coated carbonyl-iron-particle (CIP) based MCF slurry. Polishing performance (i.e. normal force and surface roughness) of the new ZrO_2-coated CIP based MCF/MRF slurry is compared with that of the non-coated HQ CIP based MCF slurry. The effect of ZrO_2-coated CIP concentration is also investigated.

Chapter V focus on eliminating the single crystal diamond turning (SCDT)-induced concentrically arranged tool marks on the nickel-phosphorus (Ni-P) plated mold with MCF slurry. Both HQ CIP based MCF slurry and ZrO_2-coated CIP based MCF slurry were employed. Spot polishing is firstly carried out and the polished surface was analyzed in terms of profile, roughness, texture, and chemical elements. Then, based on the results obtained from spot polishing process, a scanning polishing was performed by designing a certain motion path of MCF slurry carrier relative to the work surface.

Chapter VI dedicates to understanding the material removal behaviour. The pressure/shear stress distributions over the polishing zone are measured and the relationship between the pressure/shear stress and material removal rate during the MCF polishing is established. The characteristics of the removal function, the polishing spot, were also investigated in order to further elucidate the material removal behaviour. Effects of process parameters (namely magnet revolution speed n_m, MCF slurry carrier rotational speed n_c and working gap Δ) on the pressure/shear stress distributions and material removal rate are discussed, while effects of process parameters (namely magnet eccentricity r, magnet revolution speed n_m, MCF slurry carrier rotational speed n_c and working gap Δ) on the removal function are presented. Moreover, the magnetic field distribution is analysed and the geometry and internal structure of MCF slurry is examined in order to give a reasonable explanation for the removal function.

Chapter VII , the last chapter summarizes and gives suggestions for future work on MCF polishing.

References

[1] Umehara, N., Kalpakjian, S., 1994. Magnetic Fluid Grinding – a New Technique for Finishing Advanced Ceramics. CIRP Annals 43, 185–188.

[2] Li, Y., Hou, J., Xu, Q., Wang, J., Yang, W., Guo, Y., 2008. The characteristics of optics polished with a polyurethane pad. Opt. Express 16, 10285–10293.

[3] Tani, Y., Kawata, K., Nakayamac, K., 1984. Development of high-efficient fine finishing process using magnetic fluid. CIRP Ann. 33, 217–220.

[4] Umehara, N., Hayashi, T., Kato, K., 1995. In situ observation of the behavior of abrasives in magnetic fluid grinding. J. Magn. Magn. Mater. 149, 181–184.

[5] Prokhorov, I., Kordonski, W., 1992. New high-precision magnetorheological instruments-based method of polishing optics. OSA OF&T Workshop Digest 24, 134–136.

[6] Kordonski, W., Jacobs, S., 1996. Magnetorheological finishing. Int. J. Mod. Phys. B 10, 2837–2848.

[7] Jha, S., Jain, V.K., 2004. Design and development of the magnetorheological abrasive flow finishing (MRAFF) process. Int. J. Mach. Tools Manuf. 44, 1019–1029.

[8] Das, M., Jain, V.K., Ghoshdastidar, P.S., 2008. Fluid flow analysis of magnetorheological abrasive flow finishing (MRAFF) process. Int. J. Mach. Tools Manuf. 48, 415–426.

[9] Das, M., Sidpara, A., Jain, V.K., Ghoshdastidar, P.S., 2011. Parametric analysis of MR polishing fluid using statistical technique. Int. J. Precis. Technol. 2, 51–63.

[10] Jacobs, S.D., Golini, D., Hsu, Y., Puchebner, B.E., Strafford, D., Prokhorov, I. V., Fess, E.M., Pietrowski, D., Kordonski, W., 1995. Magnetorheological finishing: a deterministic process for optics manufacturing. Proc. SPIE 2576, 372–383.

[11] Golini, D., Kordonski, W.I., Dumas, P., Hogan, S.J., 1999. Magnetorheological finishing (MRF) in commercial precision optics manufacturing. Proc. SPIE 3782, 80–91.

[12] DeGroote, J.E., Romanofsky H.J., Kozhinova, I.A., Schoen, J.M., Jacobs, S.D., 2003. Polishing PMMA and other optical polymers with magnetorheological finishing. Proc. SPIE 5180, 123–134.

[13] Kim, W.B., Lee, S.H., Min, B.K., 2004. Surface Finishing and Evaluation of Three-Dimensional Silicon Microchannel Using Magnetorheological Fluid. J. Manuf. Sci. Eng. 126, 772–778.

[14] Seok, J., Kim, Y.J., Jang, K.I., Min, B.K., Lee, S.J., 2007. A study on the fabrication of curved surfaces using magnetorheological fluid finishing. Int. J. Mach. Tools Manuf. 47, 2077–2090.

[15] Cheng, H.B., Yam, Y., Wang, Y.T., 2009. Experimentation on MR fluid using a 2-axis wheel tool. J. Mater. Process. Technol. 209, 5254–5261.

[16] Singh, A.K., Jha, S., Pandey, P.M., 2011. Design and development of nanofinishing process for 3D surfaces using ball end MR finishing tool. Int. J. Mach. Tools Manuf. 51, 142–151.

[17] Singh, A.K., Jha, S., Pandey, P.M., 2012. Nanofinishing of a typical 3D ferromagnetic workpiece using ball end magnetorheological finishing process. Int. J. Mach. Tools Manuf. 63, 21–31.

[18] Preston, F. W., 1927. The theory and design of plate glass polishing machines. J. Soc. Glass Technol. 11, 214–256.

[19] Shorey, A.B., Jacobs, S.D., Kordonski, W.I., Gans, R.F., 2001. Experiments and observations regarding the mechanisms of glass removal in magnetorheological finishing. Appl. Opt. 40, 20–33.

[20] DeGroote, J.E., Marino, A.E., Wilson, J.P., Bishop, A.L., Lambropoulos, J.C., Jacobs, S.D., 2007. Removal rate model for magnetorheological finishing of glass. Appl. Opt. 46, 7927–7941.

[21] Miao, C., Shafrir, S.N., Lambropoulos, J.C., Mici, J., Jacobs, S.D., 2009. Shear stress in magnetorheological finishing for glasses. Appl. Opt. 48, 2585–2594.

[22] Miao, C., Lambropoulos, J.C., Jacobs, S.D., 2010. Process parameter effects on

material removal in magnetorheological finishing of borosilicate glass. Appl. Opt. 49, 1951–1963.

[23] Dai, Y.F., Song, C., Peng, X.Q., Shi, F., 2010. Calibration and prediction of removal function in magnetorheological finishing. Appl. Opt. 49, 298–306.

[24] Seok, J., Kim, Lee, S.O., Y.J., Jang, K.I., Min, B.K., Lee, S.J., 2009. Tribological Properties of a Magnetorheological (MR) Fluid in a Finishing Process. Tribol. Transa. 52, 460–469.

[25] Sidpara, A., Jain, V.K., 2011. Experimental investigations into forces during magnetorheological fluid based finishing process. Int. J. Mach. Tools Manuf. 51, 358–362.

[26] Shimada, K., Fujita, T., Oka, H., Akagami, Y., Kamiyama, S., 2001. Hydrodynamic and magnetized characteristics of MCF (magnetic compound fluid). Trans. Jpn. Soc. Mech. Eng. B 67, 3034–3040 (in Japanese).

[27] Shimada, K., Akagami, Y., Kamiyama, S., Fujita, T., Miyazaki, T., Shibayama, A., 2002. New microscopic polishing with magnetic compound fluid (MCF). J. Intell. Mater. Syst. Struct. 13, 405–408.

[28] Shimada, K., Wu, Y., Matsuo, Y., Yamamoto, K., 2005. Float polishing technique using new tool consisting of micro magnetic clusters. J. Mater. Process. Technol. 162–163, 690–695.

[29] Shimada, K., Shuchi, S., Kanno, H., Wu, Y., Kamiyama, S., 2005. Magnetic cluster and its applications. J. Magn. Magn. Mater. 289, 9–12.

[30] Shimada, K., Matsuo, Y., Yamamoto, K., Wu, Y., 2008. A new float-polishing technique with large clearance utilising magnetic compound fluid. Int. J. Abras. Technol. 1, 302–315.

[31] Furuya, T., Wu, Y., Nomura, M., Shimada, K., Yamamoto, K., 2008. Fundamental performance of magnetic compound fluid polishing liquid in contact-free polishing of metal surface. J. Mater. Process. Technol. 201, 536–541.

[32] Wu, Y., Sato, T., Lin, W., Yamamoto, K., Shimada, K., 2010. Mirror surface

finishing of acrylic resin using MCF-based polishing liquid. Int. J. Abras. Technol. 3, 11–24.

[33] Jiao, L., Wu, Y., Wang, X., Guo, H., Liang, Z., 2013. Fundamental performance of Magnetic Compound Fluid (MCF) wheel in ultra-fine surface finishing of optical glass. Int. J. Mach. Tools Manuf. 15, 109–118.

[34] Sato, T., Wu, Y., Lin, W., Shimada, K., 2009. Study on magnetic compound fluid (MCF) polishing process using fluctuating magnetic field. Trans. Jpn. Soc. Mech. Eng. B 75, 1007–1012 (in Japanese).

[35] Sato, T., Wu, Y., Lin, W., Shimada, K., 2010. Study of three-dimensional polishing using magnetic compound fluid (MCF). J. Jpn. Soc. Abras. Technol. 54, 425–430 (in Japanese).

Chapter II
Experimental Approach and MCF Slurry

2.1 Experimental setup

Based on the MCF polishing principle introduced in Chapter I, Fig. 2.1 shows one experimental setup constructed. A disc-shaped neodymium permanent magnet (ϕ32 mm × t10 mm, 0.45 T) was set at an eccentricity of r = 8 mm. A polishing unit composed of a magnet holder, an MCF slurry carrier (an aluminum plate), two motors, two sets of belt/pulleys is developed and mounted onto a 6-DOF robot arm. One of the motors is connected to the magnet holder via a belt to give the magnet a revolution motion. The other is used to drive the MCF slurry carrier rotationally. The working gap of Δ is determined by adjusting the vertical position of the MCF slurry carrier through the control of the robot arm. A robot program can be designed to give the MCF slurry carrier relative motion to the work surface. Nano-precision polishing of polymethyl methacrylate (PMMA) was carried out using this setup.

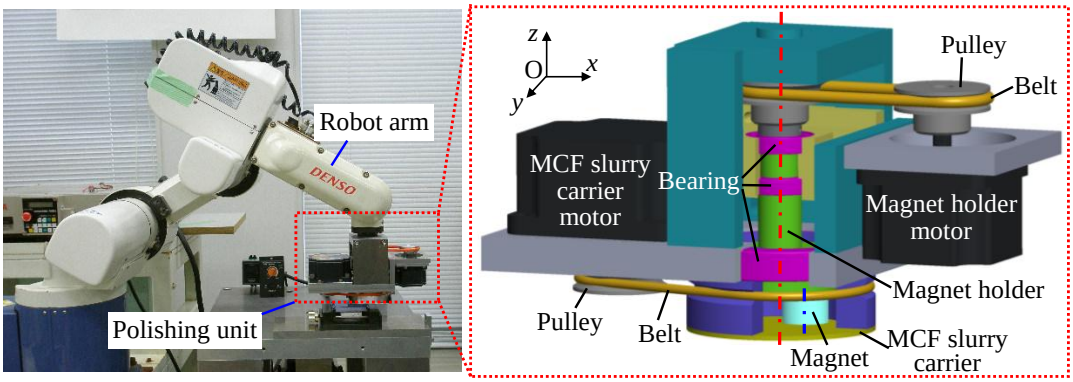

Fig. 2.1 Experimental setup constructed based on a 6-DOF robot arm

In Fig. 2.2, the other experimental setup was constructed in-house, which is composed of a magnet holder and an MCF slurry carrier, and mounted onto the spindle head of a vertical milling cutter. Magnet holder is rotated by the spindle to give the

magnet a revolution motion and MCF slurry carrier is driven to rotate by using a motor and a set of belt/pulleys. In this setup, the installed magnet was a commercially available disc-shaped neodymium permanent magnet with dimensions of 18 mm in diameter and 10 mm in thickness and its magnetic field strength is 0.4 T.

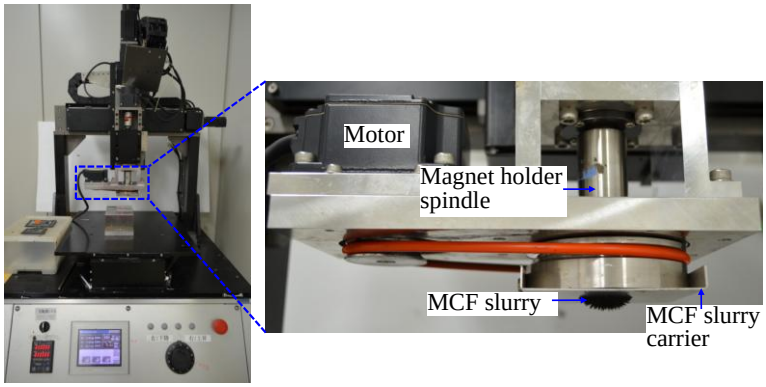

Fig. 2.2 Experimental setup constructed based on a milling cutter

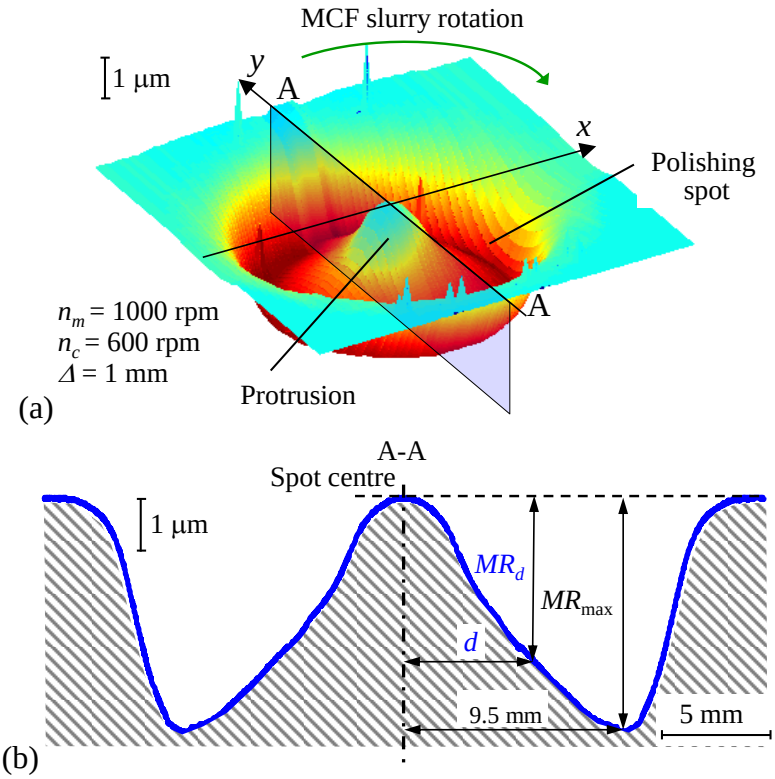

Fig. 2.3 (a) A 3D profile and (b) a cross-sectional profile of a typical polishing spot obtained at n_m = 1000 rpm, n_c = 600 rpm and Δ =1 mm

Nano-precision polishing of nickel-phosphorus (Ni-P) plating layer was performed using this setup; Moreover, the material removal behaviours in MCF polishing of optical glasses were investigated through spot polishing tests, in which no relative motion of the centre of the MCF slurry carrier to the workpiece is imposed, and a sole circular interacting area was considered as a polishing spot. The removal function in MCF polishing is characterized by the polishing spot. A 3D profile of a typical polishing spot is exhibited in Fig. 2.3(a). A cross-sectional profile of the polishing spot measured along A–A (see Fig. 2.3(a)), which passes through the polishing spot centre where the material removal (*MR*), i.e. the spot depth, is smallest as shown in Fig. 2.3(b). According to this cross-sectional profile, *MR* at a position *d*, i.e. a certain distance from the spot centre is inferred and volumetric material removal (*VR*) is calculated by integration.

2.2 Metrology and characterization

2.2.1 MCF slurry motion analysis

As displayed in Fig. 2.4, a high-speed motion analysis microscope (VW6000 by Keyence Co., Ltd.) was used to observe the behaviours of the used MCF slurry under a rotary magnetic field.

Fig. 2.4 Keyence VW6000 high-speed motion analysis microscope

2.2.2 Surface profile

As shown in Fig. 2.5, a stylus-based profilometer **(**Form Talysurf Intra by Taylor Hobson Inc.) was used to measure the cross-sectional profiles (at least three) of a work surface.

Fig. 2.5 Taylor Hobson Form Talysurf Intra profilometer

2.2.3 Surface quality characterization

As displayed in Fig. 2.6, scanning electron microscope (SEM, ERA-8900 by Elionix) were used to observe the work surface textures. Elemental composition analyses were carried out using Energy Dispersive X-Ray Analysis (EDX, Genesis APEX by EDX) to check if any embedding of particles has occurred. With this instrument, the microstructure of MCF slurry and the components were also examined.

Fig. 2.6 EDAX ERA-8900, 3D-SEM & EDX

As shown in Fig. 2.7, the surface roughness was measured (at least five locations) using a non-contacting white-light interferometer which was equipped with a 10× Mirau objective and provided a 700 μm×526 μm measurement area (New view 600, Zygo Corporation). The surface roughness was characterized by the most common arithmetic roughness average (R_a) which can be calculated from Eq. 2.1 and root mean square (*rms*) which can be calculated from Eq. 2.2.

$$R_a = \frac{1}{n}\sum_{i=1}^{n}|y_i| \tag{2.1}$$

$$rms = \sqrt{\frac{1}{n}\sum_{i=1}^{n}y_i^2} \tag{2.2}$$

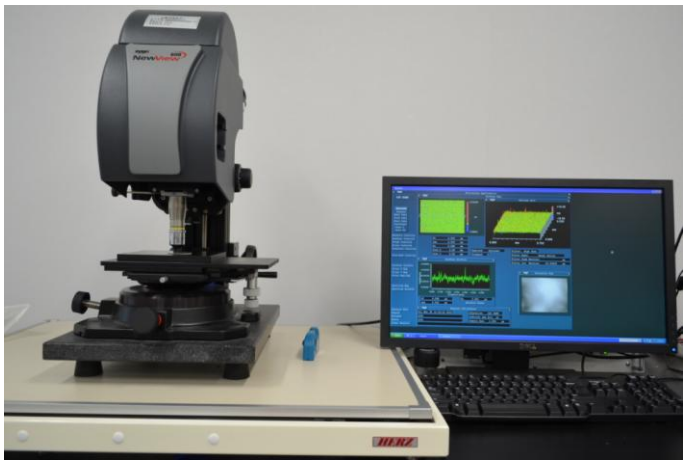

Fig. 2.7 Zygo New view 600 interferometer

2.2.4 Force measurement

A force measurement system composed of a 3-component dynamometer (9256A1 by Kistler Co., Ltd.), a charge amplifier and an oscilloscope were used to record the polishing forces. The sensitivities of the dynamometer, the charge amplifier and the oscilloscope are (−10 pC/N (Fx, Fy) and −13 pC/N (Fz)), (0.01–9990 pC/M.U.) (2 mV/div–10 V/div), respectively.

2.3 MCF slurry

Shimada et al. [1] developed a magnetic compound fluid (MCF) by mixing a magnetic (MF) and a magnetorheological (MR) fluid with the same base solvent. Hence, MCF includes not only μm-sized iron particles but also nm-sized magnetite particles whereas there are no nm-sized magnetite particles within MR fluid. They confirmed that MCFs exhibit higher magnetic pressure and apparent viscosity than MFs and a more stable distribution of particles than MR fluids under a magnetic field, while maintaining a fluid-like behaviour.

2.3.1 Components of MCF slurry

As exhibited in Fig. 2.8, components of MCF slurry used in this work are as follows: HQ carbonyl-iron-particle (CIP, mean particle size d_{50} = 2 μm, BASF made), zirconia(ZrO_2)-coated CIP (size ~1.4 μm, developed by the University of Rochester) [2], alumina (Al_2O_3) abrasive particles (grain size ~1 μm, alpha, AP-D, deagglomerated aluminas, Struers Inc.), water based magnetic fluid (MF, MSG W11 by Ferrotec Corporation) and α-cellulose (Reagnent, Nacalai tesque Inc.).

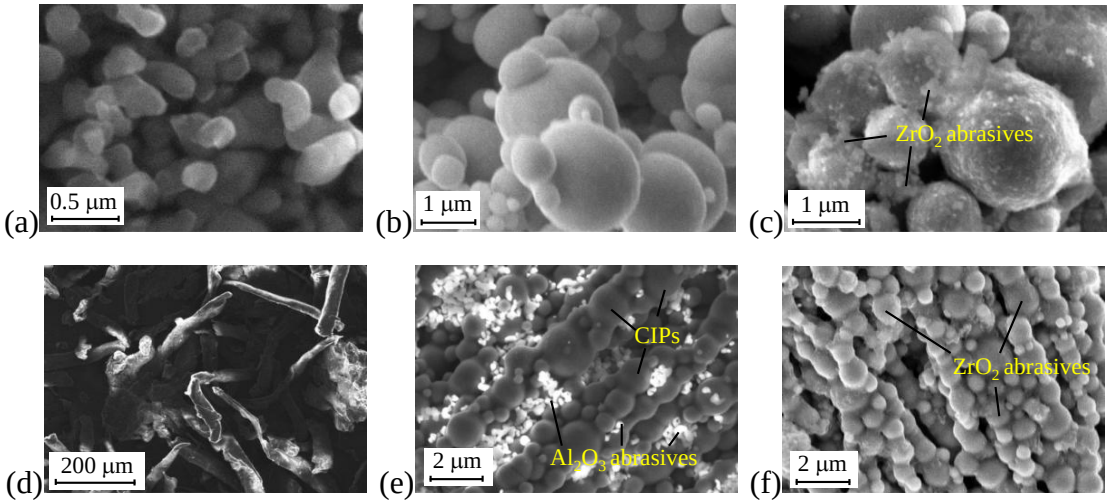

Fig. 2.8 SEM images of (a) Al_2O_3 abrasive particle, (b) the conventional HQ CIP, (c) ZrO_2-coated CIP, (d) α-cellulose and internal microstructures of (e) a typical HQ CIP based MCF slurry and a typical ZrO_2-coated CIP based MCF slurry

2.3.2 Work life of MCF slurry in spot polishing of optical glasses

Spot polishing tests were performed to investigate the work life of MCF slurry in polishing of optical glasses (borosilicate glass (Bk7) and fused silica (FS) glass). The experimental setup as shown in Fig. 2.2 was used. The experimental procedures were designed as follows: (1) the MCF slurry carrier is located at high enough vertical position and then the workpiece is fixed on the work stage, followed by putting a certain volume of MCF slurry onto the carrier; (2) the magnet holder and MCF slurry carrier are rotated at their respective speed, and then MCF carrier is lowered to make the rotating MCF slurry come in contact with the work-surface under a certain working gap of Δ to begin the spot polishing operation; (3) after a period of spot polishing, i.e. 5 min, 10 min and 15 min, MCF slurry carrier is raised, MCF slurry carrier rotation and magnet holder rotation are stopped in order, and then the polished workpiece is taken off the work stage followed by washing; subsequently the polished work-surface profile is measured using a stylus-based profilometer (Form Talysurf Intra by Taylor Hobson Inc.) and the surface roughness is also measured using a white light interferometer (New view 600, Zygo Corporation). Fresh workpieces are used to carry out each period of spot polishing. Table 2.1 shows the polishing experimental conditions.

Table 2.1 Polishing experimental conditions

Workpiece material	BK7, FS
Magnet	Nd-Fe-B
Magnet eccentricity	r = 4.5 mm
MCF slurry carrier rotational speed	n_c = 500 rpm
Magnet revolution speed	n_m = 1000 rpm
Amount of MCF slurry supplied	v = 1 mL
Working gap	Δ = 1 mm
Spot polishing period	5 min-35 min

Compositions of the used MCF slurry are as shown in Table 2.2. Slurry MCF1 is a HQ CIP based one, mixing with Al_2O_3 abrasives and water-based magnetic fluid (MF) while slurry MCF2 consists of ZrO_2-coated CIP and MF. α-cellulose fibers is not used in the presented experiment as α-cellulose fibers may increase the drying speed of slurry.

Table 2.2 Compositions of the used MCF slurry (wt. %)

Slurry type	HQ CIP (ϕ2 μm)	ZrO_2-coated CIP (ϕ1.4 μm)	Al_2O_3 abrasives (1 μm)	Water based MF
MCF1	56		12	32
MCF2		68		32

2.3.2.1 Variations of material removal rate

Fig. 2.9 shows the removal surface profiles which pass through the spot centre after spot polishing of BK7 for a period of 35 min with slurry MCF1 (Fig. 2.9(a)) and slurry MCF2 (Fig. 2.9(b)), and spot polishing of FS for a period of 35 min with slurry MCF1 (Fig. 2.9(c)) and slurry MCF2 (Fig. 2.9(d)). The surface profiles appear approximately symmetrical, depended on the compositions of MCF slurry and insensitive to the two used glasses. *dR* (depth removal) is defined as shown in Fig. 2.9(a) and Fig. 2.9(b) and *VR* (volumetric removal) is calculated according to the marked red curve. *dRR* (depth removal rate) and *VRR* (volumetric removal rate) are calculated as the *dR* and *VR* divided by the polishing time.

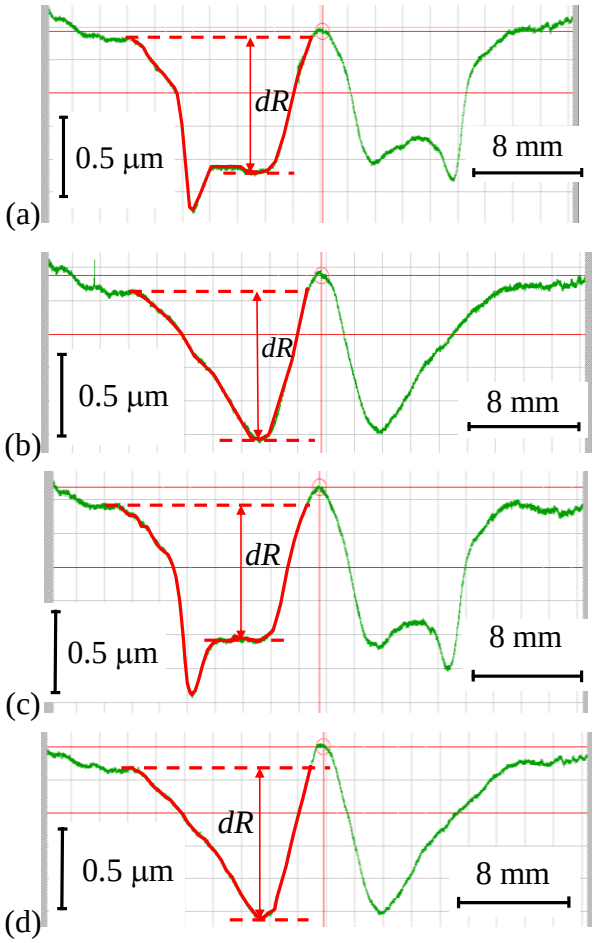

Fig. 2.9 Surface profiles after spot polishing for a period of 35 min: polishing of BK7 with (a) HQ CIP and (b) ZrO2-coated CIP based MCF slurry and Polishing of FS with (c) HQ CIP and (d) ZrO2-coated CIP based MCF slurry

Variations of *dRR* and *VRR* with increasing spot polishing period are plotted in Fig. 2.10. Fig. 2.10(a) shows that *dRR* obtained with both the MCF slurries still shows no decay and keeps at the level of ~0.0243 μm/min after spot polishing for a period of 35 min. However, it is noted that *VRR* obtained with ZrO_2-coated CIP based MCF slurry starts to decline from ~0.07 mm^3/min to 0.06 mm^3/min after spot polishing for a period of 25 min while *VRR* obtained with HQ CIP based MCF slurry still keeps at the level of ~0.08 mm^3/min after spot polishing for a period of 35 min.

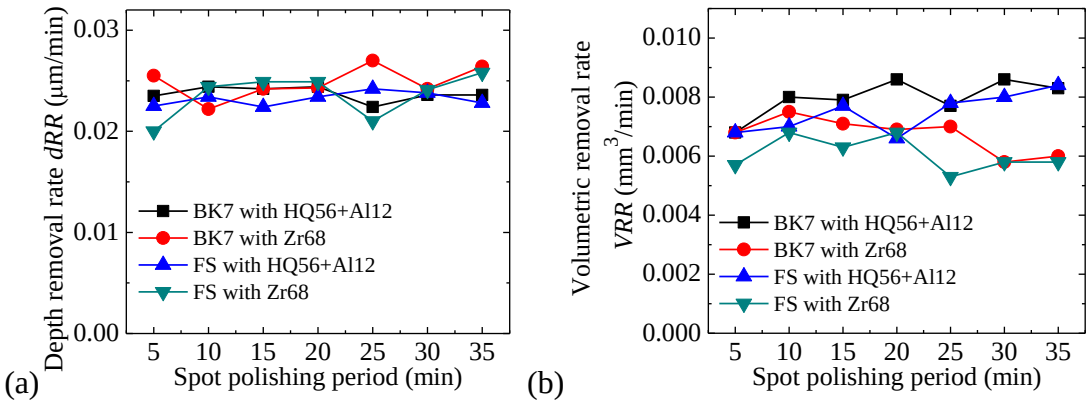

Fig. 2.10 Variations of (a) *dRR* and (b) *VRR* with spot polishing period

2.3.2.2 Variation of surface roughness *rms*

The average value of surface roughness at 4 sites of the *dR* region shown in Fig. 2.9 along two perpendicular diameters of the spot were obtained as the surface roughness of the polished work-surface. Variations of surface roughness *rms* values with increasing spot polishing period were plotted in Fig. 2.11. The surface roughness obtained with ZrO_2-coated CIP based MCF slurry is better than that obtained with HQ CIP based MCF slurry and surface roughness *rms* increases a little with the spot polishing period increasing, especially with HQ CIP based MCF slurry. Besides, surface roughness obtained with HQ CIP based MCF slurry is clearly more sensitive to working gap than that with ZrO_2-coated CIP based MCF slurry. As scratches are caused on the polished surface of BK7 samples with HQ CIP based MCF slurry, which sharply worsen the polished surface roughness, working gap is adjusted to be 1.05 mm in spot polishing of BK7 for a period of 35 min and all the polishing of FS samples. As scratches are still caused on both the polished BK7 and FS after spot polishing for a period of 35 min with HQ CIP based MCF slurry, surface roughness begin to deteriorate to over 1 nm. Surface roughness *rms* obtained with ZrO_2-coated CIP based MCF slurry is still nearly stable to be under 1 nm after spot polishing for a period of 35 min.

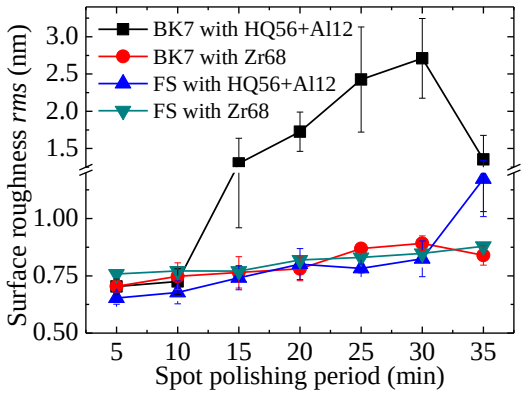

Fig. 2.11 Variation of surface roughness *rms* with spot polishing period

2.3.3 Summary

(1) Depth removal rate *dRR* obtained with both the MCF slurries still stabilizes at the level of ~0.0243 μm/min after spot polishing for a period of 35 min; *VRR* obtained with HQ CIP based MCF slurry still keeps stable at the level of ~0.08 mm^3/min after spot polishing for a period of 35 min while *VRR* obtained with ZrO_2-coated CIP based MCF slurry weakens from ~0.07 mm^3/min to 0.06 mm^3/min after spot polishing for a period of 25 min;

(2) After spot polishing for a period of 10 min, surface roughness *rms* inside spots obtained with HQ CIP based MCF slurry begin to deteriorate to over 1 nm while surface roughness inside spots obtained with ZrO_2-coated CIP based MCF slurry is still nearly stable to be under 1 nm.

(3) The removal function is depended on the compositions of MCF slurry and insensitive to the two used glasses.

References

[1] Shimada, K., Fujita, T., Oka, H., Akagami, Y., Kamiyama, S., 2001. Hydrodynamic and magnetized characteristics of MCF (magnetic compound fluid). Trans. Japan Soc. Mech. Eng. B 67, 3034–3040 (in Japanese).

[2] Shafrir, S.N., Romanofsky, H.J., Skarlinski, M., Wang, M., Miao, C., Salzman, S., Chartier, T., Mici, J., Lambropoulos, J.C., Shen, R., Yang, H., Jacobs, S.D., 2009. Zirconia-coated carbonyl-iron-particle-based magnetorheological fluid for polishing optical glasses and ceramics. Appl. Opt. 48, 6797–6810.

Chapter III
Behaviours of MCF Slurry and Its Mechanical Characteristics under a Rotary Magnetic Field

3.1 Introduction

Although MCF produced by mixing magnetic fluid (MF) and magnetorheological (MR) fluid with the same base solvent was proposed just only 13 years ago in 2001 by Shimada [1], it has a wide spectrum of applications potentially such as abrasive slurry used for precision surface finishing, damper for quake-absorbing structure, rubber-based smart materials and so on. This is attributed to its excellent properties that it yields a larger magnetic pressure and a higher apparent viscosity compared with MF, and has a greater stability of particle dispersion than MR fluid does under the same magnetic field. In the absence of magnetic field, the MCF slurry behaves as a Newtonian fluid. Once a magnetic field is applied to the MCF slurry, it is stiffened somewhat and behaves as a viscoplastic fluid due to the formation of many chain-shaped micro magnetic clusters along the magnetic lines of force generated by the applied magnetic field. For the sake of this feature, MCF slurry has so far been successfully employed for polishing a variety of engineering materials including polymer, glass, ceramics, etc. to nano-precision surface finish [2,3].

However, it has been found that the behavior of the MCF slurry under a magnetic field and its performance in surface finishing are affected significantly not only by process parameters but also by the applying way of magnetic field [4,5]. For example, if the MCF slurry is under a static magnetic field in which the magnetic flux density and the spatial distribution of the magnetic line of force are kept constant, its geometrical shape and the size/distribution of the magnetic clusters generated within the MCF slurry will be as they are. These behaviors are unfavorable for its performance in surface finishing because the abrasive particles within the MCF slurry

are hardly dispersed uniformly owing to the uneven distribution of magnetic clusters. By contrast, as a rotary magnetic field in which the magnetic flux density is kept constant but its spatial distribution is always fluctuated is applied, a certain geometrical shape will be formed by itself and the abrasive particle dispersion will be greatly improved due to the even distribution of the magnetic clusters.

Therefore, in order to dig out the potentiality of MCF slurry in surface finishing, it is important to completely understand its behaviors under the rotary magnetic field and its mechanical characteristics when used in surface finishing. In this chapter, the self-shape formation process of the MCF slurry under a rotary magnetic field is first clarified, followed by the investigation on how the magnetic field affects the time required for forming the MCF slurry to its final shape and the size of the final shape. Then, the mechanical characteristics of the MCF slurry when used in surface finishing are investigated by measuring the normal and shear forces generated in surface finishing operation.

3.2 Behaviors of MCF slurry under a rotary magnetic field

3.2.1 Generation method of rotary magnetic field

Fig. 3.1 shows the schematic illustration of the generation method of rotary magnetic field and the behavior of MCF slurry under this kind of magnetic field. A disc-shaped permanent magnet is attached on the lower end face of its holder with an eccentricity of r. An MCF slurry carrier made of an aluminum plate is located below the magnet with a gap of δ. Both the magnet holder and the carrier can be rotated around their own axis. When the magnet holder is rotated at a speed of n_m the magnet revolves around the axis of holder, subordinately resulting in the generation of a rotary magnetic field in which the magnetic flux density does not change but the spatial positions and directions of the magnetic lines of force are always fluctuated. Evidently, at $r = 0$ a static magnetic is generated because the magnetic lines of force keep in the same spatial positions and their directions are unchanged.

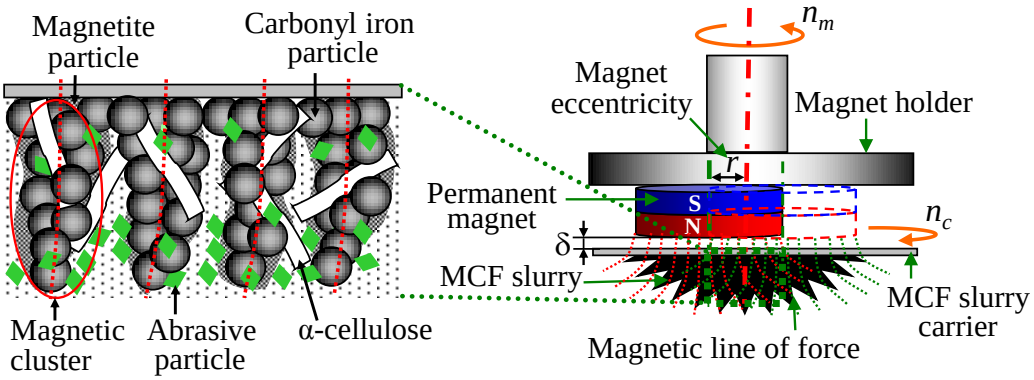

Fig. 3.1 Schematic illustration of rotary magnetic field generation method and MCF slurry behaviour

3.2.2 Self-shape formation process of MCF slurry

As a certain volume of MCF slurry is put onto the inferior surface of the carrier (see the left side of Fig. 3.1), chain-shaped magnetic clusters composed of nm-sized magnetic particles and μm-sized CIPs are formed along the magnetic lines of force immediately. Dimensions of the clusters depend on the compositions of MCF slurry and the strength/applying method of the magnetic field. Within the MCF slurry, non-magnetic abrasives particles are entrapped into the clusters or distributed between clusters, and most of them are encouraged to be close to the top of the clusters due to gravity and magnetic levitation. In addition, α-cellulose fibers have interwoven with the clusters to increase the viscosity of MCF slurry.

It can be imaged that when a rotary magnetic field is applied, the geometrical shapes and locations of the magnetic clusters will vary always due to the magnetic attraction force. This results in the variation of the external shape and dimensions of the MCF slurry. In order to experimentally clarify the variation process, an actual rotary magnetic field generation setup was constructed in-house as shown in Fig. 3.2, which is composed of a magnet holder and an MCF slurry carrier, and mounted onto the spindle head of a vertical milling cutter. Magnet holder is rotated by the spindle to give the magnet a revolution motion and MCF slurry carrier is driven to rotate by using a motor and a set of belt/pulleys. In this setup, the installed magnet was a commercially

available disc-shaped neodymium permanent magnet with dimensions of 18 mm in diameter and 10 mm in thickness and its magnetic field strength is 0.4 T. The compositions and blend ratios of the used MCF slurry are as shown in Table 3.1.

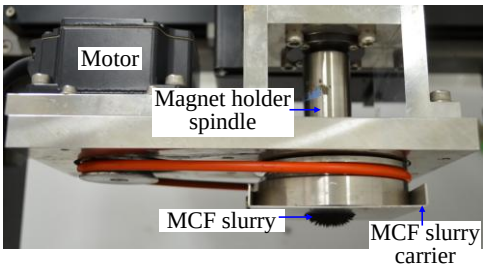

Fig. 3.2 A photograph of the main portion of experimental setup

Table 3.1 Compositions of the MCF slurry used (wt. %)

Water based MF	HQ CIP (~ϕ 2μm)	Al_2O_3 abrasives (~1μm)	α-cellulose
27	58	12	3

The variation process of the external shape of MCF slurry was investigated by observing its side-view with a high-speed motion analysis microscope as shown in Fig. 3.3 and MCF slurry carrier was not rotated. Using this setup, a typical variation process under r = 4.5 mm is obtained as shown in Fig. 3.4. At beginning at time of t = 0, 1 mL of the MCF slurry is put onto the inferior surface of the carrier without the rotation motion of the magnet holder. After the whole MCF slurry supplied is attracted onto the inferior surface of the carrier (see Fig. 3.4(a)) by the magnetic force from the magnet, the holder starts to rotate around its own axis at n_m = 1000 rpm, resulting in the generation of a rotary magnetic field. Under the application of this magnetic field, the external shape of the MCF slurry changes with working time as shown in Fig. 3.4(b–g). It can be observed that for the first one second the external shape does not change significantly and is not clean-cut, but soon later the shape gradually become

clean-cut, eventually to a terminal shape like a mountain at t = 3 s. Hereafter, this process is called self-shape formation process, and the time required for reaching the terminal shape is expressed with T.

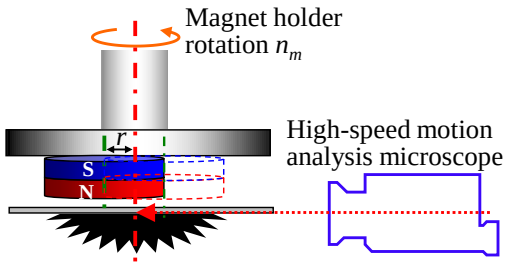

Fig. 3.3 Observation method using high-speed motion analysis microscope

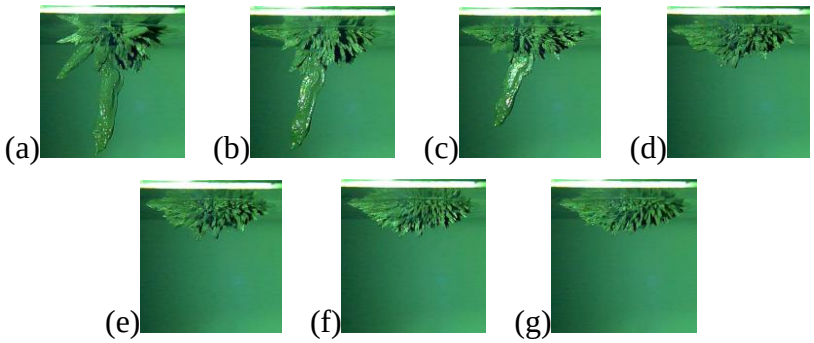

Fig. 3.4 A typical slurry shape formation process observed at: (a) t = 0 s, (b) t = 0.5 s, (c) t = 1 s, (d) t = 1.5 s, (e) t = 2 s, (f) t = 2.5 s and (g) t = 3 s

Fig. 3.5 shows photos of a top-view and a side-view of the MCF slurry terminal shape (at a moment) which is dried for one day naturally. Obviously, the MCF slurry is terminally formed like a mountain with circular base of W in diameter and maximum height of H_{max} at the mountaintop. However, it was also observed that the location of the mountaintop is not at the central point of the circular base and constantly varies with the revolution of the magnet. As shown in Fig. 3.5(b), values of the maximum height h_{max} at positions along the slurry diameter direction were also measured by the microscope at intervals of 0.5 mm (0.4394 mm actually) and their actual values (as shown in Fig. 3.6) were calculated proportionally according to the W and H_{max} exactly

measured before. Fig. 3.6 also shows an approximate curve of h_{max}, which is considered to be the cross section profile of the formed slurry.

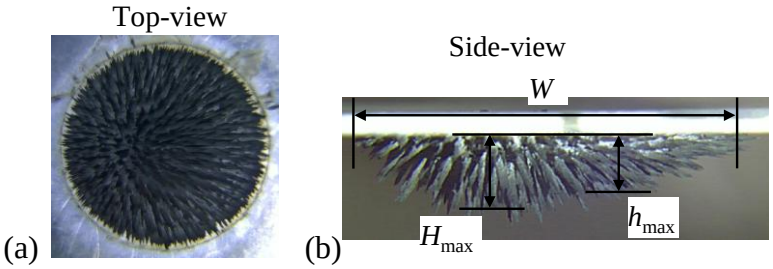

Fig. 3.5 Photos of a (a) facial- and a (b) side-view of the MCF slurry terminal shape (at a moment)

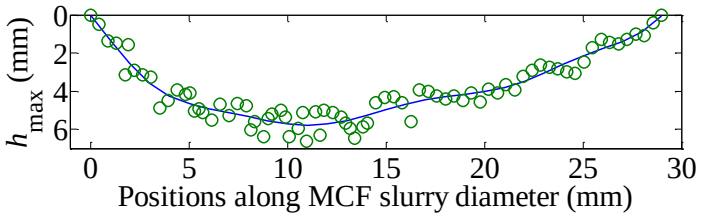

Fig. 3.6 Cross section profile of the formed slurry: curve of the h_{max} in Fig. 3.5(b)

Fig. 3.7 exhibits the variations of the terminal cross section profile and the mountaintop location for t = 68 ms during which the magnet has rotated for 408 °. It is shown that at each moment (Fig. 3.7(a–r) the cross section profile is just like the cross section of a mountain and the mountaintop location moves left and right towards. It is especially interesting to notice that comparing Fig. 3.7(p–r) with Fig. 3.7(a–c) indicates that the cross section profile and the mountaintop location are returned to those at t = 0 ms (0 °) after the magnet has revolved for 360 °(60ms). This means that the external shape and dimensions of the MCF slurry are repeated periodically with the revolution of the magnet at a frequency equal to the magnet revolution speed.

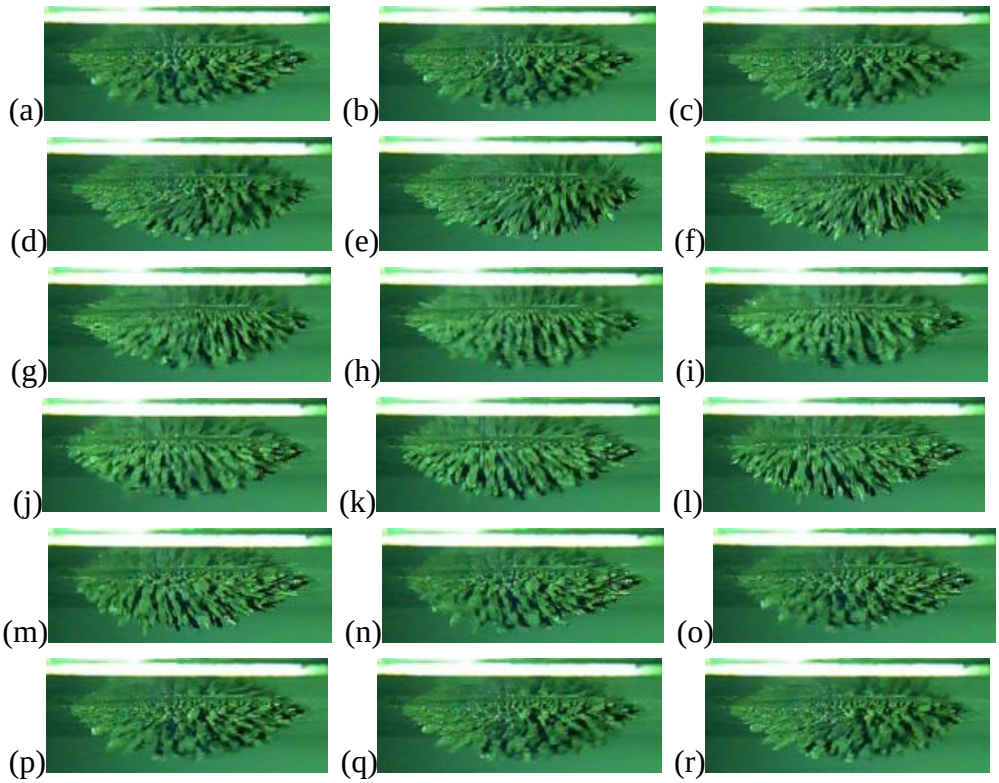

Fig. 3.7 Variations of the terminal cross section profile and the mountaintop location (frame rate = 250 fps) at: (a) 0 ms (0 °), (b) 4 ms (24 °), (c) 8 ms (48 °), (d) 12 ms (72 °), (e) 16 ms (96 °), (f) 20 ms (120 °) (g) 24 ms (144 °), (h) 28 ms (168 °), (i) 32 ms (192 °), (j) 36 ms (216 °), (k) 40 ms (240 °), (l) 44 ms (264 °), (m) 48 ms (288 °), (n) 52 ms (312 °), (o) 56 ms (336 °), (p) 60 ms (360 °), (q) 64 ms (384 °) and (r) 68 ms (408 °)

3.2.3 Effects of process parameters on shape formation

In order to further understand the MCF slurry behavior, effects of process parameters on the terminal shape formation T and its dimensions, i.e. W and H_{max}, have been investigated. The selected variable process parameters are magnet eccentricity r, magnet revolution speed n_m and supplied MCF slurry volume v (see Table 3.2). The terminal slurry shape formation process under each experimental condition was observed using the setup shown in Fig. 3.3. W and H_{max} (as shown in Fig. 3.5) of the terminal slurry shape were measured exactly.

Table 3.2 Process parameters for shape formation investigation

Magnet eccentricity r (mm)	0, 1.5, 3, 4.5, 6, 9, 10
Magnet revolution speed n_m (rpm)	500, 1000, 1500, 2000
Supplied MCF slurry volume v (mL)	1, 1.5, 2

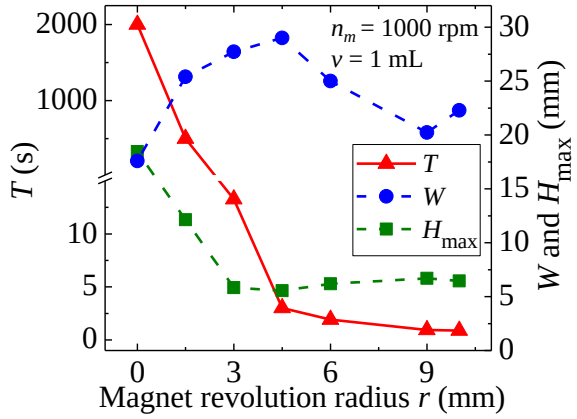

Fig. 3.8 Effect of the r on the T, W and H_{max} (n_m = 1000 rpm and v = 1 mL)

Fig. 3.8 shows the obtained variation of T, W, H_{max} with the increase in the r. It is evident that when the magnet eccentricity r is less than 4.5 mm the slurry shape formation time T decreases rapidly with the increase in the r while the decrease rate gets low significantly once the r is over 4.5 mm. This indicates that a longer time is required to bring the initial shape of MCF slurry to its terminal one when the used r is smaller. In addition, it can be foreseen that the terminal shape of MCF slurry is difficult to become clean-cut because the rotary action of the applied magnetic field is weaker with smaller r. This phenomenon was experimentally confirmed as shown in Fig. 3.9. Obviously, when the r is set at a quite small value close to 0 (see Fig. 3.9(a)), not only an extremely long time of T > 2000 s is required for the formation of the terminal shape but also little change can be observed on the external shape compared the terminal shape with its initial one. It should be further noted from Fig. 3.8 and Fig. 3.9 that at r = 4.5 mm, the terminal shape can be formed in a reasonable time of T = 3 s and a most clean-cut shape like a mountain can be achieved. As for the values of W

and H_{max}, it can be seen that they reach their peak and valley, respectively, at the same value of r = 4.5 mm. Therefore, the value of r is kept constant at r = 4.5 mm for the rest work of this chapter. Because the distance between the spatial positions of MCF slurry and the magnet increases with r increasing, the strength of the stiffed slurry is weakened when larger r is used. Hence, the eccentricity r of 4.5-6 mm (1/4 - 1/3 of the diameter of the used magnet) is recommended to make MCF slurry reach its terminal shape quickly also with certain strength.

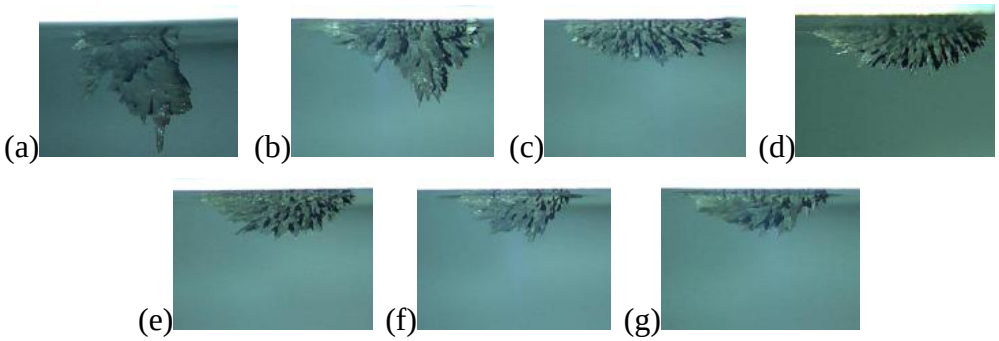

Fig. 3.9 Terminal external shapes of MCF slurry for different values of r: (a) 0 mm, (b) 1.5 mm, (c) 3 mm, (d) 4.5 mm, (e) 6 mm, (f) 9 mm and (g) 10 mm

Next, the effect of the magnet revolution speed n_m on T, W and H_{max} were obtained as shown in Fig. 3.10. As the magnet revolution speed n_m increases, the variation of magnetic lines of force direction is accelerated so that MCF slurry seems being stirred with increasing speed. Hence, it is noticed that the time T decreases linearly with the magnet revolution speed n_m increasing. However, the dimensions of the terminal MCF slurry shape, i.e. the W and the H_{max}, are kept constant practically with respect to n_m because the density and distribution of the used magnetic field are not changed. These indicate that when the time T needs to be shortened but the dimensions of terminal shape should be kept constant a larger value should be given to the magnet revolution speed n_m.

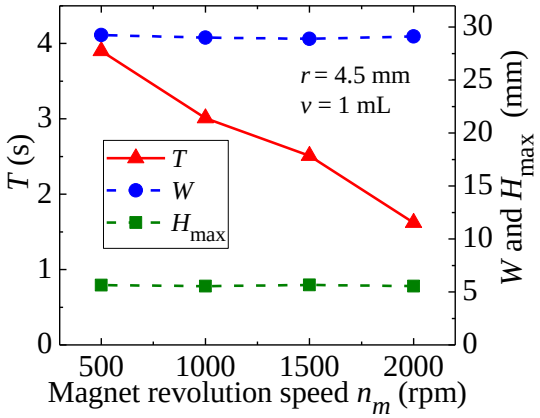

Fig. 3.10 Effect of the n_m on T, W and H_{max} (r = 4.5 mm and v = 1 mL)

Finally, it was investigated that how the supplied MCF slurry volume v affects the T, W and H_{max}. When the supplied MCF slurry volume v increases, the amount of the chain structure clusters increases. But the used magnetic field flux density and its distribution keep constant. Consequently, it becomes difficult to make a larger amount of supplied slurry become clear-cut. Therefore, it is seen from Fig. 3.11, both the T and the H_{max} increase with the increase in the v but no change can be observed on the W.

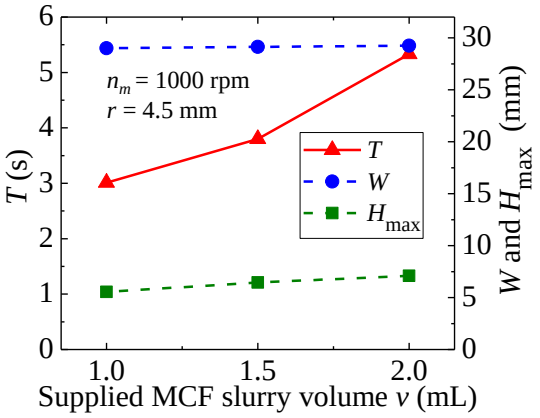

Fig. 3.11 Effect of the v on T, W and H_{max} (n_m = 1000 rpm and r = 4.5 mm)

3.3 Mechanical characteristics: the normal and shear forces

3.3.1 Experimental investigation method

Although a few researchers [6-8] have investigated polishing forces in magnetorheological finishing (MRF) process in which a wheel-shaped polishing tool is

employed. The polishing forces in MCF surface finishing process are still unclear. This section is contributed to investigate the mechanical characteristics of MCF slurry under the rotary magnetic field, i.e. the normal and shear forces.

Fig. 3.12 shows polishing process and forces measurement with MCF slurry under the application of a rotary magnetic field. As shown in the left side of Fig. 3.12, two workpieces are used. When the carrier is also rotated at a speed of n_c and MCF slurry is in contact with the workpiece under a certain working gap of Δ, a relative motion between MCF slurry and work-surface is generated and work-surface experiences normal polishing force due to compression and shear polishing force due to the relative motion. Eventually work-materials are removed by the micro-cutting action of abrasive particles carried by clusters within MCF slurry. According to Preston principle [9], it is known that in polishing process the material removal rate is affected significantly by the polishing force, indicating that quantitatively understanding the polishing force is essential to clarify the mechanical characteristics of polishing process using MCF slurry. Therefore, in order to know the effects of process parameters, i.e. n_c, Δ, n_m, on the polishing forces, a 3-component dynamometer is installed below the workpiece2 for measuring the normal force F_n in z-axis and the shear force F_{ty} in y-axis acting on the workpiece2 for different values of the parameters. If the relative position of the MCF slurry with the terminal shape to the workpieces is set up so that the contact line of the two workpieces passes through the centre of the MCF slurry, the value of F_n would be the half of the total normal force and that of the F_{ty} would be the half of the component in y-axis of the total shear force.

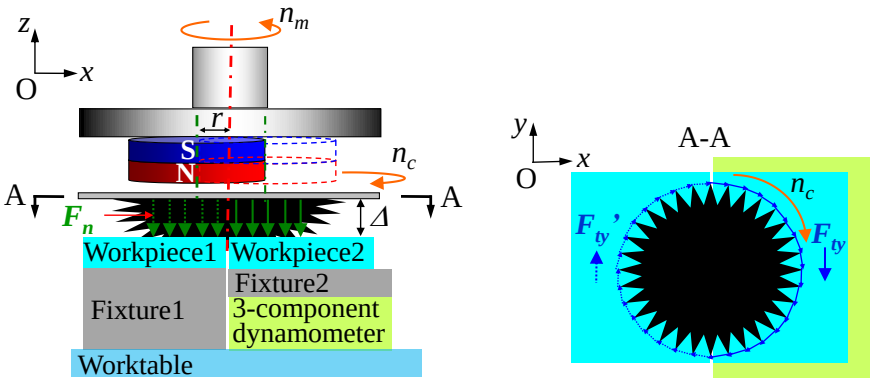

Fig. 3.12 Polishing process and forces measurement

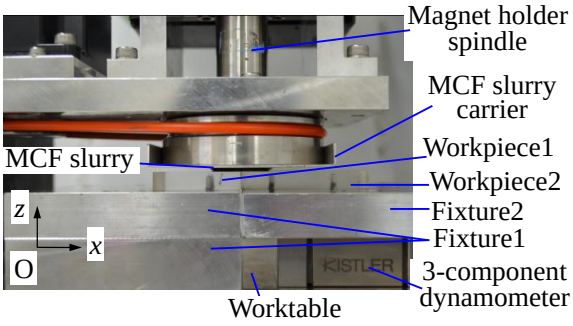

Fig. 3.13 A photo of experimental setup established in-house

Fig. 3.13 shows a photo of experimental setup established in-house and spot experiments have been carried out. The workpiece1 is held on the work-table through a fixture only whereas the workpiece2 is through not only a fixture but also a dynamometer (9256A1 by Kistler Co., Ltd.) The height of the left fixture is equal to the height of the right fixture plus that of the dynamometer. The working gap of Δ is determined by adjusting the vertical position of the MCF slurry carrier, and the relative position of the MCF slurry carrier to the workpiece is set up by adjusting the work-table position in *x*-axis and *y*-axis. The workpiece material is polymethyl methacrylate (PMMA, L60 mm × W40 mm × t9 mm). The process parameters considered in forces measurement are tabulated in Table 3.3.

Table 3.3 Process parameters for force measurement

MCF slurry carrier rotational speed n_c (rpm)	300, 450, 600, 750, 900
Magnet revolution speed n_m (rpm)	500, 750, 1000, 1250, 1500
Working gap Δ (mm)	0-5

3.3.2 Variations of forces with working time

After both the magnet holder and the MCF slurry carrier were rotated, the MCF slurry with repeated terminal shape started to get close to the workpiece. Measurement of forces was started before the slurry came in contact with the work surface and continued for 90 s. As shown in Fig. 3.14, when the MCF slurry interacted with the workpiece, the values of forces (F_n and F_{ty}) increased gradually with the working gap of Δ decreasing first and kept stabilized as the Δ was kept to be the set value 1 mm later. Although initially a certain value of the force in x-axis F_{tx} was also observed, hereafter it decreased to 0 with working time increasing. The F_{tx} is generated when the slurry tried to pass through the small gap between the two workpieces. When the working gap of Δ is not less than 1 mm, stable values of forces (as shown in Fig. 3.14) have been achieved. However, under a small working gap of Δ (i.e. Δ = 0.75 mm), initially a higher value of forces was observed and later decreased due to the messing of MCF slurry.

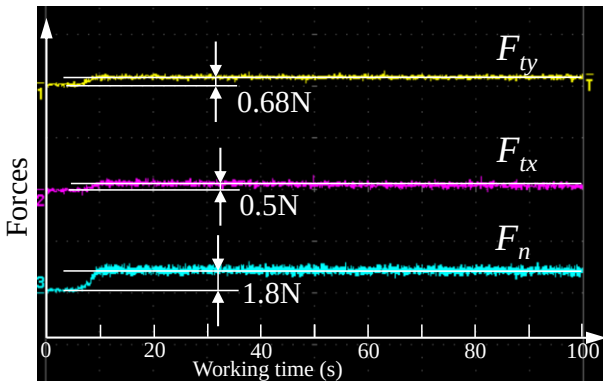

Fig. 3.14 Variations of normal and shear forces with working time (Δ = 1 mm, n_m = 1000 rpm, n_c = 600 rpm)

3.3.3 Effect of parameters on forces

Due to relative high magnetic flux density, MCF slurry sticks onto the inferior surface of the carrier. It is assumed that MCF slurry moves with the same speed as the carrier. Hence, as MCF slurry carrier rotational speed n_c increases, the relative motion speed of magnetic clusters and abrasive particles also increases. Hence, the amount of abrasive particles interacting with the work surface increases and forces generated by abrasives on the work surface also increase. It is observed in Fig. 3.15 that both forces increase slightly with carrier rotational speed n_c increasing.

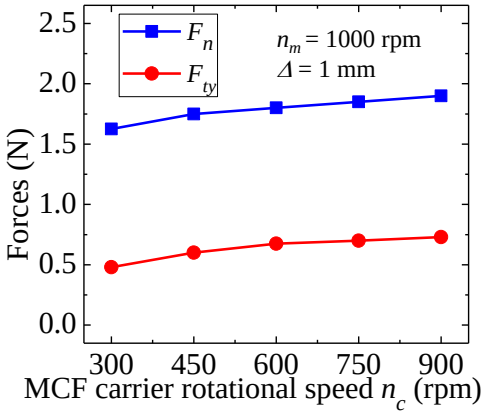

Fig. 3.15 Effect of the n_c on the F_n and F_{ty} (n_m = 1000 rpm, Δ = 1 mm)

As shown in Fig. 3.16, both forces increase slightly with magnet revolution speed n_m increasing from 500 rpm to 1000 rpm. After that, they change little. When magnet revolution speed n_m increases, the motion speed of clusters also increase a little. Hence, forces acting on the work surface also increase. When magnet revolution speed n_m increases over a certain value (say 1000 rpm), MCF slurry has been in a stable state and forces acting shows little change with respect to the further increase of magnet revolution speed n_m.

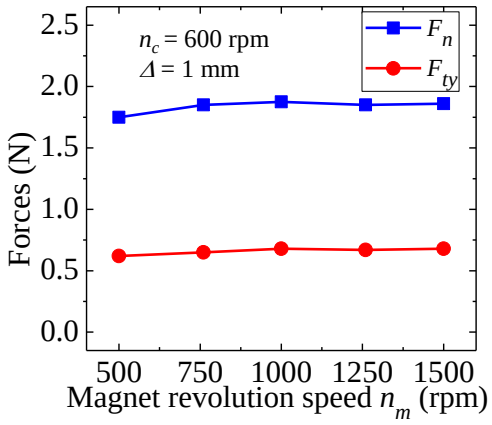

Fig. 3.16 Effect of the n_m on the F_n and F_{ty} (n_c = 600 rpm, Δ = 1mm)

From Fig. 3.17, both forces decrease significantly with the increase of working gap of Δ. As the working gap decreases, the work surface is close to the magnet and strong MCF clusters interacts with the work-surface because the closer to the magnet the higher magnetic flux density is. The supplied MCF slurry volume v is constant. Hence, the same amount of MCF slurry tries to move in the reduced working gap. Consequently, the forces acting generated by the interaction between the carrier, abrasive particles and work-surface is increased. When working gap is larger than a certain value (say 3 mm), only the end of clusters with a little strength is in contact with work surface and CIPs chains also do not have enough strength to drive abrasive particles to move, resulting in little forces acting.

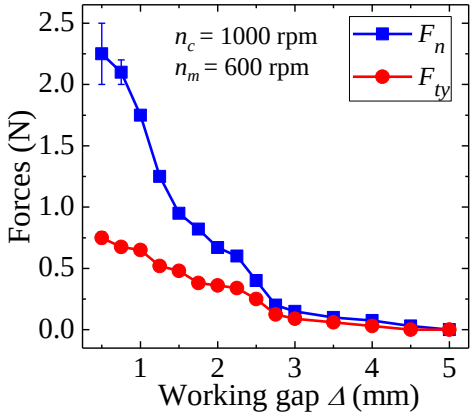

Fig. 3.17 Effect of the Δ on the F_n and F_{ty} (n_m = 1000 rpm, n_c = 600 rpm)

3.4 Mechanical characteristics: surface roughness

Fig. 3.18 presents the effect of the applying way of the magnetic field on the obtained surface roughness. Obviously, concentrically arranged tool marks were observed on the surface obtained under a static magnetic field whereas extremely smooth surface and a better surface roughness were obtained under a rotary magnetic field.

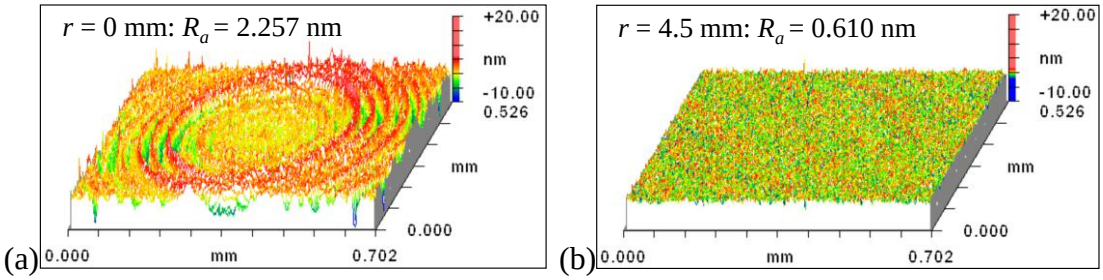

Fig. 3.18 Effect of the applying way of the magnetic field on the obtained surface roughness: (a) Under a static magnetic field and (b) Under a rotary magnetic field

In order to elucidate how the surface was smoothed under different applying ways of the magnetic field, the gemoetry and internal structure of MCF slurry during polishing was observed. Fig. 3.19 displays facial views of an instantaneous shape of the MCF slurry obtained during polishing. It is inferred from this figure that MCF slurry was distributed in a concentrically arranged shape which was centred at that of the magnet. The magnetic clusters within the slurry were driven to rotate together with not only the rotation of the slurry carrier but also the rotating magnetic lines of force under a rotary magnetic field. This leads to that the abrasives within the slurry exert micro-cutting actions in random directions rather than along constant concentric circles. Since a rotary magnetic field greatly help enhance the shape restoring ability of the slurry, the slurry was much more uniformly distributed and magnetic spikes of smaller size were formed within the slurry than under a static magnetic field.

Uniformity in the distribution of the abrasive particles within the slurry in the polishing zone is important for achieving an even material removal. Therefore, the distributions of the Al_2O_3 abrasive particles at various positions were investigated by

chemical element analysis using energy dispersive spectroscopy (EDS, Genesis EDAX). Fig. 3.20 and Fig. 3.21 show the SEM images and the aluminum element distributions, respectively, under a static magnetic field and a rotary one, at positons a–g as shown in Fig. 3.19. Obviously, the abrasives within the slurry were much more uniformly distributed under a rotary magnetic field than under a static one. Although the abrasives at the edge part of the slurry (namely positions a and g) were hardly uniformly distributed, they almost exert no mico-cutting actions since the magnetic lines of force at this positon are parallel to the polishing zone.

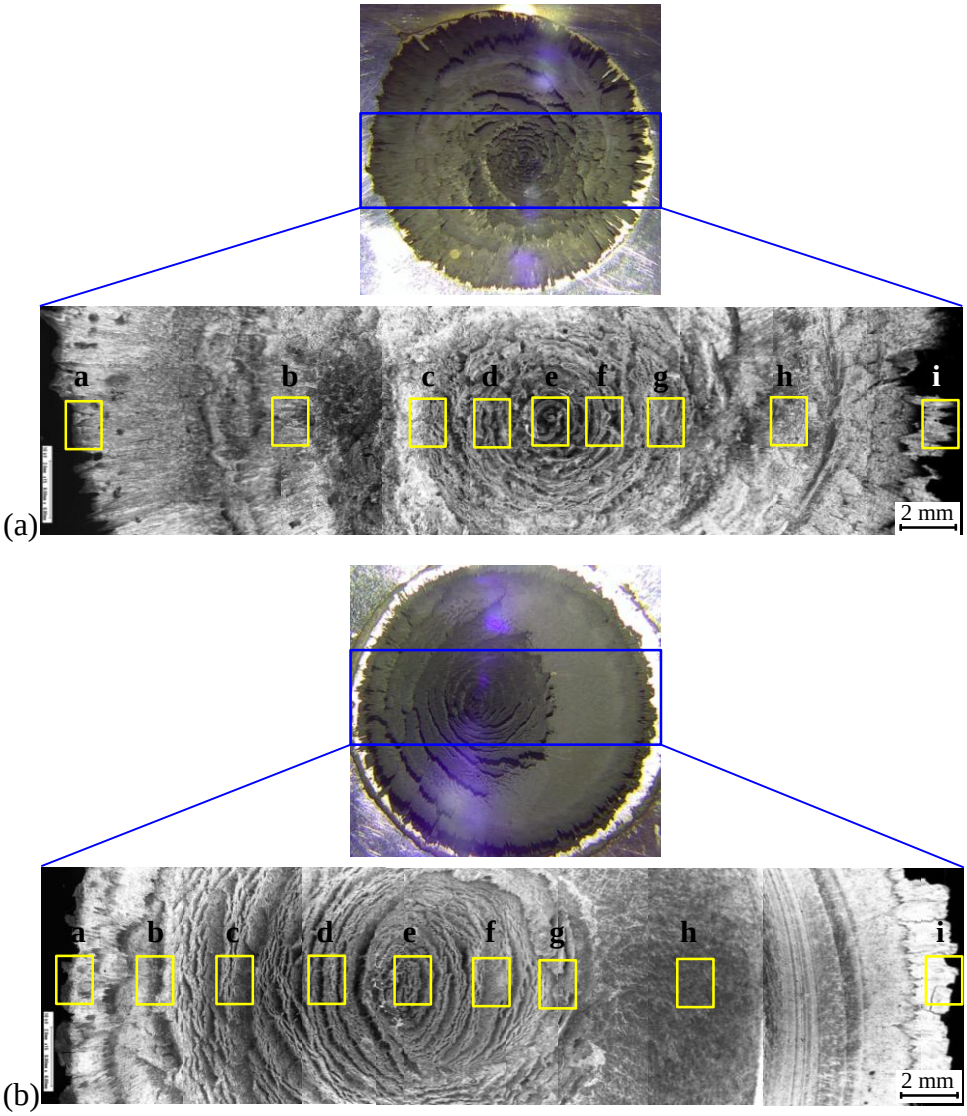

Fig. 3.19 Facial view of MCF slurry: (a) Under a static magnetic field and (b) Under a rotary magnetic field

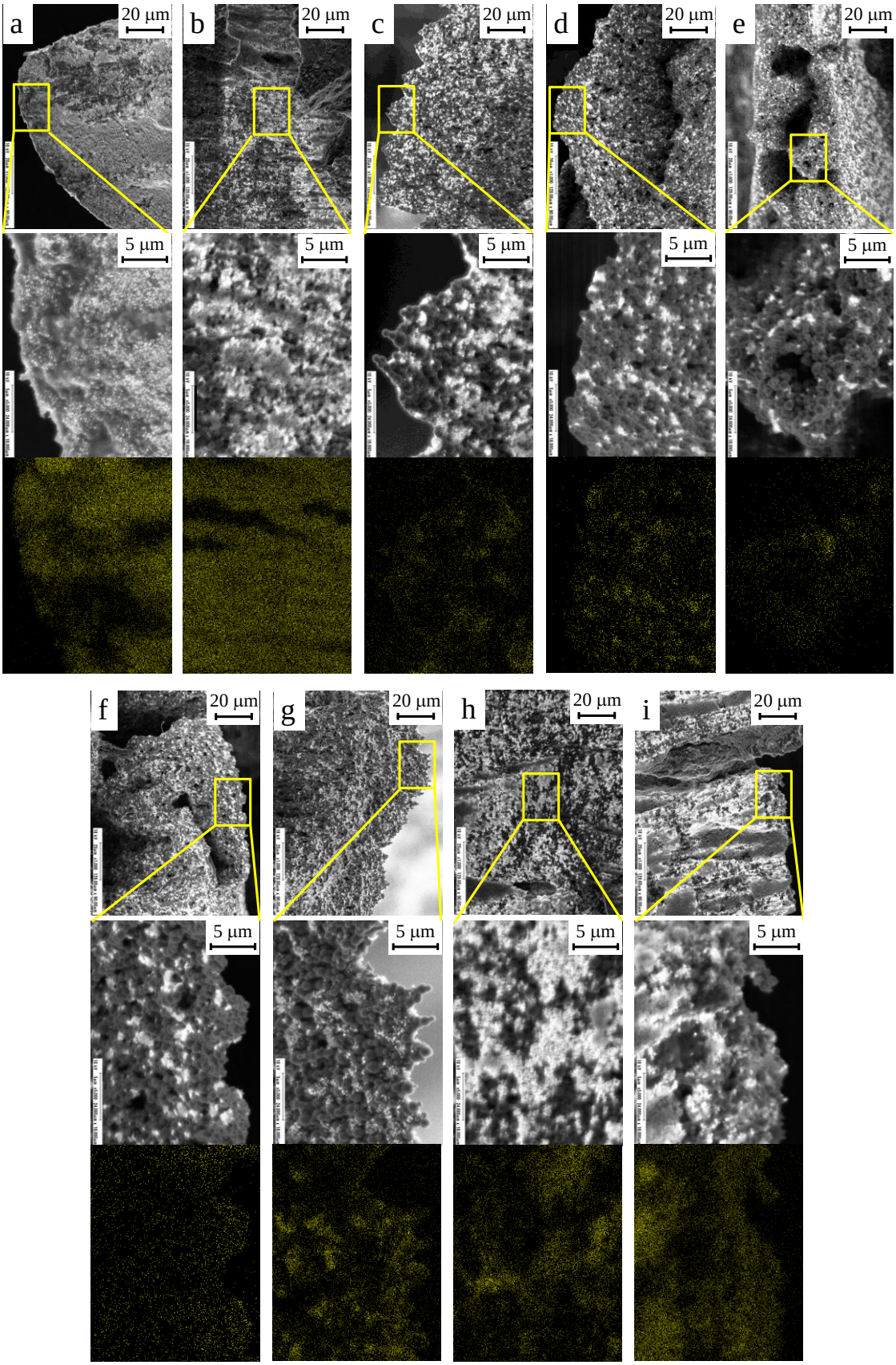

Fig. 3.20 Facial-view of internal structure of MCF slurry under a static magnetic field

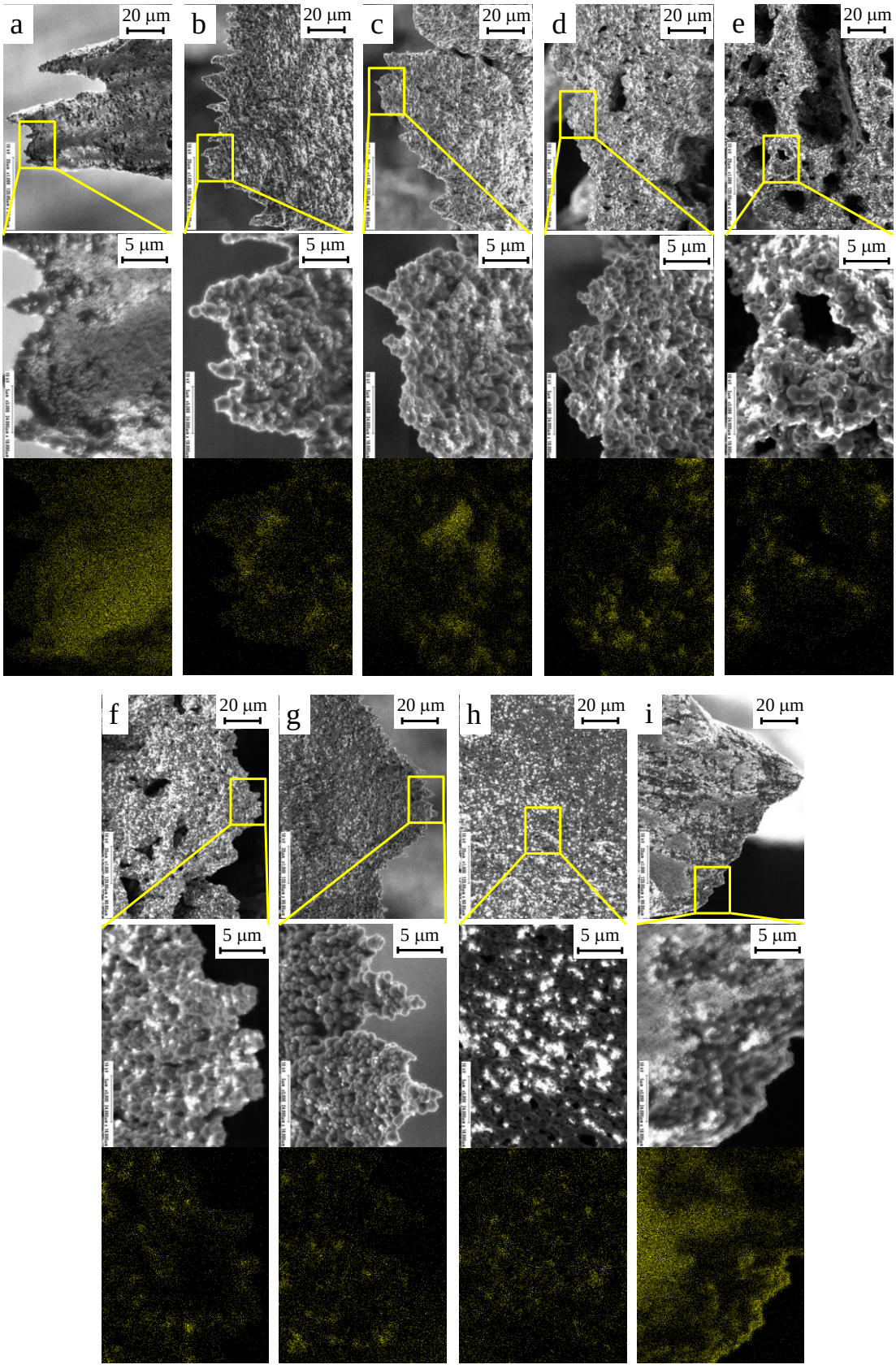

Fig. 3.21 Facial-view of internal structure of MCF slurry under a rotary magnetic field

3.5 Summary

Under a rotary magnetic field, experimental investigations are carried out to discuss the self-shape formation process of MCF slurry, and the influences of process parameters (magnet eccentricity r, revolution speed n_m and supplied MCF slurry volume v) on the terminal shape formation time T and dimensions (diameter W and the maximum height $H_{\max}$) of the terminal slurry shape. Moreover, under the rotary magnetic field, mechanical characteristics of MCF slurry: the normal and shear forces, are measured and effects of MCF slurry carrier rotational speed n_c, magnet revolution speed n_m and working gap Δ on forces are investigated. Main conclusions are summarized as follows:

(1) Under a rotary magnetic field, MCF slurry with clear-cut terminal shape is achieved and its terminal shape and dimensions are repeated periodically with the revolution of the magnet at frequency equal to the n_m.

(2) The time T decreases with the increase in the magnet eccentricity r (significantly if $r < 4.5$ mm) and the speed n_m, and increases with the supplied slurry volume v increasing. Both dimensions show significant change with variation in magnet eccentricity r and are kept constant practically with respect to the magnet revolution speed n_m. The $H_{\max}$ increase with the increase in the supplied MCF slurry volume v but no change can be observed on the W. Therefore, the maximal contribution is made by magnet eccentricity on behaviours of MCF slurry, followed by MCF slurry supplied volume, whereas minimal contribution is noted by magnet revolution speed.

(3) Both forces increase slightly with the MCF slurry carrier rotational speed n_c increasing and decrease evidently with the increase in the working gap Δ. Polishing forces increases slightly with the magnet revolution speed n_m increasing from 500 rpm to 1000 rpm and then show little change.

(4) A more uniform distribution of abrasive particles and a better surface finish are obtained under a rotary magnetic field than under a static one.

References

[1] Shimada, K., Fujita, T., Oka, H., Akagami, Y., Kamiyama, S., 2001. Hydrodynamic and magnetized characteristics of MCF (magnetic compound fluid). Trans. Jpn. Soc. Mech. Eng. B 67, 3034–3040 (in Japanese).

[2] Shimada, K., Matsuo, Y., Yamamoto, K., Wu, Y., 2008. A new float-polishing technique with large clearance utilising magnetic compound fluid. Int. J. Abras. Technol. 1, 302−315.

[3] Furuya, T., Wu, Y., Nomura, M., Shimada, K., Yamamoto, K., 2008. Fundamental performance of magnetic compound fluid polishing liquid in contact-free polishing of metal surface. J. Mater. Process. Technol. 201, 536–541.

[4] Sato, T., Wu, Y., Lin, W., Shimada, K., 2009. Study on magnetic compound fluid (MCF) polishing process using fluctuating magnetic field. Jpn. Soc. Mech. Eng. 75, 1007−1012 (in Japanese).

[5] Sato, T., Wu, Y., Lin, W., Shimada, K., 2010. Study of three-dimensional polishing using magnetic compound fluid (MCF). J. Jpn. Soc. Abras. Technol. 54, 425−430 (in Japanese).

[6] Sidpara, A., Jain, V., 2011. Experimental investigations into forces during magnetorheological fluid based finishing process. Int. J. Mach. Tools Manuf. 51, 358–362.

[7] Jung, B., Jang, K., Min, B., Lee, S., Seok, J., 2009. Magnetorheological finishing process for hard materials using sintered iron-CNT compound abrasives. Int. J. Mach. Tools Manuf. 49, 407–418.

[8] Miao, C., Lambropoulos, J., Jacobs, S., 2010. Process parameter effects on material removal in magnetorheological finishing of borosilicate glass. Appl. Opt. 49, 1951–1963.

[9] Miao, C., Shafrir, S., Lambropoulos, J., Mici, J., and Jacobs, S., 2009. Shear stress in magnetorheological finishing for glasses. Appl. Opt. 48, 2585–2594.

Chapter IV
Ultra-fine Polishing of Optical Polymer with Zirconia-coated Carbonyl-iron-particle based MCF slurry

4.1 Introduction

Optical polymers exhibit excellent ability in reducing the absorption of photons in a certain range of energy, such as 7-9 keV [1]. Hence, they are the usual construction materials of the optoelectronic devices. To meet the required performance, the surfaces of these devices must be finished to nano-level roughness. However, as optical polymers are soft, conventional grinding and/or polishing processes usually result in scratches, and the embedding of abrasive particles on the work surface [2]. Hence, it is hardly expected that nano-level surface finish of optical polymers can be achieved with the conventional finishing processes. Therefore, it is necessary to develop novel finishing methods that effectively improve the surface finish of the soft optical polymers.

Magnetic field-assisted polishing using magnetic fluids (MFs) or magnetorheological (MR) fluids is a potential candidate, in which an applied magnetic field controls the behaviour of the abrasive particles. Through fine polishing employing an MF, Tani et al. [3] appreciably improved surface roughness of a flat polypropylene workpiece. MRF successfully attained a surface roughness of 0.5 nm in *rms* for a diamond turned polymethyl methacrylate (PMMA) part [2]. A ball end MRF process was proposed and applied to work surfaces made of EN31 magnetic steel and relatively soft nonmagnetic copper [4]. These surveys demonstrate that the magnetic field-assisted polishing potentially achieves the nano-surface finish of optical polymers. However, a given magnetic field distributes the particles more stably in an MF than in an MR fluid, whereas strengthens magnetic pressure and apparent viscosity of the latter more than that of the former.

MCF is more viscous than an MF and disperses particles more readily than an MR fluid under a static magnetic field. An MCF slurry was proposed by blending abrasive particles and α-cellulose fibres into the MCF [5]. The fundamental characteristics of contact-free MCF polishing in the flat surface finishing of stainless steel and acrylic resin were also experimentally investigated [6,7]. Following the above work, the static field applied to the MCF slurry was replaced with a rotary magnetic field [8] under which the shape restoring ability of MCF slurry was significantly enhanced and the abrasive particles within the MCF slurry were more uniformly distributed during polishing. It is confirmed the polishing performance of the MCF slurry under the rotary magnetic field was much higher than under the static magnetic field [9]. The behaviours of MCF slurry has been clarified that once a rotary magnetic field is applied, the MCF slurry rapidly self-assembles into a clear-cut terminal shape [10], which well favours surface finishing.

However, CIP (carbonyl-iron-particle) used in MCF has low ability against aqueous corrosion when the water is employed as the solvent. A zirconia-coated CIP has been developed via sol-gel synthesis and applied in the MRF in University of Rochester [11]. Its long-time stability against aqueous corrosion has been experimentally confirmed. By spot polishing tests, stable material removal and smooth surfaces in spot were obtained with the ZrO_2-coated CIP based MR fluid. In what follows we describe our work to polish PMMA with the novel kind of ZrO_2-coated CIP based MCF slurry. Polishing performance (normal force and surface roughness) of the new ZrO_2-coated CIP based MCF/MRF slurry is compared with that of the conventional non-coated CIP (i.e., HQ) based MCF slurry. The effect of ZrO_2-coated CIP concentration on normal force during the polishing process and surface roughness is also investigated.

4.2 Experimental details

4.2.1 Experimental apparatus and MCF slurries

Fig. 4.1 shows an experimental apparatus constructed based on the polishing

principle mentioned above. A disc-shaped neodymium permanent magnet (ϕ32 mm × t10 mm, 0.45 T) was set at an eccentricity of r = 8 mm. A polishing unit, which is composed of a magnet holder, a slurry carrier (namely an aluminum plate), two motors and two sets of belt/pulleys, was developed and mounted onto the arm toe of a 6-joint robot. One of the motors is connected to the magnet holder to give the magnet a revolution motion. The other is used to drive the slurry carrier rotationally. The working gap Δ is determined by adjusting the vertical position of the carrier through the control of the robot arm.

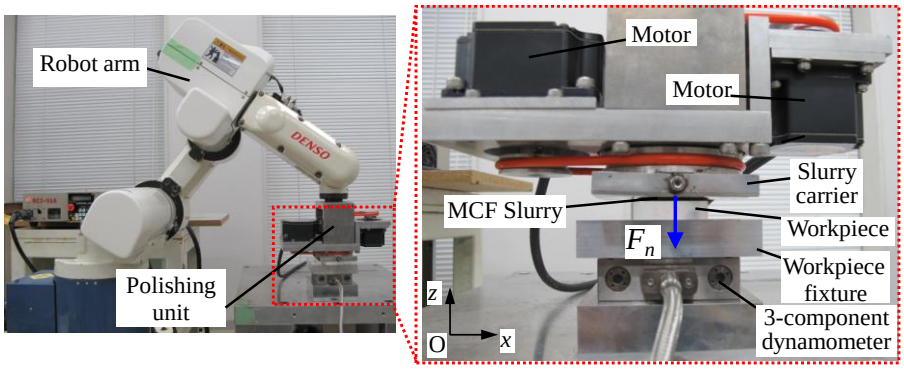

Fig. 4.1 Experimental apparatus

As summarized in Table 4.1, six MCF slurries (MCF1–MCF6) with different compositions and an MR fluid slurry were prepared and used in experiments. MCF1 was a conventional one, which was composed of HQ CIPs, alumina (Al_2O_3) abrasive particles, α-cellulose and water based MF, whilst MCF2 was a ZrO_2-coated CIPs based one prepared by just replacing the HQ CIPs in MCF1 with the ZrO_2-coated CIPs. Considering that there is a ZrO_2 layer over the CIPs' surface and the use of α-cellulose would result in relatively large polishing force and thereby hinder the nano-level surface finish, MCF3 was made up of only ZrO_2-coated CIPs and water based MF, of which the component blend ratio was the same as that of the MR fluid slurry employed in MRF process in Shafrir's work [12] (who developed the ZrO_2-coated CIPs) but the DI water used in the MR fluid was replaced with water based MF. The other MCF slurries, i.e. MCF4 – MCF6, contained the same components as that of MCF3 but with different blend ratios.

In experiments, three different tests were designed for their respective purposes. The first test was conducted using MCF1 and MCF2 for the performance comparison

between the conventional MCF slurry containing non-coated CIPs and the new one containing ZrO_2-coated CIPs. The second test was carried out using MCF3 and MR fluid for the comparison between the new one and the ZrO_2-coated CIPs based MR fluid slurry in order to evaluate the performance of the ZrO_2-coated CIPs based MCF slurry. Finally, the third test was performed using MCF3, MCF4, MCF5 and MCF6 to further study the effect of the concentration of ZrO_2-coated CIPs in order to determine a suitable composition, under which a nano-level surface roughness can be efficiently achieved.

Table 4.1 Compositions of MCF slurries and MR fluid slurry (wt.%)

Slurry	MCF1	MCF2	MR fluid	MCF3	MCF4	MCF5	MCF6
HQ CIPs (~ϕ2 μm)	58						
ZrO_2-coated CIPs (~ϕ1.4 μm)		58	78	78	73	70	68
Water based MF	27	27		22	27	30	32
DI water			22				
Al_2O_3 abrasive particles (~1 μm)	12	12					
α-cellulose	3	3					

Fig. 3 shows the scanning electron microscope (SEM) images of Al_2O_3 abrasive particles (median size ~1 μm), HQ CIPs (median diameter ~2 μm), ZrO_2-coated CIPs (median diameter ~1.4 μm), α-cellulose, and internal micro-structures of MCF1 and MCF6 under the applied magnetic field, respectively. Compared with HQ CIPs (Fig. 4.2(b)), there is a thin and rough ZrO_2 layer over the ZrO_2-coated CIPs' surface (Fig. 4.2(c)). This layer consists of overlapping nanocrystallites of faceted ZrO_2, about 50−100 nm in size [12]. It can be seen from the images of internal micro-structures (Fig. 4.2(e) and (f)) that both ZrO_2-coated CIPs and HQ CIPs are uniformly distributed along the magnetic lines of force to form chain-shaped clusters and non-magnetic abrasive particles within the MCF1 are entrapped into the clusters or distributed between the clusters whilst α-cellulose fibers have interwoven with the clusters to increase the viscosity of the slurry (see left side of Fig. 4.2(e)).

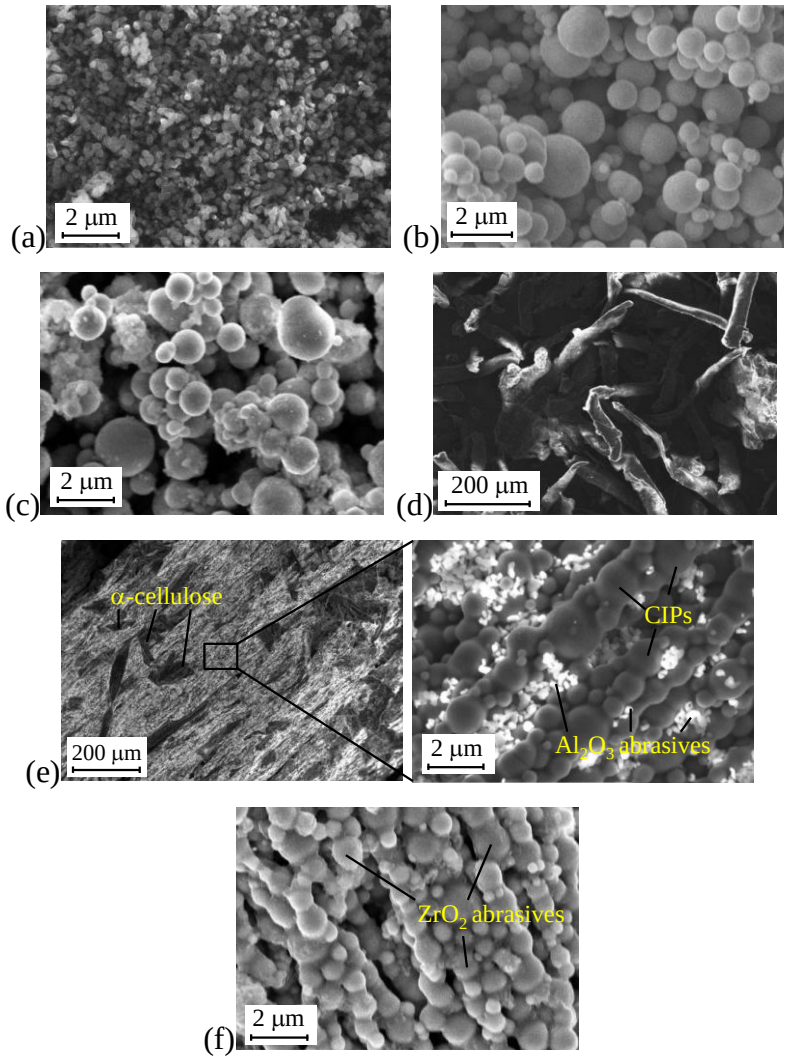

Fig. 4.2 SEM images of (a) Al_2O_3 abrasive particles, (b) HQ CIPs, (c) ZrO_2-coated CIPs, (d) α-cellulose, and internal microstructures of (e) MCF1 and (f) MCF6

4.2.2 Experimental procedures and conditions

The experimental procedures were as follows: (1) the slurry carrier is located at a high enough vertical position through the control of the robot arm, and then the workpiece is fixed on the worktable, followed by putting a certain volume of a slurry (1 mL in this work) onto the carrier; (2) the magnet holder and the carrier are rotated at their respective speeds (n_m = 1000 rpm and n_c = 800 rpm), and then a robot motion program is ran to give the working gap Δ and a reciprocation of the slurry carrier relative to the work surface (in this work the reciprocation was in y-direction with a stroke of 30 mm and a speed of 15 mm/s) to start the polishing operation; (3) the robot program, magnet holder rotation and carrier rotation are orderly stopped after polishing for a certain period (3 min or 6 min), and then the polished workpiece is taken down

from the worktable followed by washing; subsequently, the surface roughness of the workpiece is measured using a white light interferometer (which is equipped with a 10× Mirau objective and provides a 700 μm × 526 μm measurement area) and the average value of the surface roughness measured at five different sites are regarded as that of the polished workpiece; (4) the workpiece is reset on the worktable and the same volume of the slurry is supplied, then procedures (1)-(3) are repeated until the surface roughness is no longer decreased with the polishing time.

In experiments, the situations of the used slurries, which reflect the slurry behaviour during polishing, were observed whenever necessary with a digital camera in the way as shown in Fig. 4.3. In addition, the normal polishing force F_n during polishing can be used to explain the experimental results because the material removal rate (MRR) strongly relate to the F_n according to Preston's equation of $MRR = C_pPV$ [13], where C_p is the coefficient depending on the work material, the abrasive and so on, P is the pressure determined by dividing the F_n by the interacting area between the MCF slurry and the workpiece, and V is the relative speed between the slurry and the workpiece. Therefore, the F_n for all the used slurries under the corresponding working gap were obtained during polishing using a 3-component dynamometer (model-9256A1 by Kistler Co., Ltd.) which was mounted below the fixture of workpiece (see Fig. 4.1).

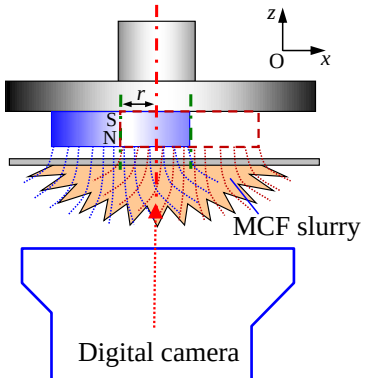

Fig. 4.3 Illustration of the slurry observation method

Table 4.2 shows experimental polishing conditions. Workpieces (L60 mm × W40 mm × t9 mm) were prepared from a commercially available PMMA plate, and their work surfaces were ground with sandpapers of # 800 and # 1500 so that the initial work-surface roughness were $R_a \approx 300$ nm.

Table 4.2 Experimental polishing conditions

Workpiece	PMMA
Magnet	Nd-Fe-B, ϕ32 mm × t10 mm
Magnet eccentricity	r = 8 mm
MCF slurry carrier rotational speed	n_c = 800 rpm
Magnet revolution speed	n_m = 1000 rpm
Amount of MCF slurry supplied	v = 1 mL
Relative speed	V = 15 mm/s

4.3. Results and discussion

4.3.1 Performance comparison of conventional CIPs based MCF slurry and ZrO_2-coated CIPs based MCF slurry

Fig. 4.4 displays the performance comparison of the conventional CIPs based MCF slurry, i.e. MCF1, and the ZrO_2-coated CIPs based MCF slurry, i.e. MCF2. Fig. 4.4(a) shows the variations of the surface roughness R_a during polishing obtained with both slurries at working gap Δ = 1.5 mm. It is seen from this figure the surface roughness decreased dramatically for the first 3 min either with MCF1 or with MCF2 and then the decrease rate became considerably small, eventually reached their respective stable levels. It is also obvious that the surface roughness decrease rate with MCF1 was higher than that with MCF2, and better final surface finish was achieved with MCF1 than with MCF2. Fig. 4.4(b) shows the optical microscopic images and the best work-surface roughnesses after polishing with MCF1 and MCF2 for 18min, respectively. It is seen that the resultant surface roughness of R_a 1.748 nm with MCF1 is much smaller than that of R_a 4.523 nm with MCF2. In order to explain this phenomenon, both the MCF1 and the MCF2 used for 3min at Δ = 1.5 mm were observed in the way shown in Fig. 4.3 and the obtained optical images are exhibited in Fig. 4.4(c). The images of slurries after being used for 3 min revealed that both slurries changed little after being used, which implies that these two slurries have good particle dispersion and shape restoring ability during experiments. Fig. 4.4(d) exhibits the

variations of normal force F_n during polishing. The F_n with MCF2 was much smaller than that with MCF1, accordingly leading to a smaller roughness improvement rate with MCF2 as shown in Fig. 4.4(a).

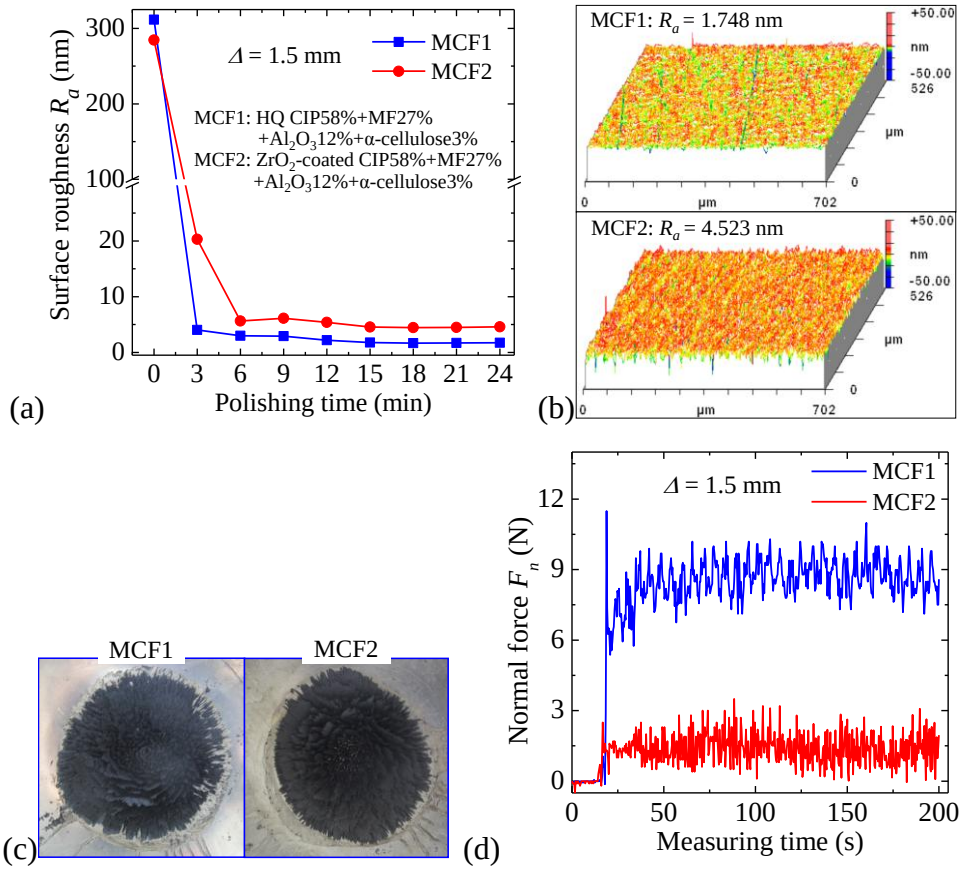

Fig. 4.4 Comparison of conventional HQ CIPs based MCF slurry and ZrO_2-coated CIPs based MCF slurry in terms of (a) the variations of surface roughness R_a obtained at Δ = 1.5 mm, (b) the respective best surface roughnesses after polishing with MCF1 and MCF2 for 18min, (c) the optical images of slurries after polishing for 3 min at Δ = 1.5 mm, and (d) the variations of normal forces during polishing at Δ = 1.5 mm

The reason why MCF1 performed better than MCF2 is considered as follows: because the ZrO_2-coated CIPs and the HQ CIPs were employed at the same weight percentage and the HQ CIPs specific gravity within MCF2 was smaller than that within MCF1, smaller amount of the magnetic clusters were formed within MCF2; the size of the ZrO_2-coated CIPs (1.4 μm) was a little smaller than that of the HQ CIP (2 μm) and thus magnetic clusters formed within MCF2 were slenderer than those within MCF1,

then the ZrO_2-coated CIPs based clusters within MCF2 would grab the relatively large Al_2O_3 abrasives (1 μm) , so it is more difficult to control their behaviours during polishing than to control the behaviours of the HQ CIPs based clusters within the MCF1. Therefore, the use of relative large abrasives (i.e. > 1 μm) in this kind of ZrO_2-coated CIPs based MCF slurry cannot result in better polishing performance. However, the slenderer ZrO_2-coated CIPs based magnetic clusters, which are capable of grapping nano-sized ZrO_2 abrasives, potentially favor the nano-level surface finish. In the next section, polishing with ZrO_2-coated CIPs based MCF slurry was studied in the absence of both Al_2O_3 abrasives and α-cellulose.

4.3.2 Performance comparison of ZrO_2-coated CIPs based MCF slurry and MR fluid slurry

This section described the performance comparison of the ZrO_2-coated CIPs based MCF slurry, i.e. MCF3, and the MR fluid slurry containing the same CIPs at working gap Δ = 1.5 mm (Fig. 4.5) in the absence of both Al_2O_3 abrasives and α-cellulose. As shown in Fig. 4.5(a), the roughness variation trends during polishing with MCF3 and MR fluid were similar with those with MCF1 and MCF2 (Fig. 4.4(a)). However, the required polishing time for surface roughness to reach the stable level with MR fluid was 9 min. It is 2 times longer than that with MCF3, which was 3 min. Fig. 4.5(b) shows the optical images and the best surface roughnesses of the work-surfaces after polishing with MR fluid for 18 min and with MCF3 for 15 min. It reveals that the surface roughness in the stable level obtained with MCF3 (e.g. R_a 1.334 nm) is much smaller than that with MR fluid (e.g. R_a 3.238 nm). These indicate that not only the surface finish improvement rate with MCF3 was higher than that with MR fluid but also the resultant surface finish was better. This suggests that the use of Al_2O_3 abrasives and α-cellulose hinders the further improvement of surface roughness. The probable reason is that they are relatively large and frequently remove the soft work-material with large cutting depths.

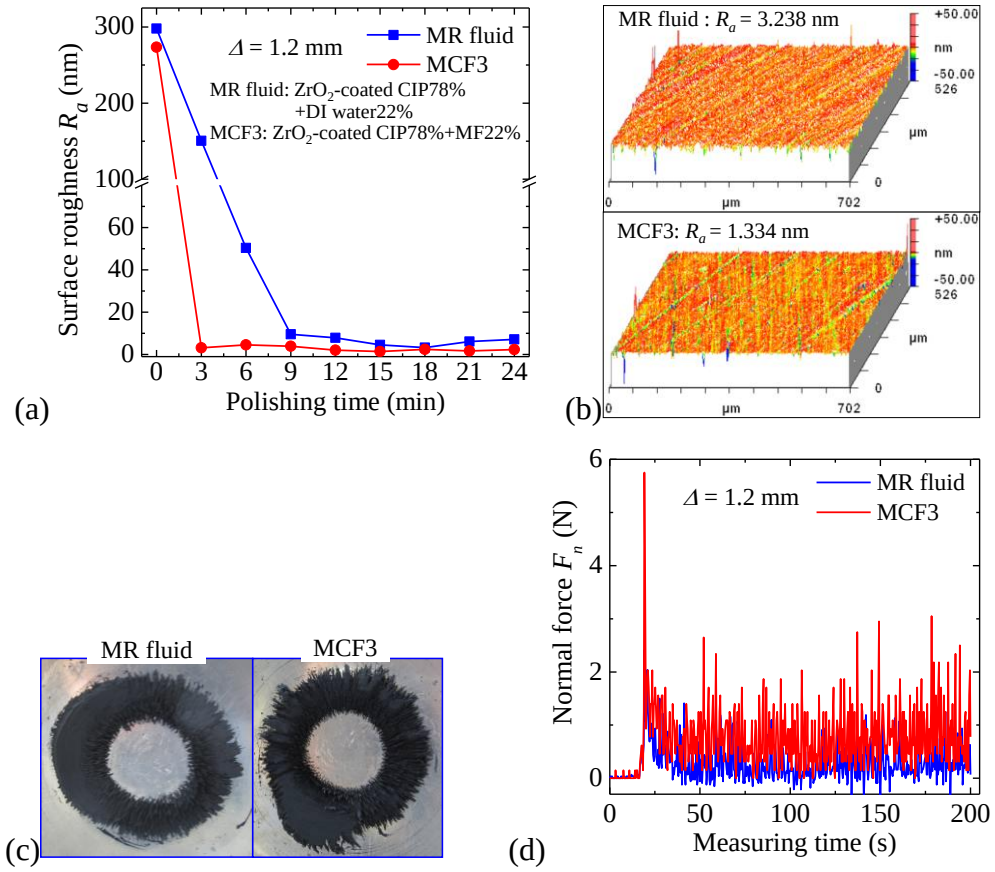

Fig. 4.5 Comparison of the ZrO_2-coated CIPs based MCF slurry and MR fluid slurry in terms of (a) the variations of surface roughness R_a obtained at Δ = 1.2 mm, (b) the respective best surface roughnesses after polishing with MR fluid for 18 min and with MCF3 for 15 min, (c) the optical images after polishing for 3 min at Δ = 1.2 mm, and (d) the variations of normal forces during polishing at Δ = 1.2 mm

The optical images of the slurries after polishing for 3 min at Δ = 1.2 mm (Fig. 4.5(c)) manifest that both slurries were distributed in donut shapes and became a little dried after being used. This implies that the concentration of the ZrO_2-coated CIPs under this composition was relatively high, which leads to that large magnetic force was generated and the magnetic clusters within the MCF slurry moved away from the carrier centre. As observed from Fig. 4.5(c), MR fluid became more dried than MCF3. This indicates that MCF3 has better restoring ability than MR fluid during polishing, which helps enhance the surface finish. Fig. 4.5(d) displays the variations of normal force F_n during polishing. Regardless of the slurry, the F_n increased rapidly at beginning to a peak, and then decreased quickly, eventually its average value reached a stable value but varied in a certain range because the slurries were easily dried. It is

also evident that MCF3 exerted higher normal force than MR fluid, thereby resulting in a higher roughness improvement rate as shown in Fig. 4.5(a). Better polishing performances of MCF3 than MR fluid are considered to be the benefits of the use of MF containing magnetite particles, which help disperse the abrasive particles uniformly, and enhance the toughness and flexibility of the magnetic clusters within the MCF slurry during polishing. It is in particular worth noting that the resultant work-surface finish in the stable level with MCF3 without Al_2O_3 abrasives and α-cellulose (see Fig.6(a) and (b)) was better than that with MCF1 containing Al_2O_3 abrasives and α-cellulose (see Fig.6(a) and (b)).

4.3.3 Effect of the concentration of ZrO_2-coated CIPs

As revealed in the above section, the ZrO_2-coated CIPs based MCF slurry without Al_2O_3 abrasives and α-cellulose, e.g. MCF3, performed better not only than that with Al_2O_3 abrasives and α-cellulose, e.g. MCF2, but also than MR fluid slurry, even than the conventional HQ CIPs based MCF slurry, e.g. MCF1. However, it has been yet unclear what is the optimum ZrO_2-coated CIPs concentration for this kind of MCF slurry in terms of its polishing performance. Therefore, in this section, the effect of the concentration of ZrO_2-coated CIPs on the work-surface roughness was investigated using MCF slurries, namely MCF3 – MCF6, with different concentrations of ZrO_2-coated CIPs.

Fig. 4.6(a) shows the obtained variations of surface roughness R_a during polishing with various slurries. It is evident that the highest surface finish improvement rate was achieved with MCF3 whereas the smoothest work-surface with the final surface roughness of around R_a 1 nm and few visible polishing scratches seems to be eventually attained with MCF5 or MCF6 (Fig. 4.6(b)). These phenomena can be understood from the slurry distributions and the normal polishing force variations as shown in Fig. 7(c) and (d), respectively. When the CIP concentration was relatively high at 78 wt.%, the major part of magnetic clusters within the MCF slurry likely moved away from the carrier centre and hence possessed larger relative speed to the work surface, and additionally more abrasives interacted with the work-surface,

thereby leading to a higher surface finish improvement rate. However, it was observed that the slurries with relatively high CIP concentration, such as MCF3 and MCF4, easily became dried and changed from liquid state to solid state, and hence their shape restoring abilities became too weak to keep their performances, which disfavors the nano-precision polishing. Among them, as MCF4 was easily dried and showed very low polishing efficiency, polishing operation with it was only carried out for 12 min and then continued with MCF5 for another 36 min. The surface finish with MCF5 was rapidly improved. MCF6 showed the similar performance with MCF5. Therefore, both MCF5 and MCF6 were considered to be suitable for nano-precision polishing of PMMA.

Fig. 4.6(d) exhibits the variations of normal force F_n during polishing with MCF3 – MCF6 at Δ = 1.0 mm. F_n increased as the ZrO_2-coated CIPs concentration increased from 68 wt.% (i.e. MCF6) to 70 wt.% (i.e. MCF5) because more magnetic clusters are formed within the slurry and more ZrO_2 abrasives interact with the work-surface at a higher CIP concentration, leading to a higher surface finish improvement rate as exhibited in Fig. 4.6(a). Although F_n also increased as the concentration increased from 73 wt.% (i.e. MCF4) to 78 wt.% (i.e. MCF3), F_n value firstly increased significantly to a relatively large value, and then decreased significantly to a value even smaller than that with MCF6 because the slurries were easily dried when the concentration is larger than 70 wt.%. It is inferred from Fig. 4.6(c) that MCF5 and MCF6 have better particle dispersion and restoring abilities than MCF3 and MCF4 during polishing. Therefore, they exerted more stable normal forces and thereby stable micro-cutting action during polishing (Fig. 4.6(d)), leading to the stable improvement of surface finish at a considerable rate. It is believed that the relatively high concentrations of MF used in MCF5 and MCF6 greatly helped enhance the particle dispersion and restoring abilities during polishing. Moreover, it is observed from Fig. 4.6(c) that the slurry is prone to a donut shaped distribution with the increase in the ZrO_2-coated CIPs concentration because the larger the ZrO_2-coated CIPs concentration is, the larger the magnetic force becomes.

Consequently, a surface roughness less than R_a 1nm can be achieved under a proper ZrO_2-coated CIPs concentration (i.e. 70 wt.%) and the concentration should be less than a certain value (in the current work, 70 wt.%), otherwise MCF slurry shows

bad particle dispersion ability and is easily dried, resulting in the loss of polishing ability.

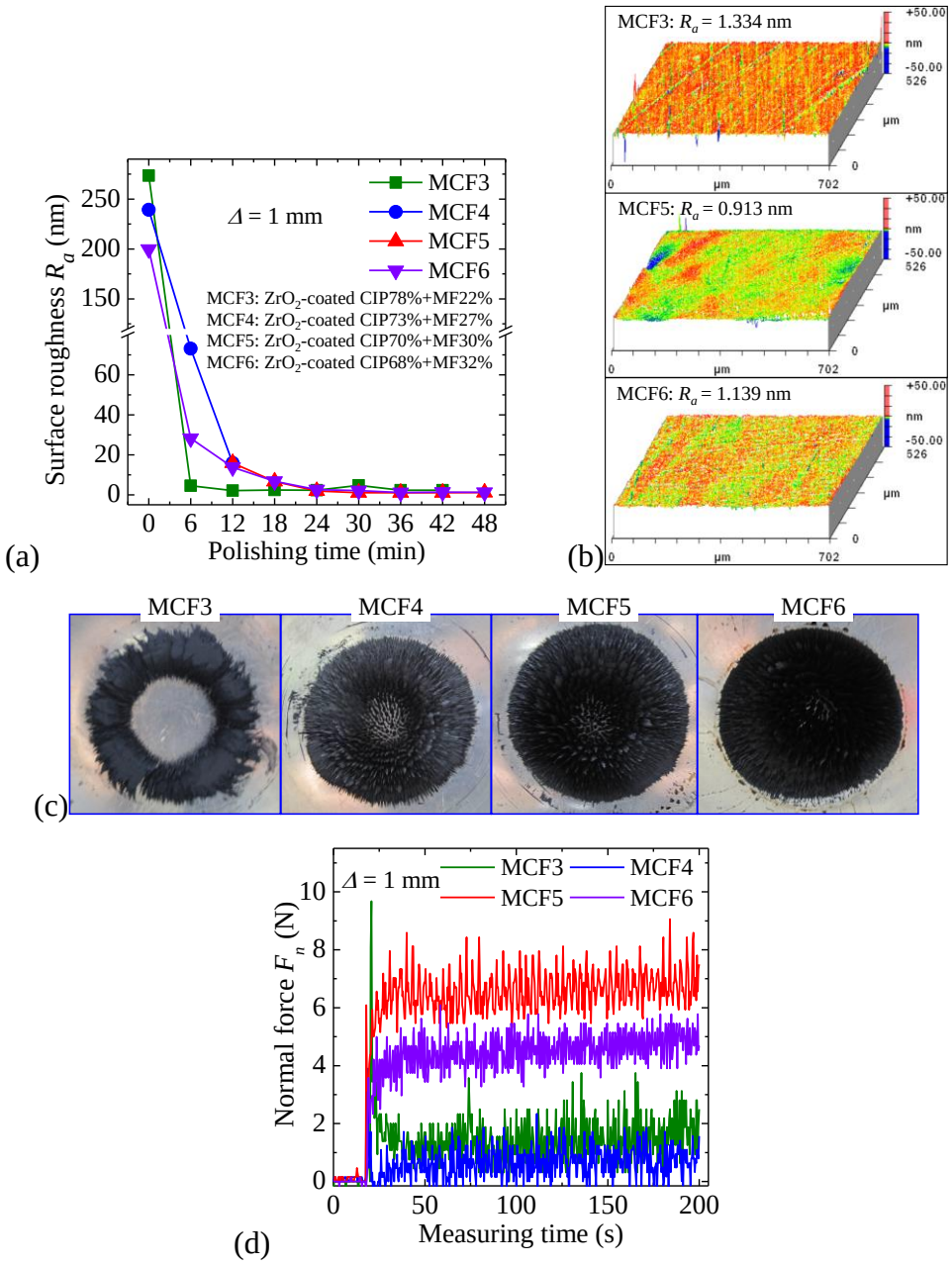

Fig. 4.6 Effect of slurry composition under different concentrations of ZrO_2-coated CIPs in terms of (a) the variations of surface roughness R_a obtained at Δ = 1 mm, (b) the best surface roughnesses obtained with MCF3, MCF5 and MCF6 after polishing for 18 min, 30 min and 36 min, respectively, (c) the optical images of MCF3, MCF4, MCF5 and MCF6 after polishing for 3 min at Δ = 1.0 mm, and (d) the variations of normal forces during polishing at Δ = 1.0 mm

4.4. Summary

This work dealt with the preliminary experimental investigations on the ultrafine polishing of PMMA using ZrO_2-coated CIPs based MCF slurry. For comparison, the conventional MCF slurry containing non-coated CIPs, and MR fluid slurry, in which DI water is employed instead of water based MF, were also examined. The main conclusions are summarized as follows:

(1) The use of relative large abrasive particles (i.e. > 1 μm) in the ZrO_2-coated CIPs based MCF slurry cannot result in better surface roughness and higher surface finish improvement rate compared with the conventional HQ CIPs based MCF slurry.

(2) ZrO_2-coated CIPs based MCF slurry produced smoother work surface at a higher improvement rate than ZrO_2-coated CIPs based MR fluid slurry. The reason is that the use of MF containing magnetite particles in MCF slurry helps disperse the abrasive particles uniformly and enhance the toughness of the magnetic clusters within the MCF slurry during polishing.

(3) In the absence of both Al_2O_3 abrasive particles and α-cellulose, better surface roughness was attained using ZrO_2-coated CIPs based MCF slurry and a best surface roughness R_a less than 1 nm was achieved under a proper CIP concentration (i.e. 70 wt.%) at a considerable improvement rate; the ZrO_2-coated CIPs concentration should be less than a certain value (in the current work, 70 wt.%), otherwise MCF slurry shows bad particle dispersion ability and is easily dried, resulting in the loss of polishing ability.

References

[1] Kim, G.B., Lee, S.J., Lee, J.P., 2007. Fabrication of PMMA X-ray compound refractive lenses for the pohang light source and performance tests. J. Korean. Phys. Soc. 51, 1256–1262.

[2] DeGroote, J.E., Romanofsky, H.J., Kozhinova, I.A., Schoen, J.M., Jacobs, S.D., 2003. Polishing PMMA and other optical polymers with magnetorheological finishing. Proc. SPIE 5180, 123–134.

[3] Sidpara, A., Das, M., Jain, V.K., 2009. Rheological Characterization of Magnetorheological Finishing Fluid. Mater. Manuf. Processes 24, 1467–1478.

[4] Tani, Y., Kawata, K., Nakayamac, K., 1984. Development of high-efficient fine finishing process using magnetic fluid. CIRP Ann. 33, 217–220.

[5] Singh, A.K., Jha, S., Pandey, P.M., 2012. Magnetorheological Ball End Finishing Process. Mater. Manuf. Processes 27, 389–394.

[6] Singh, A.K., Jha, S., Pandey, P.M., 2012. Nanofinishing of a typical 3D ferromagnetic workpiece using ball end magnetorheological finishing process. Int. J. Mach. Tools Manuf. 63, 21−31.

[7] Shimada, K., Fujita, T., Oka, H., Akagami, Y., Kamiyama, S., 2001. Hydrodynamic and magnetized characteristics of MCF (magnetic compound fluid). Trans. Jpn. Soc. Mech. Eng. B 67, 3034–3040 (in Japanese).

[8] Shimada, K., Wu, Y., Matsuo, Y., Yamamoto, K., 2005. Float polishing technique using new tool consisting of micro magnetic clusters. J. Mater. Process. Technol. 162−163, 690–695.

[9] Wu, Y., Sato, T., Lin, W., Yamamoto, K., Shimada, K., 2010. Mirror surface finishing of acrylic resin using MCF-based polishing liquid. Int. J. Abras. Technol. 3, 11–24.

[10] Sato, T., Wu, Y., Lin, W., Shimada, K., 2009. Study on magnetic compound fluid (MCF) polishing process using fluctuating magnetic field. Trans. Jpn. Soc. Mech. Eng. B 75, 1007–1012 (in Japanese).

[11] Guo, H., Wu, Y., 2012. Behaviors of MCF (magnetic compound fluid) slurry and its mechanical characteristics: normal and shearing forces under a dynamic magnetic field. Jpn. Soc. Exp. Mech. 12, 369–374.

[12] Shafrir, S.N., Romanofsky, H.J., Skarlinski, M., Wang, M., Miao, C., Salzman, S., Chartier, T., Mici, J., Lambropoulos, J.C., Shen, R., Yang, H., Jacobs, S.D., 2009.

Zirconia-coated carbonyl-iron-particle-based magnetorheological fluid for polishing optical glasses and ceramics. Appl. Opt. 48, 6797–6810.

[13] Preston, F.W, 1927. The theory and design of plate glass polishing machines. J. Soc. Glass Technol. 11, 214–256.

Chapter V
Polishing of Nickel-Phosphorus Plated Mold with MCF Slurry

5.1 Introduction

The electroless nickel-phosphorus (Ni-P) plated mold has been extensively applied to the mass-production of optical lens by hot press. As the Ni-P plating layer is soft and shows good machinability, a mirror surface finish is generally obtained through the use of the ultra-fine single crystal diamond turning (SCDT) process. However, the SCDT process frequently results in unwanted tool marks on the mold surface. Therefore, the mold has to be further finished to nano-level surface roughness in order to eliminate the SCDT-induced tool marks. Although conventional mirror grinding, lapping, and polishing processes are available, scratches, and the embedding of abrasive particles are usually caused on the work surface when attempting to improve surface finish of soft materials, e.g., optical polymers [1] and potassium dihydrogen phosphate (KDP) [2]. Hence, it is hard to expect that the finish of the Ni-P plated mold surface that had undergone the SCDT process can be improved via conventional finishing processes. Therefore, novel finishing methods that effectively eliminate the tool marks and improve the surface finish of the Ni-P plated mold are of high priority.

Promising finishing techniques are magnetic field-assisted polishing using magnetic fluids (MFs) or magnetorheological (MR) fluids. In these techniques, the behaviour of the abrasive particles is controlled by an applied magnetic field. Tani et al. [3] implemented fine polishing by magnetically controlling an MF, and reported an appreciably improved surface roughness of a flat polypropylene workpiece. DeGroote et al. [1] successfully smoothed a diamond turned polymethyl methacrylate (PMMA) part to 0.5 nm in *rms* with MRF. Singh et al. [4] proposed a ball end MRF process, and applied it to flat and 3D ferromagnetic work surfaces. Hence, the magnetic field-assisted polishing is supposed to be an excellent candidate for polishing the soft

Ni-P plated mold. However, under a given magnetic field, the particles are more stably distributed in an MF than in an MR fluid, whereas magnetic pressure and apparent viscosity of the former are smaller than that of the latter.

To overcome the disadvantages and exploit the advantages of MFs and MR fluids, Shimada et al. [5] developed a magnetic compound fluid (MCF) by mixing an MF and an MR fluid with the same base solvent. Hence, MCF includes not only μm-sized iron particle but also nm-sized magnetite particle whereas there is no nm-sized magnetite particle within the MR fluid. They found that MCF is more viscous than an MF and disperses particles more readily than an MR fluid under a static magnetic field. Shortly afterwards, Shimada et al. [6] proposed an MCF slurry by blending abrasive particles and α-cellulose fibres into the MCF. Following the work by Shimada et al., Sato et al. replaced the static field applied to the MCF slurry with a rotary magnetic field [7], which helps enhance the shape restoring ability of the MCF slurry and disperses the abrasive particles within the MCF slurry more uniformly during polishing. The magnetic field in the polishing process with MCF slurry (i.e. MCF polishing) is generated by a permanent magnet whilst the magnetic field in MRF is usually produced by an intricately structured electromagnet. Therefore, the MCF polishing also exhibits good cost-performance as compared with other similar techniques such as the MRF. Being aware of the benefits of the rotary magnetic field, Guo et al. [8] polished a flat PMMA specimen with an MCF slurry containing zirconia abrasive particles (ZrO_2)-coated CIPs [9] under a rotary magnetic field and successfully achieved a surface roughness below 1 nm R_a with no visible scratches. These results verify the crucial role that rotary magnetic field MCF polishing has in the ultra-precision surface finishing of soft materials.

This chapter reports the polishing of Ni-P plated mold with MCF slurry under the application of a rotary magnetic field. Two kinds of MCF slurry containing different magnetic particles and abrasive grains were used to eliminate the SCDT-induced tool marks. Two polishing tests, one is spot polishing and another is scanning polishing,

were carried out. Spot polishing in which there is no scanning motion between the centre of the MCF slurry carrier and the workpiece, was first carried out, and the polished surface was analyzed in terms of profile, roughness, texture, and chemical elements to determine an appropriate set of process parameters. Then, based on the results obtained from the spot polishing process, a scanning path of the carrier on the work surface was designed to obtain a high form accuracy.

5.2 Experimental details

Fig. 5.1(a) shows a photograph of the experimental setup constructed in the laboratory. A disc-shaped neodymium permanent magnet (ϕ18 mm × t10 mm, 0.4 T) was set at an eccentricity of r = 4.5 mm. A workpiece was installed on a worktable via a set of fixtures and a 3-component dynamometer (9256A1, Kistler). The fixtures were designed to have a circular through hole (ϕ29.9 mm) within which the workpiece was constrained. Under a rotary magnetic field, a circular interacting area is established between the MCF slurry and the work surface [10]. This interacting area is centred at the rotational axis of the magnet holder, i.e. the revolution axis of the magnet. In order to create a stable circular interacting area, the top surfaces of the fixtures were adjusted to be at the same vertical level with that of the workpiece. Fig. 5.1(b) shows a photo of a workpiece. In practice, this kind of workpieces was produced by depositing an electroless Ni-P plating layer on the upper top surface of a disc-shaped body (ϕ30 mm × t25 mm) made of magnetic stainless steel. After the SCDT process, interferometric fringes are visibly observed from the Ni-P plating surface owing to the tool marks.

Two MCF slurries, i.e. MCF1 (Fig. 5.2(a)), which consists of HQ CIPs (median diameter ~2 μm, 56 wt. %), water based MF (32 wt. %) and alumina abrasives (Al_2O_3, median size ~1 μm, 12 wt. %), and MCF2 (Fig. 5.2(b)), which is made up of ZrO_2-coated CIPs (median diameter ~1.4 μm, 68 wt. %) and water based MF (32 wt. %), were prepared and employed. MCF2 did not contain abrasives as there is a thin and

rough abrasive layer over the CIPs' surface. This layer consists of overlapping nanocrystallites of faceted ZrO_2 that are about 50-100 nm in size [9]. According to the scanning electron microscope (SEM) images of MCF slurries, chain-shaped magnetic clusters composed of nano-sized magnetite particles and μm-sized CIPs are formed along the magnetic lines of force. Non-magnetic abrasive particles are entrapped in the clusters or distributed between the clusters if abrasives are employed.

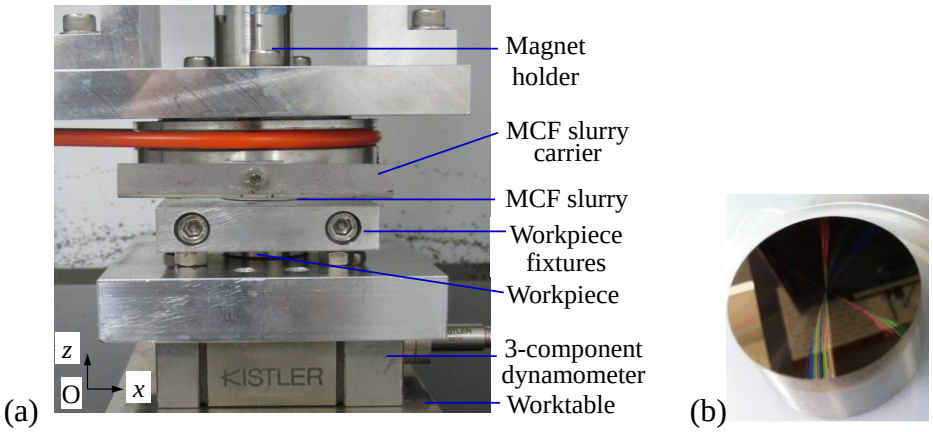

Fig. 5.1 (a) Experimental setup and (b) a workpiece

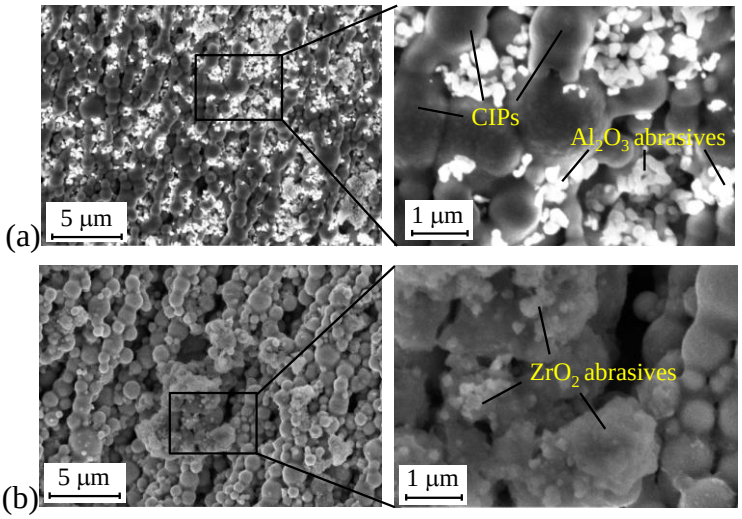

Fig. 5.2 SEM images of internal microstructure of (a) MCF1 slurry and (b) MCF2 slurry

Table 5.1 shows the experimental conditions. The two tests, i.e. spot polishing and scanning polishing, were carried out with different MCF slurries for different

polishing time and the MCF slurry carrier had different motion paths on the work surface. The process parameters of r, n_m, n_c, v and Δ were kept constant. Spot polishing was performed without the carrier motion to reveal the effects of two key conditions, namely MCF slurry compositions and polishing time, on the polishing characteristics. Based on the knowledge previously obtained in MCF polishing of nonmagnetic materials [8], a relatively large working gap of Δ = 2.2 mm was used in the spot polishing process to avoid the occurrence of sever scratches on the Ni-P plating surface. The spot polishing process was divided into three successive stages: in the first stage, the MCF2 slurry was used for 30 min; in the second stage, the MCF2 slurry was replaced with the MCF1 slurry for another 15 min; finally in the third stage, the MCF2 slurry was used again for a further 30 min. Through spot polishing, the feasibility of eliminating the SCDT-induced tool marks on the work surface can be confirmed, and the appropriate process parameters, including the MCF slurry composition and polishing time, can be determined.

Table 5.1 Experimental conditions

Parameters \ Tests	Spot polishing	Scanning polishing
Magnet	Nd-Fe-B, ϕ18 mm × t10 mm	
Magnet eccentricity	r = 4.5 mm	
MCF carrier rotational speed	n_c = 600 rpm	
Magnet revolution speed	n_m = 1000 rpm	
Amount of MCF slurry supplied	v = 1 mL	
Working gap	Δ = 2.2 mm	
MCF slurry	MCF1, MCF2	MCF2
Polishing time	30 min with MCF2 + 15 min with MCF1 + 30 min with MCF2	60 min

Subsequently, the scanning polishing was carried out with a scanning motion of the MCF carrier to ensure the required form accuracy of the mold. The scanning path was designed based on the results previously obtained in the spot polishing process as shown in Fig. 5.3. As the polishing operation starts at point A, the MCF carrier moves along the forward road heading to point B, and returns back to the start point A along the backward road. This movement is repeated until the total polishing time has reached the given value. In practice, the scanning path is generated by controlling the movement of the worktable along the *x*- and *y*-axes. The relative motion speeds along the *x*- and *y*-axes were the same, at V_f = 10 mm/s. The scanning polishing was performed using only the MCF2 slurry for 60 min.

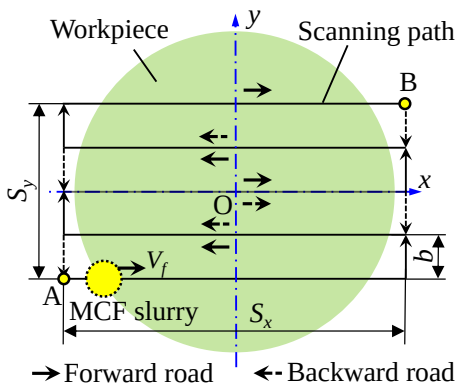

Fig. 5.3 Scanning path of MCF slurry carrier on work surface

During both the spot polishing and scanning polishing processes, the MCF slurry was supplied in 1 mL quantities and renewed every 3 min. After polishing, the workpieces were washed using deionized water and quickly dried with a compressed air gun. Following this, the work surfaces were characterized by measuring the cross-sectional profiles along the *x*- and *y*-axes (Fig. 5.4) using a stylus-based profilometer **(**Form Talysurf Intra, Taylor Hobson) and the surface roughness in the selected areas A, B and C (Fig. 5.4) using a white-light interferometer (Newview600, Zygo). Both the SEM (ERA-8900 by Elionix) and digital micro-scope (VHX-2000 by Keyence) were used to observe the work surface textures. In addition, considering that

the magnetic particles within the MCF slurry are likely to be embedded in the magnetic work surfaces, elemental composition analyses were carried out using the Energy Dispersive X-Ray Analysis (EDX, Genesis APEX by EDAX) to check if any particles had been embedded.

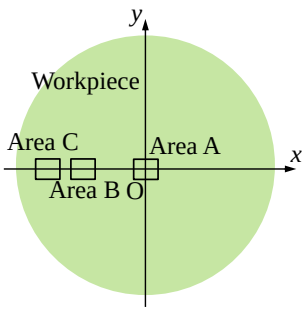

Fig. 5.4 Locations of the selected measurement areas

5.3 Spot polishing

Fig. 5.5(a) shows that the work surface right after the SCDT process was shaped like a conical mountain with a height of about 200 nm. Fig. 5.5(b) displays the x-/y-axial cross-sectional profiles (the x-axial profile is similar to the y-axial one) that has a characteristic symmetrical W-shape after spot polishing for 75 min (30min with MCF2 + 15min with MCF1 + 30min with MCF2). Little material removal was attained around the central area of the polishing spot, i.e. area A in Fig. 5.5, because the relative speed of the MCF slurry to the work surface in this area is extremely small. Contrastingly, the maximal material removal MR_{max}, i.e. the maximal spot depth, occurred at a circle with a radius of about 8 mm. Hence, the area B is located at a distance of 8 mm from the polishing spot centre. Shifting the attention to the work surface textures as shown in Fig. 5.6, the SCDT-induced tool marks on the work surface have been eliminated after a 75 min spot polishing but distinct scratches were caused.

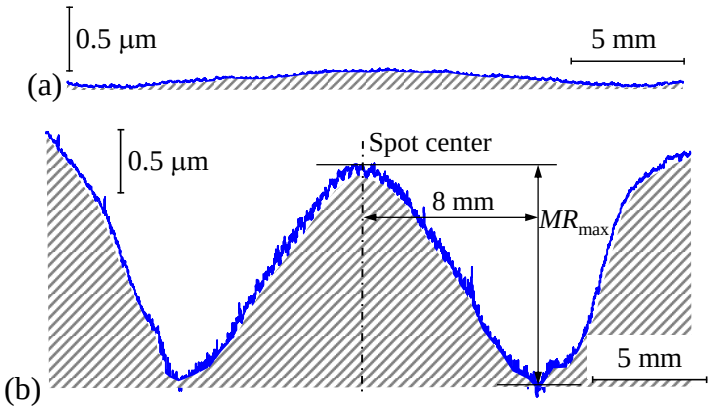

Fig. 5.5 Cross-sectional profiles of workpiece along *x*/*y*-axis after (a) SCDT and (b) spot polishing for 75 min

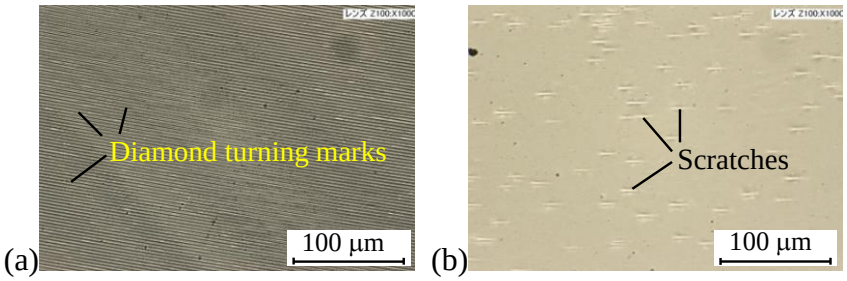

Fig. 5.6 Surface textures of workpiece after (a) SCDT and (b) spot polishing for 75min

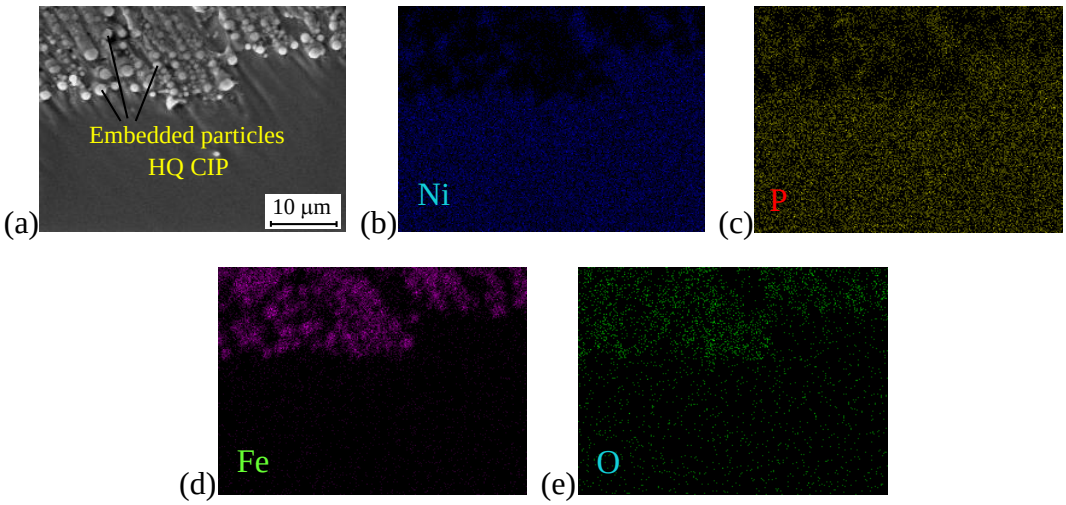

Fig. 5.7 Elements mapping analysis of the embedding of particles: (a) SEM image, distributions of (b) Ni, (c) P, (d) Fe, and (e) O

The first stage of the spot polishing process, during which the MCF2 slurry containing ZrO_2-coated CIPs was used for 30 min, resulted in the removal of the tool marks to some extent, which led to a slightly improved work surface roughness. During the second stage of the spot polishing process, the MCF2 slurry was replaced with the MCF1 slurry containing HQ CIPs and Al_2O_3 abrasives for another 15 min in an attempt to elevate the improvement rate of work surface roughness. Although the second stage significantly eliminated the tool marks, evident scratches were newly created on the work surface and particles were found to be embedded in the scratches in a few areas. Fig. 5.7(a) shows a typical embedding phenomenon of particles. The element mapping analysis of the embedding of particles, which is exhibited in Fig. 5.7(b–e), indicates that the elements of Ferrum (Fe) and Oxygen (O) were detected besides the original elements of Ni and P. Therefore, it is inferred that HQ CIPs had been embedded into the Ni-P plating surface.

Fig. 5.8(a) shows that although the concentrically arranged tool marks are visible in area A before polishing, no scratches can be observed. By contrast, as shown in Fig. 5.8(b–d), although a part of the tool marks in area A still remained after polishing, the tool marks either in both areas B and C (about 10.2 mm from the polishing spot centre) are no longer visible. However, lots of scratches appeared in all of the areas. It is worth noting that dot-shaped scratches appeared in area A, while the scratches become long and thin in areas B and C. The reasons why the scratch shapes vary in different polishing areas can be considered as follows.

During polishing, Al_2O_3 abrasive particles within the MCF1 slurry (Fig. 5.2(a)) revolve around the magnet holder axis together with the rotational motion of the MCF slurry carrier and exert micro-cutting action in random directions, hence successfully eliminating the tool marks. However, the Al_2O_3 abrasive particles are relatively large and considerably harder than the Ni-P plating layer, resulting in the easy occurrence of scratches. Dot-shaped scratches (Fig. 5.8(b)) were generated in the central area (area A) of the polishing spot because there was almost no relative motion between the

abrasive particles and the work surface in this area and the abrasive particles remained almost stationary. The length of the scratches increases with the increase in the distance from the polishing spot centre (Fig. 5.8(c) and (d)) because the relative velocity of abrasive particles to work surface increases. Once the scratches are made, CIPs are easily embedded in the scratches during polishing. The scratches and the embedded particles were yet not removed even after the third stage of spot polishing process using MCF2 slurry again for a further 30 min.

Due to the occurrence of scratches and the embedding of HQ CIPs, the R_a values of the work surface roughness increased significantly from 1.911 nm (Fig. 5.8(a)) to 4.729 nm in area A (Fig. 5.8(b)), 9.469 nm in area B (Fig. 5.8(c)) and 6.188 nm in area C (Fig. 5.8(d)) after spot polishing. Therefore, it can be concluded that it is difficult to improve the surface finish of the Ni-P plating layer through spot polishing with MCF1 slurry that contains conventional HQ CIPs and Al2O3 abrasive particles.

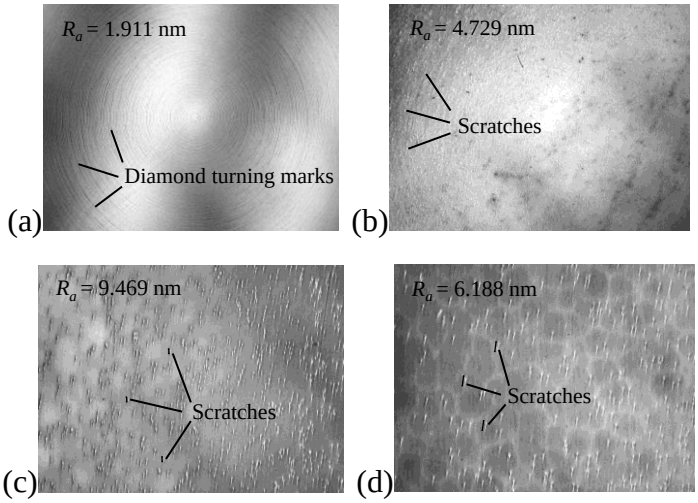

Fig. 5.8 Optical images of work surface in: (a) area A after SCDT, and (b) area A, (c) area B, and (d) area C after spot polishing using MCF1 slurry

5.4 Scanning polishing

Based on the abovementioned results of the spot polishing process, in particular, the characteristic symmetrical W-shape (Fig. 5.5(b)), the parameters for the scanning

motion path of the MCF slurry carrier on the work surface were determined at S_x = 32 mm, S_y = 16 mm, b = 4 mm (Fig. 5.3) for the scanning polishing process. The initial x- and y-axial cross-sectional profiles of the workpiece used were also similar to each other and approximately the same as those of the workpiece used in the spot polishing process (Fig. 5.5(a)). Although the x-axial cross-sectional profile in Fig. 5.9(a) was still similar to the initial one (Fig. 5.5(a)) and the x-axial flatness stayed almost at the same level of 0.2 μm after scanning polishing for 60 min using only the MCF2 slurry, the obtained y-axial cross-sectional profile in Fig. 5.9(b) demonstrates that the y-axial flatness was improved greatly from about 0.2 μm to about 0.1 μm. The improvement is considered to be the result of the overlap of the instantaneously formed W-shaped polishing spots (Fig. 5.5(b)) due to the instantaneous movement of the MCF slurry, which moves together with the carrier, along the designed motion path.

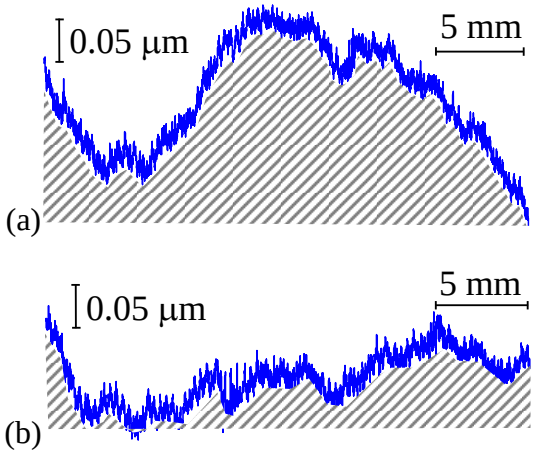

Fig. 5.9 (a) x-axial and (b) y-axial cross-sectional profiles of workpiece after scanning polishing for 60 min

Fig. 5.10(a) and (b) show that distinct tool marks are visible on the initial work surface in both areas A and B before the scanning polishing process. Contrastingly, as demonstrated in Fig. 5.10(c) and (d), the tool marks in both areas have been eliminated after scanning polishing for 60 min. Moreover, no scratches or the embedding of particles occurred over the entire work surface as in Fig. 5.11. The

optical microscopic images of work surface also revealed that the visible concentrically arranged tool marks induced by the SCDT process in both areas A (Fig. 5.12(a)) and B (Fig. 5.12(b)) have become random after scanning polishing (Fig. 5.12(c) and (d)). The work surface roughness was improved from 1.810 nm R_a after SCDT to 1.761nm R_a after scanning polishing in area A and from 1.697 nm R_a after SCDT to 1.497 nm R_a after scanning polishing in area B.

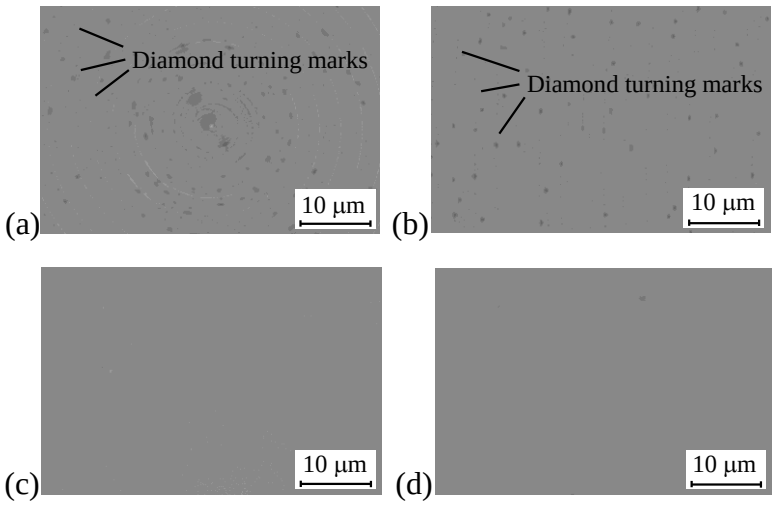

Fig. 5.10 SEM images of work surface in: (a) area A, and (b) area B after SCDT, and (c) area A, and (d) area B after scanning polishing for 60 min

Fig. 5.11 Elemental mapping analysis of work surface after scanning polishing for 60 min: (a) SEM image, and distributions of (b) P and (c) Ni

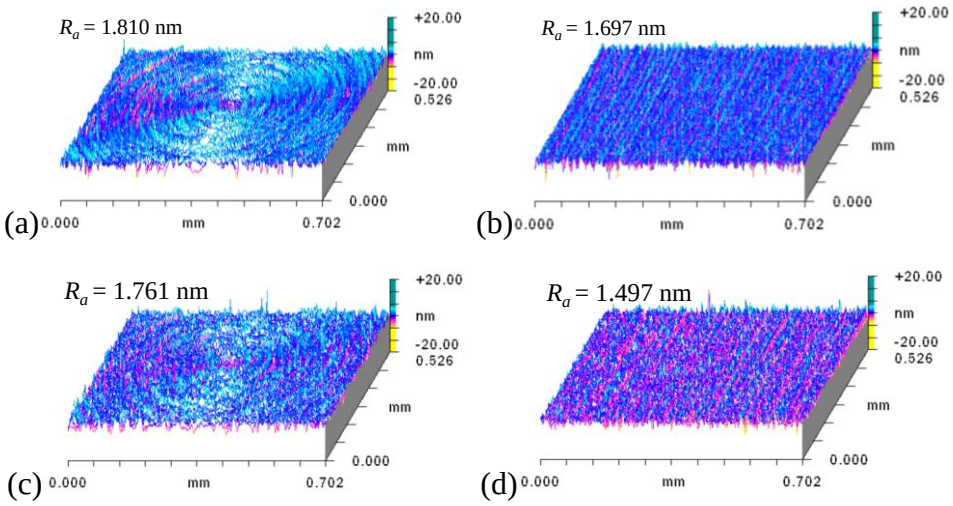

Fig. 5.12 Work surface roughness in: (a) area A, and (b) area B after SCDT, and (c) area A, and (d) area B after scanning polishing for 60 min

Under the designed scanning path, relatively small ZrO_2 abrasive particles (50–100 nm) within the MCF2 slurry move with the fluctuating magnetic lines of force and all of the particles within the MCF slurry have relative motion to the work surface, thereby removing the tool marks with no scratches or the embedding of particles and improving the surface finish of the Ni-P plating layer. Hence, a certain scanning path is beneficial for improving both the surface finish and the flatness.

5.5 Summary

MCF polishing of the SCDT Ni-P plating layer was carried out to eliminate the SCDT-induced tool marks. The MCF1 slurry containing HQ CIPs and Al_2O_3 abrasive particles and the MCF2 slurry containing ZrO_2-coated CIPs were prepared and employed. Spot polishing was carried out using both slurries whilst scanning polishing was performed only using the MCF2 slurry. The main conclusions are summarized below:

(1) The tool marks can be eliminated by both slurries. Although the MCF1 slurry evidently removes the tool marks, the Al_2O_3 abrasive particles within MCF1 are relatively large and considerably harder than the Ni-P plating layer, frequently

resulting in scratches and the embedding of CIPs. Contrastingly, the MCF2 slurry containing relatively small ZrO_2 abrasive particles slightly improves the work surface roughness without leaving scratches or the embedding of particles.

(2) The cross-sectional profile of the polishing spot has a characteristic symmetrical W-shape. Dot-shaped scratches are easily made at the spot centre and longer scratches are likely to be induced in the area farther from the polishing spot centre.

(3) Under the designed scanning path, the polishing spot with W-shaped cross-sectional profile moves along the motion path, thus greatly improving the work surface flatness from 0.2 μm to 0.1 μm. Moreover, all of the particles within the MCF slurry are made to move relative to the work surface, consequently improving the surface roughness without creating scratches or the embedding of particles.

The abovementioned results demonstrate that MCF polishing is applicable to ultra-fine polishing of soft magnetic as well as non-magnetic materials. It also has greater potential in industrial application in terms of cost-performance compared with other similar techniques such as the MRF, in which an intricately electromagnet is employed for the magnetic field generation and a costly fluid delivery system is required for supplying and circulating the MR fluid slurry.

References

[1] DeGroote, J.E., Romanofsky H.J., Kozhinova, I.A., Schoen, J.M., Jacobs, S.D., 2003. Polishing PMMA and other optical polymers with magnetorheological finishing. Proc. SPIE 5180, 123–134.

[2] Wang, Q., Cong, W., Pei, Z.J., Gao, H., Kang, R., 2009. Rotary ultrasonic machining of potassium dihydrogen phosphate (KDP) crystal: An experimental investigation on surface roughness. J. Manuf. Processes 11, 66–73.

[3] Tani, Y., Kawata, K., Nakayama, K., 1984. Development of high efficiency fine finishing process using magnetic fluid. CIRP Ann. 33, 217–220.

[4] Singh, A.K., Jha, S., Pandey, P.M., 2012. Nanofinishing of a typical 3D ferromagnetic workpiece using ball end magnetorheological finishing process. Int. J. Mach. Tools Manuf. 63, 21–31.

[5] Shimada, K., Fujita, T., Oka, H., Akagami, Y., Kamiyama, S., 2001. Hydrodynamic and magnetized characteristics of MCF (magnetic compound fluid). Trans. Jpn. Soc. Mech. Eng. B 67, 3034–3040 (in Japanese).

[6] Shimada, K., Wu, Y., Wong, Y.C., 2003. Effect of magnetic cluster and magnetic field on polishing using magnetic compound fluid (MCF). J. Magn. Magn. Mater. 262, 242–247.

[7] Sato, T., Wu, Y., Lin, W., Shimada, K., 2009. Study on magnetic compound fluid (MCF) polishing process using fluctuating magnetic field. Trans. Jpn. Soc. Mech. Eng. B 75, 1007–1012 (in Japanese).

[8] Guo, H., Wu, Y., Li, Y., Cao, J., Fujimoto, M., Jacobs, S.D., 2012. Technical performance of zirconia-coated carbonyl-iron-particles based magnetic compound fluid Slurry in ultrafine polishing of PMMA. Key Eng. Mater. 523–524, 161–166.

[9] Shafrir, S.N., Romanofsky, H.J., Skarlinski, M., Wang, M., Miao, C., Salzman, S., Chartier, T., Mici, J., Lambropoulos, J.C., Shen, R., Yang, H., Jacobs, S.D., 2009 Zirconia-coated carbonyl-iron-particle-based magnetorheological fluid for polishing optical glasses and ceramics. Appl. Opt. 48, 6797–6810.

[10] Guo, H., Wu, Y., 2012. Behaviors of MCF (magnetic compound fluid) slurry and its mechanical characteristics: normal and shearing forces under a dynamic magnetic field. Jpn. Soc. Exp. Mech. 12, 369–374.

Chapter VI
Investigation into Material Removal in Ultra-fine Polishing of Optical Glass with MCF Slurry

6.1 Introduction

Optoelectronic devices such as photodiodes, photoresistors and light-emitting diodes, have been extensively used in the detection and control of radiation, including visible light, gamma rays, X-rays, ultraviolet and infrared. The usual construction material is optical glass. To meet the required performance, the surfaces of these devices must be finished to nano-level roughness with no sub-surface damage. Therefore, during the manufacturing of optoelectronic devices, the construction material is generally subjected to nano-precision polishing as the final process after machining (e.g. cutting and grinding). Nano-precision polishing not only reduces the surface roughness but also eliminates breaks, cracks and damaged layers on the work surface caused by previous processes such as ultra-fine grinding.

Conventionally, nano-precision polishing is accomplished by freshly feeding loose abrasive slurry in the polishing zone between a pitch lap or polyurethane pad and the workpiece. To achieve the desired surface quality, this technique requires a long processing time and a continuous plentiful supply of slurry. Li et al. [1] polished optics with a polyurethane pad and eliminated surface damage several hours later, thereby mitigating subsurface damage and achieving surface roughness of approximately 1 nm. Consequently, traditional nano-polishing is a costly and time consuming process. Maintaining the required quantity of active abrasive slurry and ensuring that abrasive particles are uniformly distributed within the polishing zone are among the main difficulties. Therefore, novel polishing methods that supply large amounts of uniformly-distributed abrasive particles in the polishing zone are of high priority.

One promising advanced finishing technique is magnetic field-assisted polishing using magnetic fluids (MFs) or magnetorheological (MR) fluids. In this technique, the behaviour of the abrasive particles is controlled by an applied magnetic field to achieve a nano-precision-polished surface with no surface and/or sub-surface damage. Tani et al. [2] developed a polishing method based on magnetohydrodynamic behaviour of MFs. They blended SiC grains into an MF and achieved an appreciable stock removal rate greater than 2 μm/min and surface roughness less than R_{max} =0.04 μm for finishing of acrylic resin. Umehara et al. [3] studied the behaviour of abrasives in an MF during polishing and reported that the number of abrasives on the work surface could be controlled by a magnetic field. Prokhorov and Kordonski [4] proposed a novel magnetorheological finishing (MRF) technique in which the MR fluid contained magnetic carbonyl-iron-particles (CIPs), abrasive grains, carrier fluid and stabilizers. Kordonski and Jacobs [5] revealed that the MR fluid becomes viscous and morphs into a kind of Bingham fluid under an applied magnetic field. This mechanism of material removal in the polishing zone is considered as a process governed by the particularities of the Bingham flow. They obtained the shear stress distribution from the experimental measurements of the pressure distribution in the polishing spot. Golini et al. [6] commercialized the MRF technique for optical fabrication and reported that this technique eliminates subsurface damage, smoothes root mean square (*rms*) microroughness to less than 1 nm, and corrects PV surface figure errors to $\lambda/20$ in minutes. Shorey et al. [7] measured the drag force in MRF involving a sapphire workpiece and found that there is a linear relation between the material removal rate (*MRR*) and the drag force in MRF. Miao et al. [8] demonstrated how the calculated shear stress governs the material removal in MRF of optical glasses based on their mechanical properties and incorporated the shear stress and material mechanical properties into a modified Preston's equation. Miao et al. [9] also investigated the effect of process parameters (nanodiamond concentration, penetration depth, the relative velocity between the part and the MR fluid and magnetic field strength) on *MRR* in

MRF of borosilicate glass (BK7). They found that shear stress is independent of the process parameters. The volumetric removal rate (*VRR*) is only insensitive to the magnetic field strength. Thereby, the *MRR* model for MRF was expanded by including nanodiamond concentration and penetration depth. Jha and Jain [10] developed a new magnetorheological abrasive flow finishing (MRAFF) process for complex internal geometries using MR fluid. They demonstrated that the roughness reduces gradually with the increase of magnetic field strength and validated the role of rheological behaviour of MR fluid in exerting finishing action. Das et al. [11] performed the theoretical investigations into the mechanism of MRAFF process and concluded that shearing action takes place during finishing when the shear force acting on the abrasive particles is greater than the reaction force due to the strength of the workpiece material opposing material removal. Das et al. [12] also experimentally characterized rheological properties of MR fluid in MRAFF process. They described that the MR fluid in MRF, MRAFF and similar other processes is a suspension of micron-sized magnetizable particles such as CIPs and non-magnetic abrasive particles dispersed in either an aqueous or non-aqueous carrier fluid like paraffin oil, silicone oil, mineral oil, or water and stabilizing additives. They observed that magnetic field has the highest contribution on the yield stress and viscosity of MR fluid than the volume concentrations of CIPs, abrasive particles and grease. Cheng et al. [13] polished aspherical optical components with an MR fluid using a 2-axis wheel-shaped tool supporting dual magnetic fields, improved the surface roughness from 3.8 nm to 1.2 nm after 10 min of pre-polishing and corrected form errors from an *rms* value of 2.27 μm to 0.36 μm after 60 more minutes of fine polishing. By analyzing MRF processes, Dai et al. [14] established a calibrated predictive model of material removal function by introducing an efficiency coefficient, thereby improving finishing determinacy and model applicability. Sidpara and Jain [15] measured the normal and tangential forces in MRF. They concluded that maximum contribution is made by a working gap on the forces developed on the workpiece surface followed by CIPs concentration, whereas

minimum contribution is noted by the wheel speed. Singh et al. [16] proposed a nano-finishing process using a ball end MRF tool and applied it to flat as well as 3D ferromagnetic work surfaces, thus verifying that the newly developed method was effective in finishing typical 3D ferromagnetic work surfaces. However, in a magnetic field, magnetic pressure and apparent viscosity of an MF are smaller than that of an MR fluid, whereas the particles are more stably distributed in the former than in the latter.

To overcome the disadvantages and exploit the advantages of MFs and MR fluids, Shimada et al. [17] developed a magnetic compound fluid (MCF) by mixing an MF and an MR fluid with the same base solvent. Hence, MCF includes not only μm-sized iron particles but also nm-sized magnetite particles whereas there are no nm-sized magnetite particles within MR fluid. They confirmed that MCFs exhibit higher magnetic pressure and apparent viscosity than MFs and a more stable distribution of particles than MR fluids under a magnetic field, while maintaining a fluid-like behaviour. As an engineering application of MCFs, Shimada et al. [18] proposed an MCF slurry, a novel magnetic polishing liquid in which abrasive particles and α-cellulose fibre are blended into the MCF. The slurry showed strong performance in constant contact-force polishing under a static magnetic field. As mentioned above, constant contact-force polishing with MCF slurry frequently does not remove the micro-groove, ribs and other three-dimensional (3D) surface defects, and frequently scratches or cracks the work surfaces. To resolve these problems, Shimada et al. [19] employed MCF slurry in a contact-free surface finishing method for work surfaces with micro 3D structures, and thereby successfully performed mirror surface finishing of a brass specimen with rib-shaped grooves. Following the work by Shimada et al., Furuya et al. [20] and Wu et al. [21] experimentally investigated the fundamental characteristics of contact-free MCF polishing in the flat surface finishing of stainless steel and acrylic resin, respectively, and optimized the respective process parameters, including the composition of the MCF slurry.

However, under a static magnetic field in which the magnetic flux density and the

spatial distribution of magnetic lines of force are retained constant, the geometrical shape/size and distribution of the magnetic clusters generated within the MCF slurry are governed by the external conditions. These behaviours disfavour surface finishing because the abrasive particles within the MCF slurry are magnetically clustered, which hinders their uniform distribution. Indeed, the shape restoring ability of MCF slurry is extremely low. To overcome this weakness, Sato et al. [22] replaced the static field applied to the MCF slurry with a dynamic magnetic field.

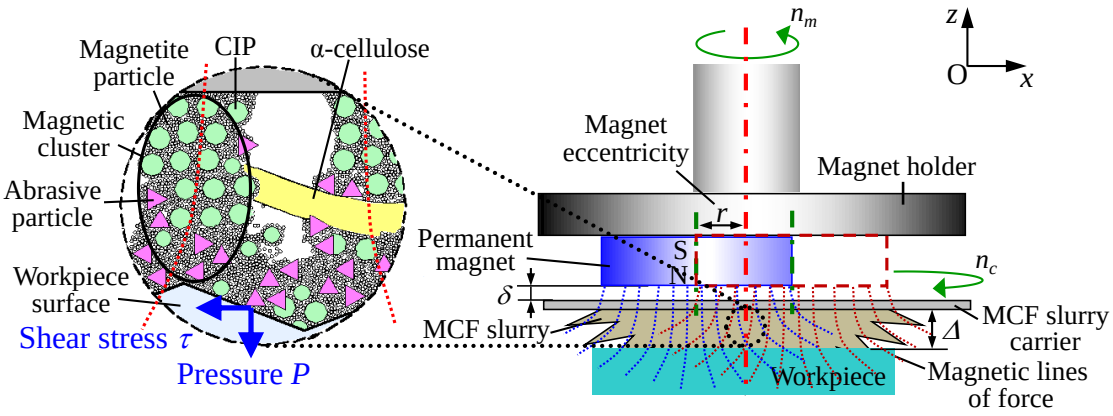

Fig. 6.1 Illustration of the process of MCF polishing under a dynamic magnetic field

The process of MCF polishing under a dynamic magnetic field is illustrated in Fig. 6.1. A disk-shaped permanent magnet is attached to the lower end face of its holder with an eccentricity r, and a non-magnetic carrier, such as an aluminium plate, is positioned between the magnet and a workpiece at distance δ from the magnet. When the magnet holder is rotated at a speed n_m the magnet revolves around the axis of the holder, thereby generating a dynamic magnetic field. The magnetic flux density is constant but the magnetic lines of force constantly revolve around the magnet holder axis. Hereafter, the dynamic magnetic field is called a 'rotary magnetic field'. Once the working gap Δ between the carrier and the workpiece has received a certain volume of MCF slurry, as shown in the left side of Fig. 6.1, chain-shaped magnetic clusters composed of nm-sized magnetite particles and μm-sized CIPs are formed along the magnetic line of force immediately; non-magnetic abrasive particles are entrapped into

the clusters or distributed between clusters and α-cellulose fibres have interwoven with the clusters if the fibres are employed. Kim et al. [23] defined magnetic levitation as forces exerted on nonmagnetic bodies by a magnetic functional fluid. Therefore, under magnetic levitation and gravitational forces, a majority of nonmagnetic abrasive particles within the MCF slurry move downward towards the workpiece surface. In addition, all of the clusters are collected forcibly by the magnetic attraction force and they are gathered in the area where the magnetic field is stronger. This leads to the generation of a pressure P (i.e. normal force F_n divided by the interacting area between the MCF slurry and the workpiece) acting on the workpiece. When the magnet holder and the carrier are rotated at their respective rotational speeds of n_m and n_c, a shear stress τ (i.e. shear force F_t divided by the interacting area between the MCF slurry and the workpiece) is imposed on the workpiece owing to the n_m/n_c-induced friction between the particles and the workpiece and the micro-cutting action of abrasive particles that remove unwanted materials.

Sato et al. [24] adopted the rotary magnetic field in an improved MCF polishing process for 3D metal components. Under the rotary magnetic field, the polishing performance of the MCF slurry was much higher than under the static magnetic field, confirming that MCF polishing is applicable to 3D-structured surface finishing. Shortly afterwards, Guo et al. [25] experimentally investigated flat surface finishing of a polymethyl methacrylate (PMMA) specimen with an MCF slurry containing zirconia-coated CIPs under a rotary magnetic field. The roughness of the resulting working surface was below 1 nm R_a, and no scratches were visible. These investigations indicate a crucial role for rotary-field MCF polishing in ultra-precision surface finishing, and justify its further development. Complete development should begin by thoroughly clarifying the fundamental characteristics of the MCF slurry under the rotary magnetic field, including its dynamic behaviour, the polishing forces during polishing and the function that describes material removal. These behaviours and polishing forces were investigated by Guo and Wu [26], as an extension of their

earlier work. They revealed that once a rotary magnetic field is applied, the MCF slurry rapidly self-assembles into a clear-cut terminal shape. The polishing forces F_n and F_t are significantly affected by the gap Δ but are insensitive to the carrier rotational speed n_c and the magnet revolution speed n_m.

As the next primary step, this chapter firstly investigates how the pressure and shear stress are distributed over the polishing zone and the relationship between the pressure/shear stress and material removal rate during the MCF polishing is also established. The measurement of the pressure and shear stress distributions and the material removal rate under varying process parameters (magnet revolution speed n_m, MCF slurry carrier rotational speed n_c and working gap Δ) are discussed. Then, effects of process parameters (magnet eccentricity r, magnet revolution speed n_m, MCF slurry carrier rotational speed n_c and working gap Δ) are presented. The magnetic field distribution is analysed and the structure of MCF slurry is examined to clarify the material removal mechanism.

6.2 Experimental details

6.2.1 Measurement of pressure and shear stress distributions

In conventional polishing processes, a pressure P is intentionally generated and uniformly distributed in the polishing zone in response to a normal force F_n applied between the polishing tool and the workpiece. As is well-known, the *MRR* depends on the pressure P and the relative velocity V between the polishing tool and the workpiece. The effects of other factors are embodied in an all-inclusive coefficient C_p, which depends on the workpiece material and abrasive properties. The *MRR* is computed from P, V and C_p by Preston's equation: $MRR = C_pPV$ [27]. Note that the *MRR* in conventional polishing processes is independent of the shear force F_t (and therefore the shear stress τ) exerted between the polishing tool and the work surface.

However, in MCF polishing, the normal force F_n (or the pressure P) is not intentionally applied, and the shear force F_t is of comparable importance to the normal

force in material removal. Additionally, since the magnetic lines of force generated by the magnet are unevenly distributed in the MCF slurry, the magnetic clusters, and the subsequent pressure P and shear stress τ are similarly unevenly distributed. Thus, the *MRR* spatially differs throughout the polishing zone. To understand how material is removed during MCF polishing, a knowledge of the P and τ distributions across the polishing zone is essential.

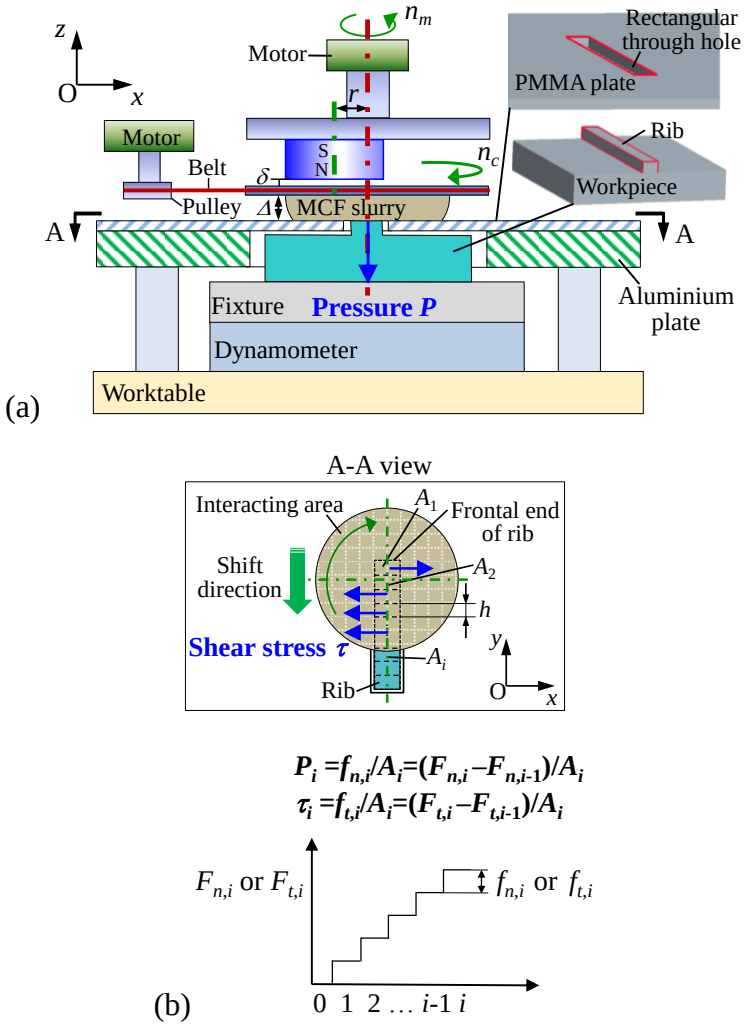

Fig. 6.2 (a) Schematic diagram of the experimental setup for measuring the distributions of P and τ and (b) the calculation method

Fig. 6.2 shows the experimental setup for measuring the distributions of P and τ in this work. The magnet revolution is provided by using a motor to rotate the magnet

holder at a speed of n_m. The motor is directly connected to the magnet holder. The MCF slurry carrier is rotationally driven at a speed of n_c by another motor via a set of belt/pulleys. Guo and Wu [26] confirmed that the rotary magnetic field establishes a circular interacting area between the MCF slurry and the workpiece. This interacting area is centred at the rotational axis of the magnet holder, i.e. at the revolution axis of the magnet. Supposedly the particles within the MCF slurry are symmetrically distributed about the revolution axis of the magnet. Thus, the pressures and shear stresses at points located some fixed distance *d* from the centre of the interacting area should be identical. Subsequently, the distributions of *P* and τ over the interacting area can be obtained if the distributions of *P* and τ along a radius of the circular interacting area have been predetermined.

To obtain the radial distributions of *P* and τ, a PMMA workpiece (L40 mm × W40 mm × t9 mm) with a rib of dimensions L40 mm × W4 mm × t2.5 mm was installed on a worktable via a fixture and a 3-component dynamometer (9256A1 by Kistler Co., Ltd.). The dynamometer recorded the polishing forces acting on the top surface of the rib. To ensure a circular interacting area, a PMMA plate (2 mm in thickness) with a rectangular through hole (L40.3 mm × W4.3 mm) was also affixed to the worktable via an aluminium plate. The height of the aluminium plate was determined such that the top surfaces of the PMMA plate and the rib were vertically level.

Prior to measuring the pressure and shear stress, the *x*-axial position of the MCF slurry carrier was adjusted so that the *y*-axial central line of the rib just passed through the centre of the interacting area (i.e. the axis of the magnet holder). The *y*-axial location of the MCF slurry was adjusted by moving the MCF slurry carrier forward or backward so that the outer rim of the circular interacting area just contacted the frontal end of the rib. Subsequently, the carrier was shifted forward at an interval *h* along the *y*-axis. Each step was held for around 3 s. Under these conditions, the forces acting on the top face of the rib increased in a step-wise fashion from $F_{n,i-1}$ or $F_{t,i-1}$ to

$F_{n,i}$ or $F_{t,i}$ (i = 1, 2, …) as shown in Fig. 6.2(b). Consequently, the force increments from step i–1 to step i were obtained as $f_{n,i} = F_{n,i} - F_{n,i-1}$ and $f_{t,i} = F_{t,i} - F_{t,i-1}$. The associated pressure P_i and shear stress τ_i generated in the area A_i were computed by dividing $f_{n,i}$ and $f_{t,i}$ by the area A_i (i = 1, 2, …). From these, the radial distributions of P_i and τ_i (i = 1, 2, …) were obtained.

Fig. 6.3 shows a photograph of the experimental setup constructed in the laboratory. A disc-shaped neodymium permanent magnet (ϕ18 mm × t10 mm) with a magnetic field strength of 0.4 T was set at an eccentricity r of 4.5 mm. Considering the sensitivity of the measurement system composed of the dynamometer (−10 pC/N (F_x, F_y) and −13 pC/N (F_z)), a charge amplifier (0.01–9990 pC/M.U.) and an oscilloscope (2 mV/div – 10 V/div), h was set at 2 mm such that the forces acting on each area A_i (i =1, 2, ...) could be distinctly detected. Thus all identical areas A_i are calculated as A_i = $h \times 4 = 2 \times 4 = 8$ mm^2 (i = 1, 2, …). The MCF slurry consists of HQ CIPs (58 wt.%, median diameter ~2 μm, BASF made), water based MF (27 wt.%), Al_2O_3 abrasives (12 wt.%, median size ~1 μm) and α-cellulose (3 wt.%). The slurry composition was retained constant throughout the experiment and supplied in 1 ml quantities.

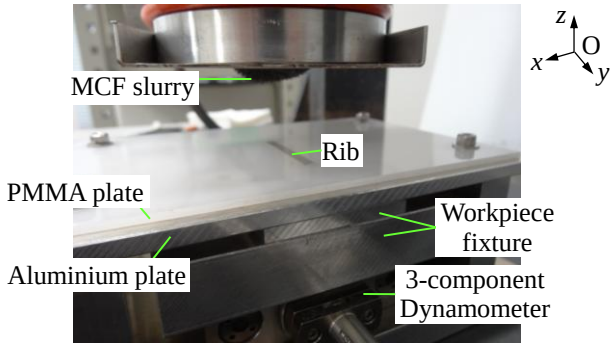

Fig. 6.3 A photograph of the experimental setup

The effects of three MCF polishing process parameters namely n_m, n_c and Δ were investigated by a classic one-factor-at-a-time experimental approach. In this approach, one parameter is varied while the others are retained constant (see Table 6.1). Under each combination of the process parameters (e.g. test No. 1), the pressure and shear

stress were measured in triplicate, and the reported values are the averages of these three measurements.

Table 6.1 Combinations of the process parameters for measurement of pressure/shear stress distributions and *MRR* investigation

Parameter \ Test No.	1	2	3	4	5	6	7
n_m (rpm)	1000	500	1500	1000	1000	1000	1000
n_c (rpm)	600	600	600	300	800	600	600
Δ (mm)	1	1	1	1	1	0.75	1.25

6.2.2 Spot polishing tests for MRR investigation

The *MRR* in MCF polishing was evaluated via spot polishing tests. Here no relative motion of the centre of the MCF carrier to the workpiece was imposed, and the sole circular interacting area was considered as the polishing spot. The experimental setup was the same as that used in the pressure/shear stress measurements, except that the PMMA plate and the PMMA workpiece (Fig. 6.2(a)) were replaced with a disc-shaped BK7 substrate (ϕ40 mm $\times$ t1 mm). BK7 is a popular optical glass for visible and ultraviolet applications due to its excellent optical properties. Seven individual BK7 substrates were used for obtaining a total number of 14 spots. Prior to MCF polishing tests, all substrates were pitch polished to a surface flatness less than 1 μm and a *rms* surface roughness of less than 1 nm. Similar to the pressure/shear stress measurements, the *MRR* investigation was conducted in a one-factor-at-a-time fashion, yielding seven rounds of spot polishing tests under various combinations of process parameters (Table 6.1). During polishing, the MCF slurry was renewed every 4 min. *y*-axial (see Fig. 6.2) cross-sectional profile of each obtained spot was measured by a stylus-based profilometer **(**Form Talysurf Intra by Taylor Hobson Inc.), and the *MRR* distributions were inferred from spot depths at

different radial positions. Each test was performed for 32 min and was repeated, yielding two spots for each combination of process parameters. The reported *MRR* is the mean value of the *MRRs* of the two spots.

6.3 Effects of pressure and shear stress on material removal

6.3.1 Distributions of pressure and shear stress

Fig. 6.4 shows a typical dynamometer output. As the MCF carrier shifts stepwise along the *y*-axis, the shear force F_t increases from 0, peaks at the 8th step and then declines to 0 at the 15th step. The normal force F_n monotonically increases with distance. The different trends of F_n and F_t can be understood from Fig. 6.2(a): before the frontal end of the rib reaches the centre of the interacting area, the negative *x*-component of F_t alone acts on the rib; consequently, F_t increases as the MCF carrier shifts in the negative *y*-direction. Once the frontal end of the rib has passed through the centre of the interacting area, the rib becomes subjected to the positive *x*-component of F_t. As the positive and negative *x*-components of F_t increasingly negate each other, F_t declines. Contrastingly, the normal force F_n acting on the rib monotonically increases because, as the MCF carrier shifts in the negative *y*-direction, it allows more interacting area between the rib and the MCF slurry. Once the entire MCF slurry has interacted with the rib, F_n remains at its final value while the positive and negative *x*-components of F_t are eventually completely balanced, and F_t falls to 0. The position where the shear force F_t peaks can be regarded as the centre of the interacting area. Thereby, the radial distributions of the forces were obtained by calculating the increments of normal and shear forces at each step. Then the distributions of the pressure and shear stress were attained as the increments of normal and shear forces at each step divided by the measurement area respectively.

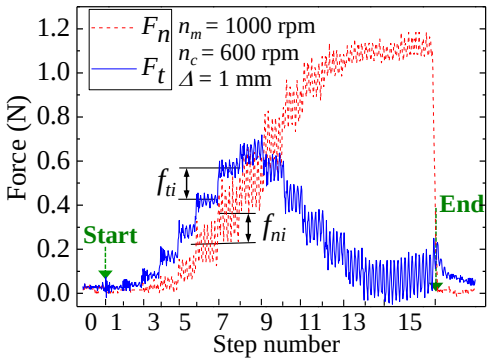

Fig. 6.4 A typical dynamometer output

6.3.1.1 Magnet revolution speed n_m

Using the data of Fig. 6.4, the distributions of pressure P and shear stress τ were plotted over the interacting area for varying values of three process parameters (n_m, n_c and Δ). Fig. 6.5 plots the distributions of P and τ as n_m is varied for fixed n_c and Δ. In Fig. 6.5(a), no obvious relationship appears between P and n_m, indicating that the magnet revolution speed n_m exerts a negligible effect on P. Contrastingly, τ is maximized at n_m = 1000 rpm (Fig. 6.5(b)), most likely for the following reason: as n_m increases, the magnetic lines of force change direction more rapidly. Consequently, the particles within the MCF slurry become more active and more of them interact with the work surface, increasing the shear stress τ. However, beyond a critical n_m (in the current work, n_m > 1000 rpm), particles rapidly slide over the work surface, with slight decrease in τ.

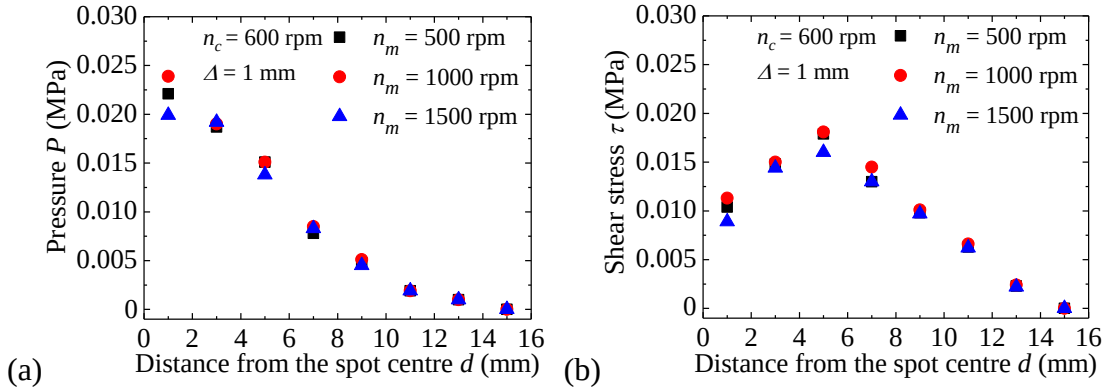

Fig. 6.5 Distributions of (a) P and (b) τ at different magnet revolution speeds n_m

6.3.1.2 MCF slurry carrier rotational speed n_c

Fig. 6.6(a) and (b) shows the distributions of P and τ at different MCF slurry carrier rotational speeds n_c but fixed n_m and Δ. Although both P and τ overall increase as n_c rises from 300 rpm to 800 rpm, when n_c is below 600 rpm, the increase in τ is much more pronounced than that in P. Once the n_c exceeds 600 rpm, τ increases only slightly, while P decreases slightly. It is briefly thought that the MCF slurry is assumed to move with the carrier; hence as n_c increases, the relative speed of the magnetic clusters within the MCF slurry increases; accordingly, more of the particles interact with the work surface per unit time; as the stiffness of the magnetic clusters is kept constant under the given magnetic field, the indented contact pressure of the abrasive particles on the work surface only increases slightly; contrastingly, the dragging of the MCF slurry in the working gap relative to the work surface enhances significantly, resulting in a greater increase in τ. However, at higher n_c (in the current work, n_c > 600 rpm), the MCF slurry easily splashes owing to the greater centrifugal force, resulting in a slight increase in τ and a slight decrease in P. Further detailed investigations will be carried out in the future work to explore the deeper reason.

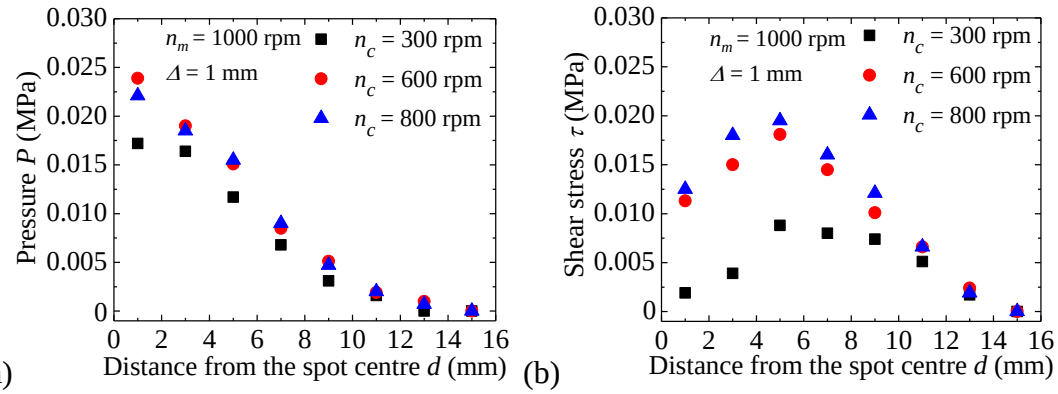

Fig. 6.6 Distributions of (a) P and (b) τ at different MCF slurry carrier rotational speeds n_c

6.3.1.3 Working gap Δ

Fig. 6.7 shows the distributions of P and τ at different working gaps Δ, with fixed

n_m and n_c. Both P and τ significantly increase as Δ is adjusted from 1.25 mm to 1 mm, and slightly increase as Δ falls from 1 mm to 0.75 mm. During this second phase, τ is slightly more affected than P. As Δ is reduced, the MCF slurry within the polishing zone (which is supplied at a constant amount) becomes more compressed and stiffer, eventually leading to increased indented pressure of the particles on the work surface; accordingly, the shear stress also increases when the stiffer MCF slurry is dragged in the decreased working gap relative to the work surface. However, as Δ is adjusted from 1 mm to 0.75 mm, these effects are small, and achieve a little pressure increase; contrastingly, more of the abrasive particles interact with the work surface and exert micro-cutting action, leading the increase of shear stress τ.

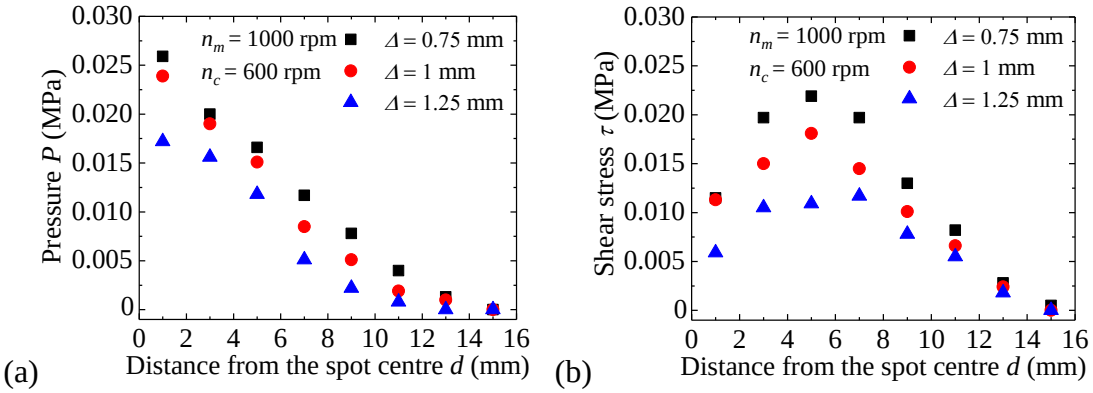

Fig. 6.7 Distributions of (a) P and (b) τ at different working gaps Δ

Obviously, regardless of the parameters, the force distributions show a similar pattern: P is higher toward the centre of the interacting area, i.e. the spot centre, and τ is maximized about 5 mm from the spot centre. To elucidate why the pressure P and the shear stress τ are distributed in this way under different rotary magnetic fields (n_m = 500 rpm, 1000 rpm and 1500 rpm), the behaviour of the used MCF slurry under a typical rotary magnetic field (n_m = 1000 rpm) was observed under a high-speed motion analysis microscope (VW6000 by Keyence Co., Ltd.).

Fig. 6.8(a) and (b) displays a facial view and a side view, respectively, of an instantaneous shape of the MCF slurry without interaction with the workpiece.

Evidently, the MCF slurry develops a reverse mountain shape with a circular base of diameter W and a maximum height H_{max} at the mountaintop. According to the motion analysis, most of the MCF slurry gathers around the magnet revolution centre, (i.e. the magnet holder axis) and possesses considerable stiffness. Consequently, P is highest at the centre of the interacting area. On-the-spot microscopic observation also revealed that the mountaintop is displaced from the centre of the circular base of the MCF slurry, but revolves around the central point at a radius of about 4.5 mm as the magnet revolves around its holder axis. Considering the eccentricity of the magnet (also 4.5 mm), it is inferred that most of the magnetic clusters gather around the magnet centre, i.e. the mountaintop. At this position, the velocity of the MCF slurry relative to the work surface is sufficient to maximize the shear stress.

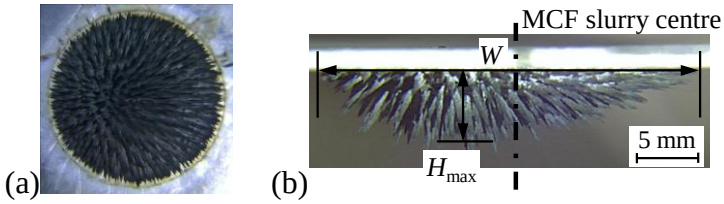

Fig. 6.8 (a) A facial view and (b) a side view of an instantaneous shape of MCF slurry under a rotary magnetic field

6.3.2 *MRRs*

By measuring the polishing spot, i.e. the circular interacting area, a 3D profile of a typical polishing spot was obtained as exhibited in Fig. 6.9(a). The procedure for obtaining the 3D profile was as follows: at first, a series of cross-sectional profile curves of the polishing spot were measured along y-axis (see Fig. 6.2(a)) at intervals of 0.5 mm on x-axis with the stylus-based profilometer. Then, the data of each cross-sectional profile curve was used to produce the 3D profile. As shown in Fig. 6.9(a), the polishing spot area appears a circular shape with a diameter of about 30 mm and a protrusion occurs in the central area of the spot owing to the much smaller speed of the MCF slurry relative to the workpiece in this area. Obviously, the

polishing spot is different from that in MRF process which is usually in the shape of a backward D and has a deepest and widest portion approximately at the position of closest approach between the workpiece and the wheel surface [7]. Among the cross-sectional profile curves, only one passes through the polishing spot centre where the material removal (*MR*), i.e. the spot depth, is smallest as shown in Fig. 6.9(b). It can be seen from Fig. 6.9(b) that this cross-sectional profile that is measured along A–A (see Fig. 6.9(a)) displays a characteristic symmetric W-shape. Little material is removed from the centre of the spot. The maximum spot depth, indicating the region of maximal material removal (MR_{max}), occurs at a circle with a radius of about 9.5 mm. Similar shapes and cross-sectional profiles of the polishing spots have been also obtained in other tests, i.e. test Nos.2–7; however, maximum material removals occurred at circles with radii of 8.2–10.2 mm depending on the process parameters (Table 6.1). Consequently, as shown in Fig. 6.9(b), a radial position *d*, i.e. a distance from the spot centre, and the material removal (i.e. the spot depth) at the position *d*, MR_d, were determined. The material removal rate at the position *d*, MRR_d, is obtained as MR_d divided by the polishing time.

As mentioned in Section 6.1, this work aims to clarify the relationships between the polishing forces and the *MRR*. To this end, the experimentally obtained pressure *P*, shear stress τ and *MRR* at different positions *d* (i.e. P_d, τ_d and MRR_d) are tabulated in Table 6.2. The data in Table 6.2, showing the effects of the process parameters n_m, n_c and Δ on the *MRR*, are plotted in Fig. 6.10 (a–c), respectively. Regardless of *d*, distinct linear relationships exist between *MRR* and n_m, between *MRR* and n_c, and between *MRR* and Δ. However, the effect of n_m on the *MRR* is weak (Fig. 6.10 (a)), and can be ignored in practice. Although larger n_m causes the locations of magnetic force lines to change more rapidly, thereby promoting particles dispersion within the MCF slurry, this parameter does not alter the quantity and stiffness of the magnetic clusters containing abrasive particles. Consequently, it induces no significant variation in the *MRR*. On the other hand, the *MRR*s are strongly linearly correlated with n_c (Fig.

6.10(b)). The strong linear correlation between the *MRRs* and n_c agrees with the Preston equation: $MRR = C_p PV$, in which the *MRR* is proportional to the relative speed between the work surface and the polishing tool [27]. The larger the n_c is, the higher the speed of MCF slurry relative to the work surface becomes. As more of the abrasive particles interact with the work surface per unit time at larger n_c, the *MRR* increases. The working gap Δ exerts a strong linear negative effect on the *MRRs* (Fig. 6.10(c)). This trend can be explained as follows: given that the supplied amount of MCF slurry is constant, the smaller the Δ, the more the MCF slurry is compressed, and active abrasive particles become concentrated within the polishing zone. Additionally, as Δ decreases, the pressure and shear stress increase (see Fig. 6.7), with associated increase in cutting depth of the abrasive particles. Eventually a marked increase in the *MRR* is achieved.

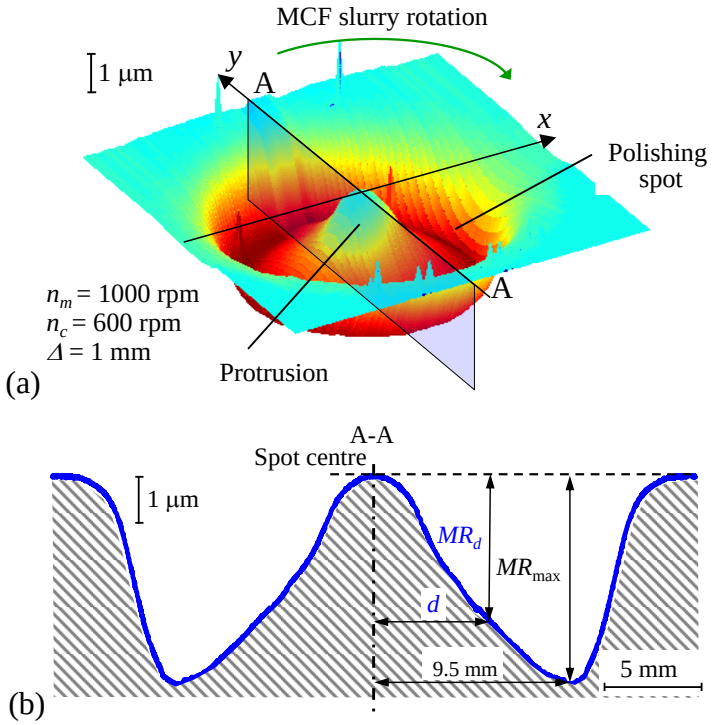

Fig. 6.9 (a) A 3D profile and (b) a cross-sectional profile of a typical polishing spot obtained at n_m = 1000 rpm, n_c = 600 rpm and Δ =1 mm

Table 6.2 Pressure P, shear stress τ and MRR at different positions d experimentally obtained in the seven tests

d (mm)	Test No. 1			Test No. 2			Test No. 3		
	P_d (MPa)	τ_d (MPa)	MRR_d (μm/min)	P_d (MPa)	τ_d (MPa)	MRR_d (μm/min)	P_d (MPa)	τ_d (MPa)	MRR_d (μm/min)
3	0.0190	0.0150	0.0474	0.0187	0.0148	0.0570	0.0192	0.0144	0.0459
5	0.0151	0.0181	0.0837	0.0151	0.0179	0.1018	0.0138	0.0160	0.0869
7	0.0085	0.0145	0.1106	0.0078	0.0130	0.1288	0.0083	0.0130	0.1152
9	0.0051	0.0101	0.1328	0.0048	0.0098	0.1446	0.0045	0.0097	0.1296
11	0.0019	0.0066	0.1240	0.0019	0.0063	0.1227	0.0019	0.0062	0.1204
13	0.001	0.0024	0.0299	0.001	0.0023	0.0258	0.001	0.0022	0.0399

d (mm)	Test No. 4			Test No. 5			Test No. 6			Test No. 7		
	P_d (MPa)	τ_d (MPa)	MRR_d (μm/min)	P_d (MPa)	τ_d (MPa)	MRR_d (μm/min)	P_d (MPa)	τ_d (MPa)	MRR_d (μm/min)	P_d (MPa)	τ_d (MPa)	MRR_d (μm/min)
3	0.0164	0.0039	0.0196	0.0185	0.018	0.0607	0.0200	0.0197	0.0361	0.0156	0.0105	0.0256
5	0.0117	0.0088	0.0361	0.0155	0.0195	0.1379	0.0166	0.0219	0.1268	0.0118	0.0109	0.0431
7	0.0068	0.0080	0.0582	0.0090	0.0160	0.1608	0.0117	0.0197	0.2191	0.0051	0.0117	0.0494
9	0.0031	0.0074	0.0827	0.0047	0.0121	0.1812	0.0078	0.0130	0.2279	0.0022	0.0078	0.0505
11	0.0016	0.0051	0.0597	0.0020	0.0066	0.1652	0.004	0.0082	0.1945	0.0008	0.0055	0.0315
13	0	0.0017	0.0216	0.0007	0.0019	0.0344	0.0013	0.0028	0.0830	0	0.0018	0.0087

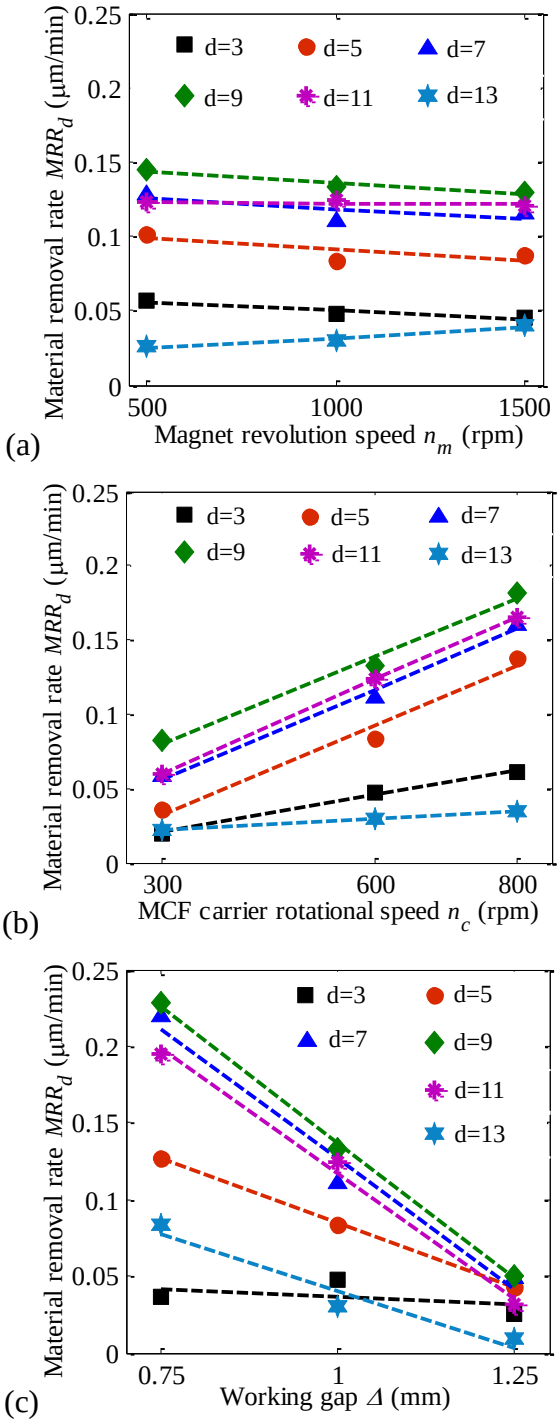

Fig. 6.10 Effects of (a) magnet revolution speed n_m, (b) MCF slurry carrier rotational speed n_c and (c) working gap Δ on the *MRR*

6.3.3 Relationship between the pressure/shear stress and the *MRRs*

As mentioned in Section 6.2.1, in conventional polishing process where the pressure is intentionally applied and uniformly distributed over the polishing zone, the

MRR depends on the pressure *P* and the velocity *V* of the polisher relative to the workpiece, but is independent of the shear stress τ. These three dependent quantities are related by Preston's equation, $MRR = C_p PV$ [27]. However, Preston's equation seems non-applicable to MCF polishing because the maximum depths of the polishing spots are located about 8.2–10.2 mm from the spot centre. According to Preston's equation, this distance should be half the spot radius, i.e. about 7.5 mm. This indicates that, besides the pressure *P* and the relative velocity *V*, *MRR* also depends on shear stress τ. Therefore, to comprehensively understand the material removal behaviours in MCF polishing, the relationships between the pressure *P*/shear stress τ and the *MRR* should be clarified. The model proposed below (Eq. (6.1)) relates the MRR_d to the pressure P_d, the shear stress τ_d and the relative velocity V_d ($= 2\pi dn_c$).

$$MRR_d = C_{pmcf} P_d^{\alpha} \tau_d^{\beta} V_d \tag{6.1}$$

The coefficient C_{pmcf} quantifies the ability of the MCF slurry to polish a specified work-piece under a specific configuration, and α and β describe the effects of *P* and τ, respectively, on the *MRR*. As an approximate quantification, the values of C_{pmcf}, α and β for all seven tests conducted under their respective process parameter settings (Table 6.1) are determined from the experimentally obtained data (Table 6.2) by least-squares fitting. That is, the values of C_{pmcf}, α and β are determined such that, when these values are inserted into Eq. (6.1), the *MRR* at a given radial position *d* of the polishing spot matches the experimentally obtained value. However, before performing detailed calculations of C_{pmcf}, α and β, their ranges are estimated as described below.

For a given test (e.g. Test No. 1 in Table 6.2), under the specified process parameters, the C_{pmcf}, α and β should be independent of the radial position *d* since the process parameters are retained constant. Computing the logarithm of Eq. (6.1) at six selected radial positions (*d* = 3, 5, 7, 9, 11 and 13 mm) yields six linear equations (Eq. (6.2)).

$$\ln MRR_d = \ln C_{Pmcf} + \alpha \ln P_d + \beta \ln \tau_d + \ln V_d \qquad d = 3, 5, 7, 9, 11 \text{ and } 13 \text{ mm} \tag{6.2}$$

Subsequently, by combining three linear equations selected randomly from Eq. (6.2), twenty simultaneous equations systems are obtained (Eq. (6.3)).

$$\begin{bmatrix} 1 & \ln P_{d,j} & \ln \tau_{d,j} \\ 1 & \ln P_{d,k} & \ln \tau_{d,k} \\ 1 & \ln P_{d,l} & \ln \tau_{d,l} \end{bmatrix} \begin{bmatrix} \ln C_{pmcf} \\ \alpha \\ \beta \end{bmatrix} = \begin{bmatrix} \ln MRR_{d,j} - \ln V_{d,j} \\ \ln MRR_{d,k} - \ln V_{d,k} \\ \ln MRR_{d,l} - \ln V_{d,l} \end{bmatrix};$$

$$j = 1\text{–}6,\ k = 1\text{–}6,\ l = 1\text{–}6;\ j \neq k \neq l \qquad (6.3)$$

Since the values of MRR (μm/min), V ($2\pi dn_c$, mm/min), P (MPa) and τ (MPa) are already known at different radial positions d (see Table 6.2), twenty sets of $\ln C_{pmcf}$, α and β are obtained by solving the twenty simultaneous equations in the above linear system. The results are summarized in Table 6.3. In Test No. 1, the $\ln C_{pmcf}$, ranges from −21.3 to −12.6; α ranges from −2.61 to 0.91, and β ranges from –1.47 to 4.42. The ranges of $\ln C_{pmcf}$, α and β in the remaining six tests (i.e. test Nos. 2–7), are listed in Table 6.4.

Table 6.3 Estimation results of $\ln C_{pmcf}$, α and β in Test No. 1

No.	1	2	3	4	5	6	7	8	9	10	11	12	13	14	15	16	17	18	19	20
$\ln C_{pmcf}$	-18.1	-18.3	-17.7	-18.5	-17.4	-13.1	-18.6	-16.7	-21.3	-19.8	-15.6	-14.7	-13.5	-13.4	-14.6	-13.5	-14.3	-12.6	-14.5	-13.5
α	-0.01	-0.03	0.03	-0.01	-0.02	-0.63	0.06	-0.24	0.91	0.51	0.26	-0.05	-0.51	-0.53	-0.58	-1.48	-0.83	-2.61	-0.90	-0.56
β	0.29	0.27	0.34	0.20	0.47	2.10	0.10	0.90	-1.47	-0.67	0.63	1.13	1.87	1.91	1.76	2.97	2.10	4.42	2.14	1.92

Table 6.4 Estimation ranges of $\ln C_{pmcf}$, α and β for the seven tests

	$\ln C_{pmcf}$		α		β	
Test No.	Lower limit	Upper limit	Lower limit	Upper limit	Lower limit	Upper limit
1	-21.3	-12.6	-2.61	0.91	-1.47	4.43
2	-25.1	-12.6	-1.51	2.22	-3.83	3.08
3	-17.1	-11.0	-1.57	-0.08	0.68	3.64
4	-27.4	-4.36	-0.98	-0.20	-1.74	4.09
5	-22.5	-11.4	-1.61	1.07	-2.02	2.75
6	-17.7	-10.9	-3.18	2.02	-1.46	5.34
7	-24.1	8.32	-0.30	1.65	-2.87	5.55

Having estimated the ranges of $\ln C_{pmcf}$, α and β, more precise values in each test were calculated by least-squares fitting. The calculation procedure is shown in Fig. 6.11. Since α and β should be non-negative in the actual polishing process, their lower limits values were set to zero in all calculations. $\ln C_{pmcf}$, α and β were incremented by 0.025 at each step to ensure calculation accuracy. The *MRR* calculated from Eq. (6.1), using the data in Table 6.2 at each *d*, is denoted MRR_{cal_d}. Following the procedure of Fig. 6.11, the $\ln C_{pmcf}$, α and β for which the *MRR* calculated by Eq. (6.1) acceptably fitted the experimental *MRR* was eventually found for all seven tests. The more precise values of $\ln C_{pmcf}$, α and β for the seven tests are summarized in Table 6.5. To confirm that the MRR_{cal_d} obtained from Eq. (6.1) using the final $\ln C_{pmcf}$, α and β indeed fits the experimental MRR_{d} values, the $MRR_{\mathrm{Cal.}_d}$s at radial positions d ($d = 3, \ldots,$ 13 mm) and the radial distributions of the experimental MRR_d for the tests Nos. 1–7 are compared in Fig. 6.12. In this figure, the radial distributions of the experimental MRR_d were plotted using the *MRR* values calculated from the data of the right halves of the cross-sectional profiles of polishing spots. The MRR_{cal_d} favourably agree with the experimental MRR_d, validating the obtained $\ln C_{pmcf}$, α and β in Table 6.5.

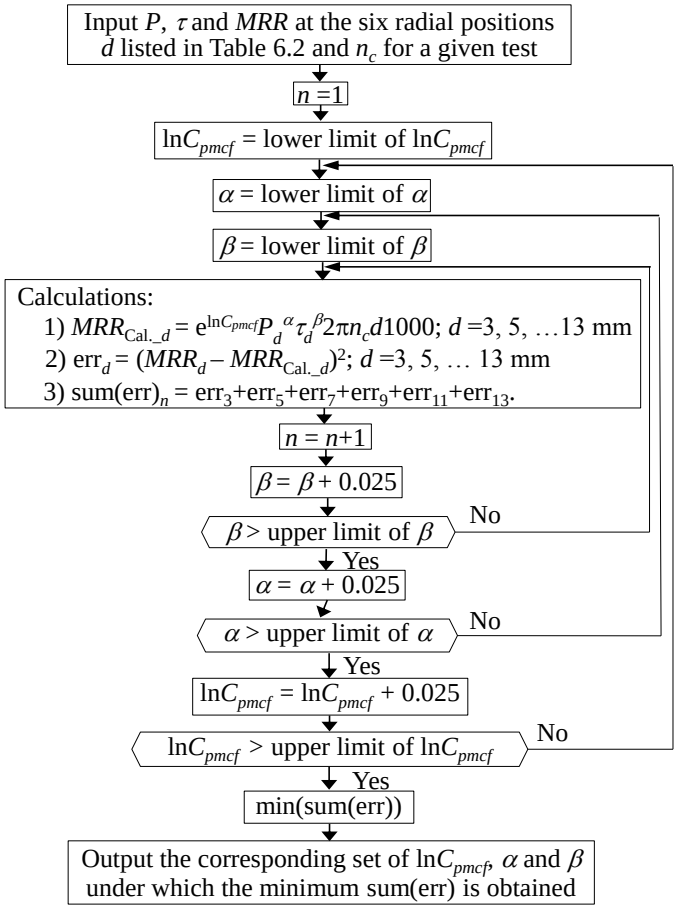

Fig. 6.11 Calculation procedure of the detailed lnC_{pmcf}, α and β in each test using least-squares fitting

Table 6.5 lnC_{pmcf}, α and β for the seven tests calculated by least-squares fitting

Test No.	lnC_{pmcf}	α	β
1	-16.05	0	0.75
2	-15.35	0	0.875
3	-15.975	0	0.75
4	-14.5	0	0.975
5	-16.05	0	0.75
6	-16.125	0	0.65
7	-16.525	0.225	0.525

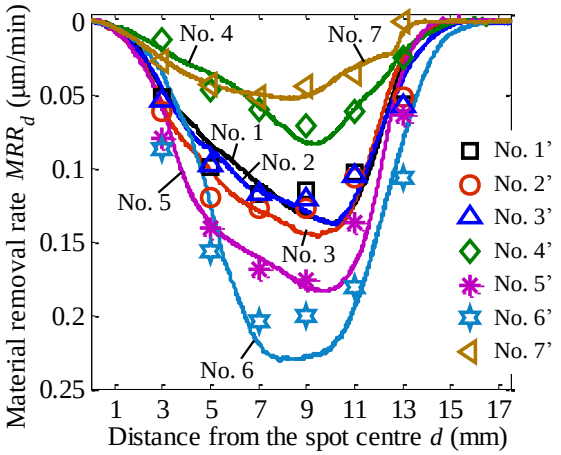

Fig. 6.12 Comparison of the $MRR_{Cal.\_d}$ (scatter points: Nos. 1'–7') at radial positions d (d = 3, …, 13 mm) and the radial distributions of the experimental MRR_d (solid lines: Nos. 1–7) in the seven tests

Table 6.5 shows that β exceeds α for all combinations of process parameters, indicating that the *MRR* in MCF polishing is governed more by shear stress τ than by pressure *P*. Miao et al. [8,9] reached a similar conclusion in MRF; that material removal is dominated by shear stress. In most of the cases investigated here, α was close to zero, implying that the pressure exerts minimal influence on the *MRR* in MCF polishing. Notably, the value of α at Δ = 1.25 mm (Test No. 7) was much larger than at Δ = 0.75 mm (Test No. 6) and at Δ = 1 mm (Test Nos. 1–5), implying that as the working gap increases, pressure contributes more to the *MRR*.

6.4 Removal function

6.4.1 Experimental details

For removal function investigation, 26 individual BK7 substrates were used for obtaining a total number of 51 spots. The effects of four MCF polishing process parameters namely r, n_m, n_c and Δ were investigated by the classic one-factor-at-a-time experimental approach (see Table 6.6). 17 rounds of spot polishing tests were yielded under various combinations of process parameters. Each test was performed for 32 min and in triplicate, yielding three spots for each combination of process parameters.

The reported *MRR* values are the averages of these three spots. During polishing, the MCF slurry was renewed every 4 min. Cross-sectional profile of each obtained spot was measured by a stylus-based profilometer **(**Form Talysurf Intra by Taylor Hobson Inc.). The *MRR* values were inferred from spot depths.

Table 6.6 The combinations of process parameters for removal function investigation tests

Parameter \ Test No.	1	2	3	4	5	6	7	8	9	10	11	12	13	14	15	16	17
r (mm)	4.5	4.5	4.5	4.5	4.5	4.5	4.5	4.5	4.5	4.5	4.5	4.5	4.5	0	1.5	3	6
n_m (rpm)	1000	500	750	1250	1500	1000	1000	1000	1000	1000	1000	1000	1000	1000	1000	1000	1000
n_c (rpm)	600	600	600	600	600	300	450	700	800	600	600	600	600	600	600	600	600
Δ (mm)	1	1	1	1	1	1	1	1	1	0.75	0.875	1.125	1.25	1	1	1	1

For convenience, Fig. 6.13(a) again exhibits the 3D profile of a typical polishing spot, which is considered as the removal function. The removal function appears a circular shape and a protrusion occurs in the central area of the spot owing to the much smaller speed of the MCF slurry relative to the workpiece in this area. Obviously, the removal function is different from that in MRF process which is usually in the shape of a backward D and has a deepest and widest portion approximately at the position of closest approach between the workpiece and the wheel surface [7]. To characterize the removal function, Fig. 6.13(b) again shows a typical cross-sectional profile of the removal function, which passes through the polishing spot centre where the material removal (*MR*), i.e. the spot depth, is smallest. This cross-sectional profile that is measured along A–A (see Fig. 6.13(a)) displays a characteristic symmetric W-shape. Little material is removed from the centre of the spot. The maximal spot depth, indicating the region of maximal depth removal ($dR_{\max}$), occurs at a circle with a certain radius. Consequently, as shown in Fig. 6.13(b), the removal function is

characterized by its radius R, the maximal depth removal rate (dRR_{max}, dR_{max} divided by the polishing time) and the radial position d_{max} (i.e. a distance from the spot centre) where the dRR_{max} occurs. Volumetric material removal (VR) was calculated using integration according to the data of the right half of the cross-sectional profile as shown in Fig. 6.13(b), and the volumetric material removal rate (VRR) was also reported as VR divided by the polishing time.

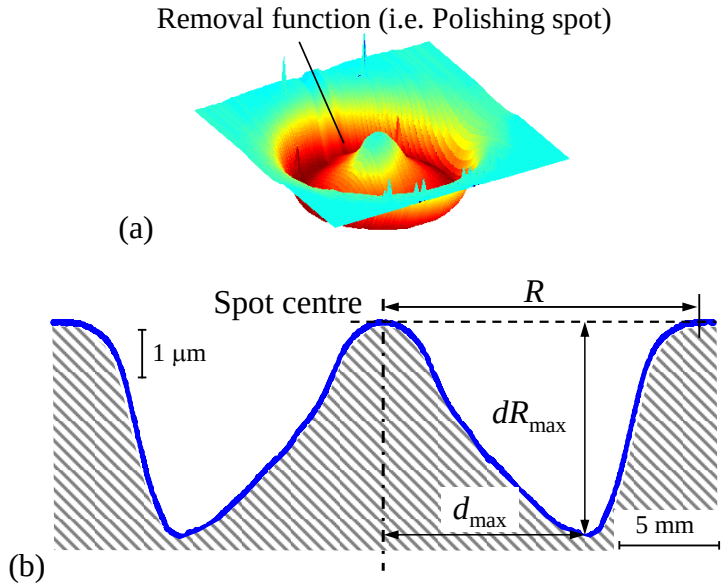

Fig. 6.13 (a) A 3D removal function and (b) a cross-sectional profile of a typical removal function obtained at n_m = 1000 rpm, n_c = 600 rpm, Δ =1 mm

6.4.2 Effects of process parameters on removal function

6.4.2.1 Magnet revolution speed n_m

Fig. 6.14 manifests the radial distributions of dRR under different magnet revolution speeds n_m and the effect of the n_m on the characteristics of removal function. The radius of the removal function R increases by 5.08 % and the d_{max} rises up by 7.32 % while the dRR_{max} decreases by 2.42 % and the VRR declines by 5.25 % as the n_m increasing from 500 rpm to 1500 rpm. The reason can be considered as follows: the higher the n_m is, the faster the directions of the magnetic lines of force change and the larger the centrifugal force acting on the abrasive particles is. This leads the particles within the MCF slurry

to become more active and move far away from the magnet revolution centre slightly, resulting in the slight increase in the R and d_{max}. Moreover, the larger the n_m is, the more rapidly particles slide over the work surface and hence the dRR_{max} and VRR decrease a little. However, both the VRR and the characteristics of removal function overall appear insensitive to the magnet revolution speed, meaning that the influence of the n_m on the removal function can be ignored in practical cases. Although when the n_m is set at a larger value, the change in the location of magnetic lines of force becomes quicker and subsequently the dispersion of particles within the MCF slurry is promoted and the restoring abilities of the MCF slurry is enhanced, the amount and stiffness of magnetic clusters containing abrasive particles are not changed with the increase in the n_m, and thus the extinct variation of removal function is not obtained.

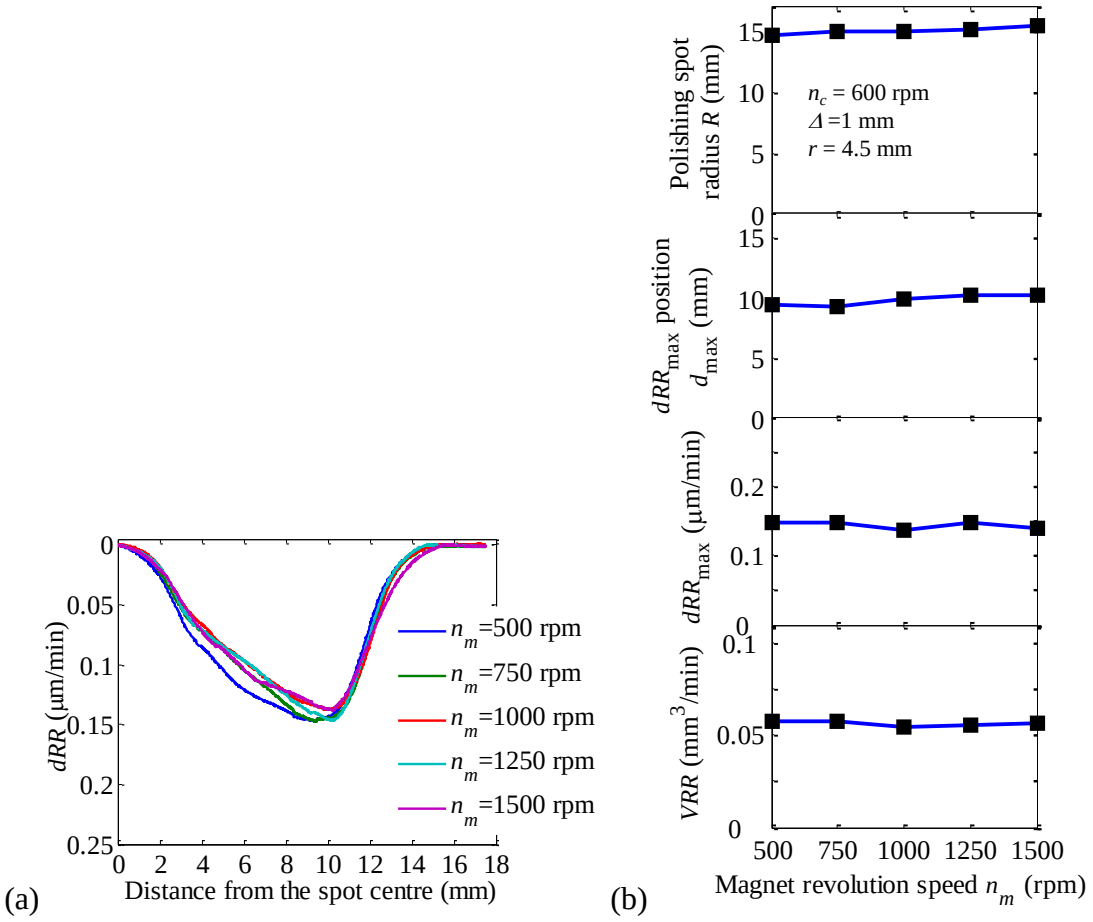

Fig. 6.14 (a) Radial distributions of dRR under different magnet revolution speeds n_m and (b) Effect of the n_m on the characteristics of removal function

6.4.2.2 MCF slurry carrier rotational speed n_c

Fig. 6.15 shows the radial distributions of *dRR* under different MCF slurry carrier rotational speeds n_c and the effect of the n_c on the characteristics of removal function the removal function. The *R* only decreases by 3.33 % as the n_c increasing from 300 rpm to 450 rpm and then keeps constant approximately. The d_{max} rises up by 8.11 % as the n_c increasing from 300 rpm to 800 rpm. Both the dRR_{max} and *VRR* manifest a strong positive linear correlation with the n_c. The centrifugal force acting on the abrasive particles increases as n_c increases, with a little increase in d_{max}. The strong linear correlation between the *MRRs* and n_c agrees with the Preston equation: $MRR = C_p PV$, in which the *MRR* is proportional to the relative speed between the work surface and the polishing tool [27].

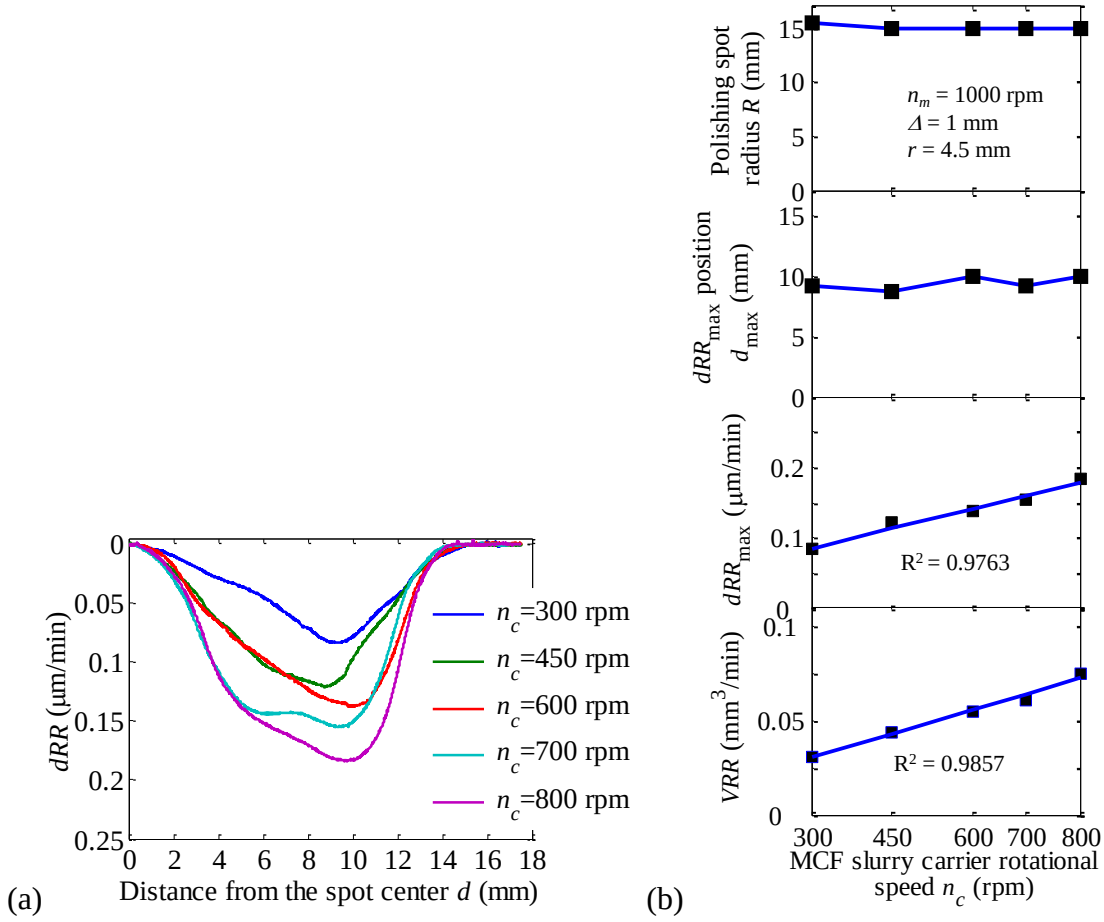

Fig. 6.15 (a) Radial distributions of *dRR* under different MCF slurry carrier rotational speeds n_c and (b) Effect of the n_c on the characteristics of removal function

6.4.2.3 Working gap Δ

Fig. 6.16 shows the radial distributions of *dRR* under different working gaps Δ and the effect of the Δ on the characteristics of removal function. The *R* declines by 15.15 % as the Δ increasing from 0.75 mm to 1.25 mm. The d_{max} is maximized at Δ = 1 mm, which is still not clear. Both the dRR_{max} and *VRR* exhibit a strong negative linear correlation with the Δ. This trend can be explained as follows: given that the supplied amount of MCF slurry is constant, the smaller the Δ, the more the MCF slurry is compressed, and active abrasive particles become concentrated within the polishing zone and the interacting area is expanded, leading to a larger *R*. Additionally, as Δ decreases, the cutting depth of the abrasive particles increases. Eventually a marked increase in the *MRR* is achieved.

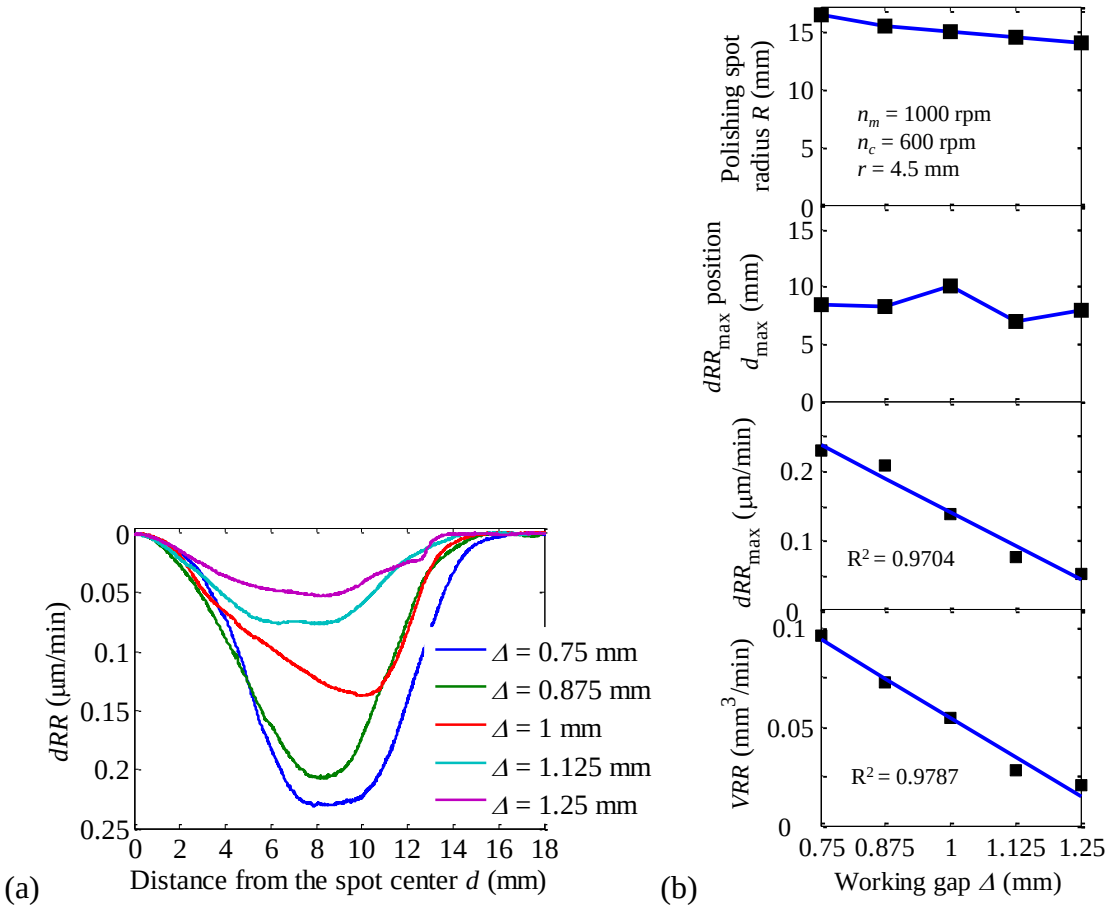

Fig. 6.16 (a) Radial distributions of *dRR* under different working gaps Δ and (b) Effect of the Δ on the characteristics of removal function

6.4.2.4 Magnet eccentricity *r*

Fig. 6.17 displays the radial distributions of *dRR* under different magnet eccentricities *r* and the effect of the *r* on the characteristics of removal function. The radius *R* of the removal function increases by 6.67 % with the *r* increasing from 0 to 4.5 mm. At *r* = 3 mm, both *VRR* and dRR_{max} are maximized while d_{max} is minimized. It is noteworthy that $d_{max}s$ in the cases of *r* = 0 mm and *r* = 1.5 mm are positions of 8.5 mm and 7 mm from the spot centre, respectively, which are close to the magnet edge.

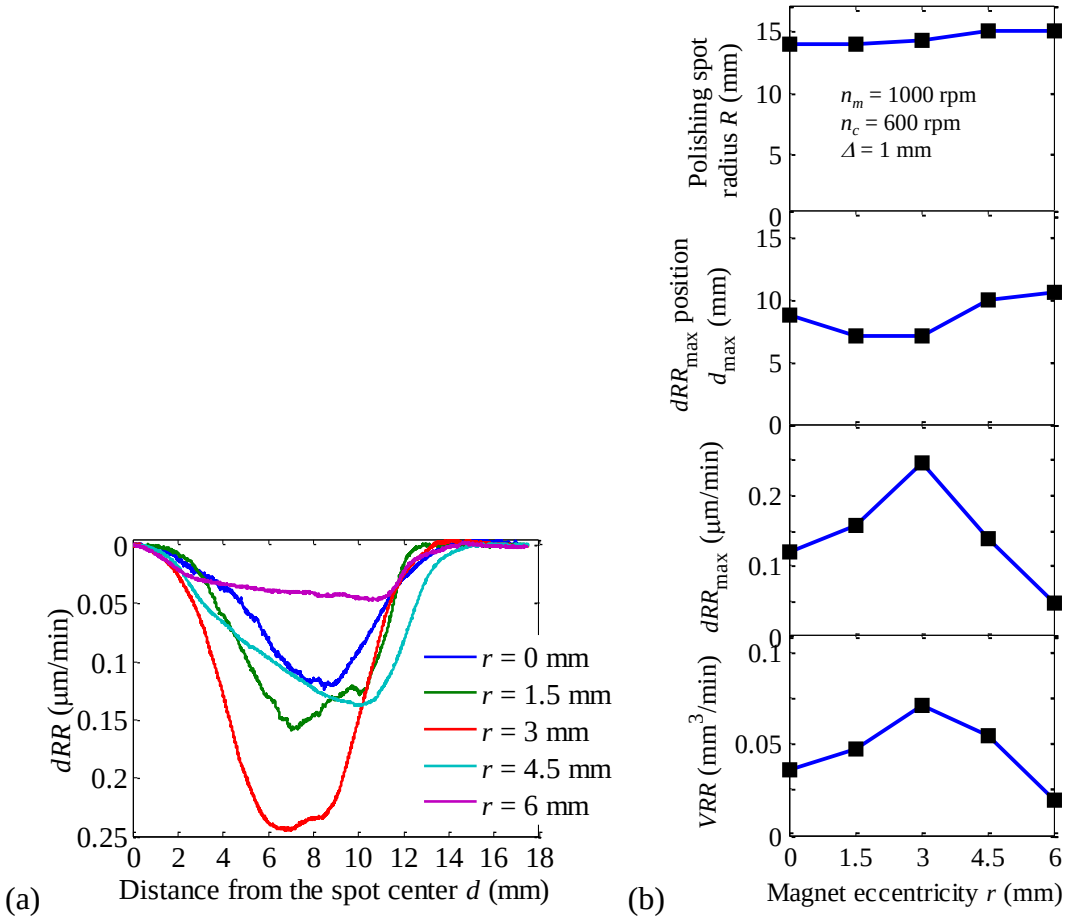

Fig. 6.17 (a) Radial distributions of *dRR* under different magnet eccentricities *r* and (b) Effect of the *r* on the characteristics of removal function

To elucidate why the removal function varies with magnet eccentricity in this fashion, the behaviours of the used MCF slurry under constant n_m = 1000 rpm and different magnet eccentricities were observed under a high-speed motion analysis

microscope (VW6000 by Keyence Co., Ltd.). Fig. 6.18 exhibits that the terminal shapes of MCF slurry at different eccentricities *r* without interacting with work surface. As the *r* increases, the directions of magnetic lines of force change more violently, resulting that the magnetic clusters within MCF slurry revolve around the magnet revolution axis violently. As $r < 3$ mm in the present work, only a few magnetic clusters within MCF slurry can revolve around magnet revolution axis and the MCF slurry shape restoring ability is extremely poor. Consequently, uniform distribution of MCF slurry can not be obtained as in Fig. 6. 18(a) and (b). At the magnet edge, MCF slurry containing abrasive particles possesses maximal relative speed to work surface, maximizing the *MRR* at this position. When $r > 3$ mm in this work, MCF slurry is frequently dragged to revolve around the magnet revolution axis and abrasive particles contained in MCF slurry slide over the work surface vary rapidly, decreasing the *MRR*.

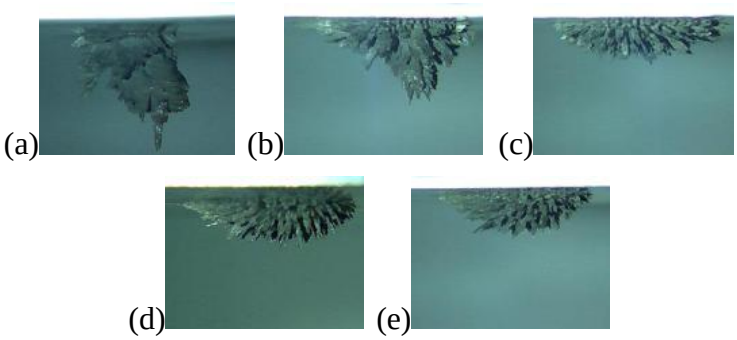

Fig. 6.18 Terminal external shapes of MCF slurry at different eccentricities *r* (namely (a) 0 mm, (b) 1.5 mm, (c) 3 mm, (d) 4.5 mm and (e) 6 mm) without interacting with work surface

6.4.3 Effects of α-cellulose concentration on removal function

For removal function investigation, 6 individual BK7 substrates were used for obtaining a total number of 12 spots. The effect of the concentration of α-cellulose was investigated by the classic one-factor-at-a-time experimental approach (see Table 6.7). The experiments were carried out at $r = 4.5$ mm, $n_m = 1000$ rpm, $n_c = 500$ rpm and $\Delta =$

1 mm. 4 rounds of spot polishing tests were yielded under various combinations of slurry compositions. Each test was performed for 32 min and in triplicate, yielding three spots for each combination of process parameters. The reported *MRR* values are the averages of these three spots. During polishing, the MCF slurry was renewed every 4 min. Cross-sectional profile of each obtained spot was measured by a stylus-based profilometer **(**Form Talysurf Intra by Taylor Hobson Inc.). The *MRR* values were inferred from spot depths.

Table 6.7 The combinations of slurry composition for removal function investigation tests

HQ CIPs (~ϕ2 μm)	Al_2O_3 abrasives (~1 μm)	Water based MF	α-cellulose
58	12	30	0
		28.5	1.5
		27	3
		25.5	4.5

Fig. 6.19 displays the radial distributions of *dRR* under different α-cellulose concentrations and the effect of the α-cellulose concentration on the characteristics of removal function. The radius *R* of the removal function increases by 27.1 % with the concentration increasing from 0 wt.% to 4.5 wt.%. Both *VRR* and dRR_{max} peak at concentration of 3 wt.%. d_{max} is maximized at concentration of 1.5 wt.%. This trend can be explained as follows: the larger the concentration of the α-cellulose is, the larger the viscosity of the slurry becomes, leading to a larger interacting area and a larger material removal. However, the material removal switches to decrease at a relatively high concentration (more than 3 wt.% in the current work) probably because the dispersity of particles is worsened and the slurry is easily dried.

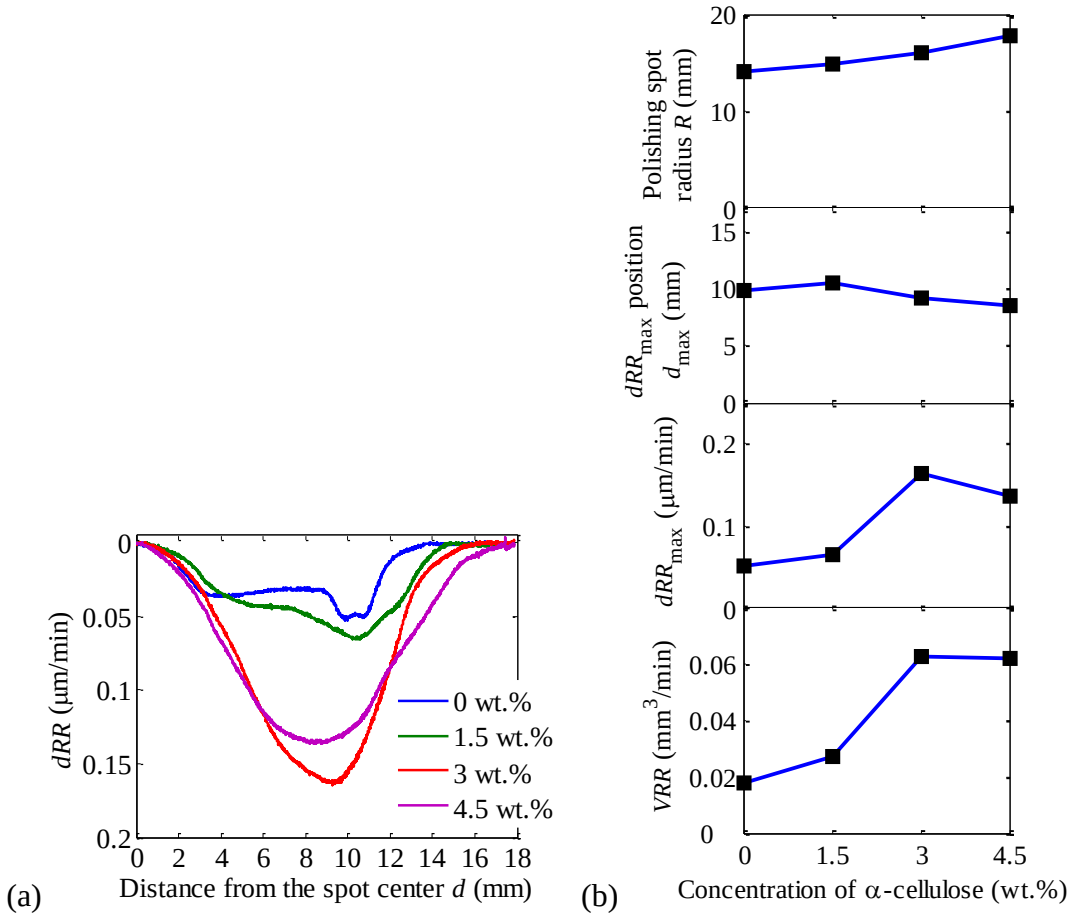

Fig. 6.19 (a) Radial distributions of *dRR* under different α-cellulose concentrations and (b) Effect of the α-cellulose concentration on the characteristics of removal function

6.4.4 Magnetic field

The magnetic field distribution of the magnet was analysed to further clarify the material removal mechanism. Fig. 6.20 exhibits the magnetic field strength distribution of the used magnet at the lower end face of the MCF slurry carrier, i.e. at a distance of 1.5 mm from the magnet (namely at working gap Δ = 1 mm), using a teslameter (5070 G/Teslameter). It is noticed that H_x is maximized at the edge of the magnet while H_z appears maximized in a circle region with a radius of 6.5 mm. It is though that the H_z mainly governs the material removal. Hence, when r = 3 mm, the magnetic clusters within MCF slurry possess not only the strongest stiffness but also large enough relative speed, thereby achieving the largest material removal. Fig. 21 displays the vector graph of magnetic field in the *x*O*z* plane. It is observed that the magnetic lines of

force at the centre of the magnet are vertical to its lower end face and become parallel to its lower end face at the edge of magnet gradually.

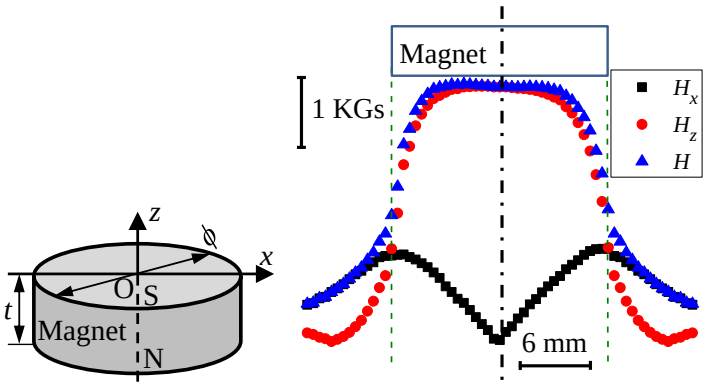

Fig. 6.20 Magnetic field strength distribution at the lower end face of MCF slurry carrier

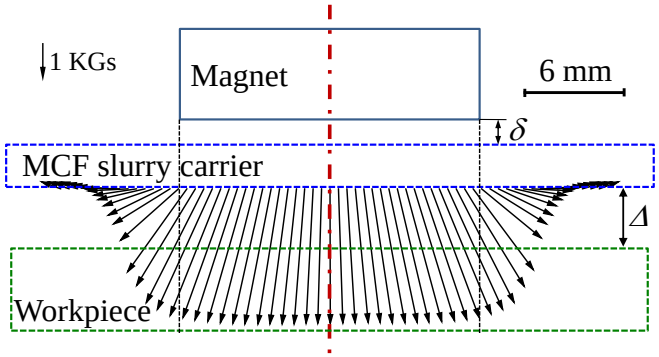

Fig. 6.21 Vector graph of magnetic field in the *x*O*z* plane at the lower end face of MCF slurry carrier

6.4.5 Geometry and internal structure of MCF slurry

In order to make clear the material removal behaviour during MCF polishing, the cross-sectional structures of MCF slurry during polishing were analyzed under a static magnetic field (Fig. 6.22) and a rotary one (Fig. 6.23). Obviously, Fig. 6.22 presents that magnetic clusters were formed along the magnetic lines of force as shown in Fig. 6.21 and the slurry is symmetrically distributed during polishing under a static magnetic field. Therefore, only the left side of the cross-sectional structure of the

slurry was detailed analyzed at positions a, b and c. The formed clusters are vertical to the work surface at the position C where is considered to be the slurry center. The thickness of the slurry is maximized in a circular range with radius of about 9 mm (namely the position b). Therefore, the maximal material removal occurs at a circle with a radius of about 9 mm because considerable amount abrasives are collected at this position and they possess moderate relative speed to the work surface. However, the cross-sectional distribution of the element aluminum manifests that the abrasive particles is hardly uniformly distributed under a static magnetic field. The abrasive particles are distributed along the clusters at the position near to the edge of the magnet (e.g. position a) because the directions of the magnetic lines of force change little at this position.

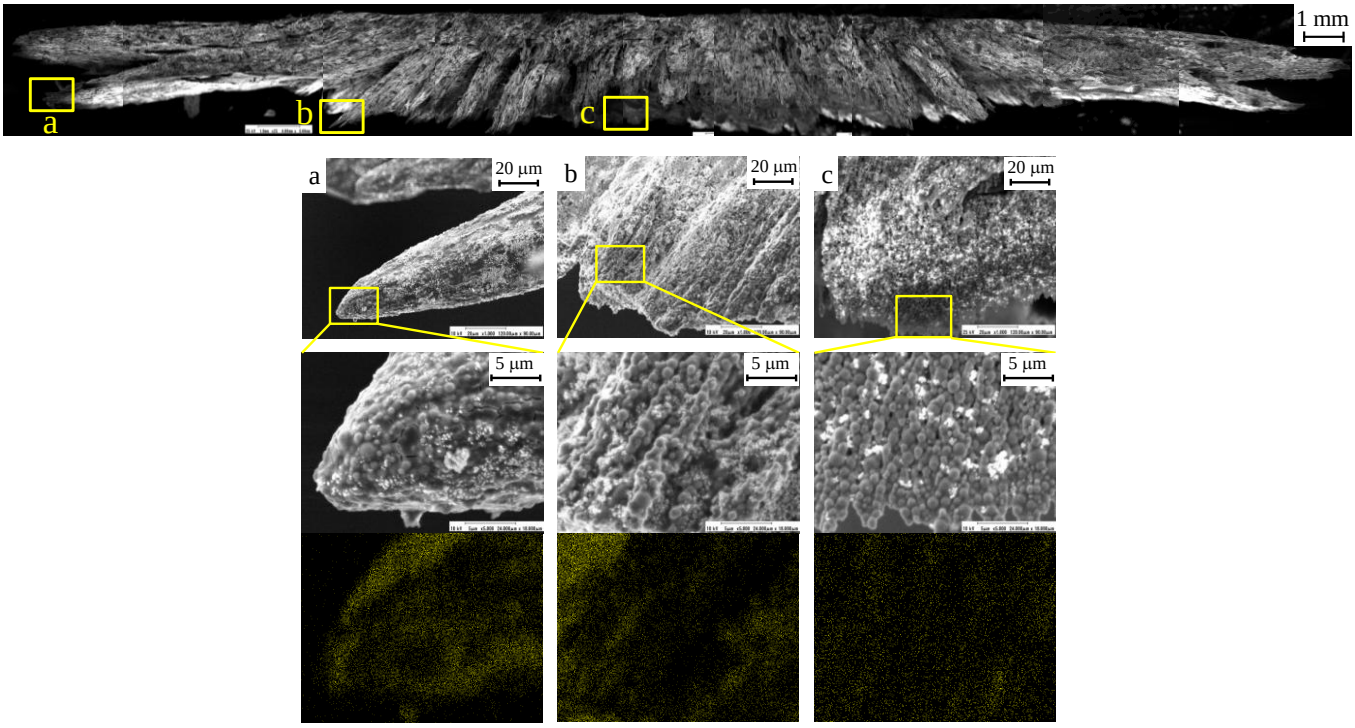

Fig. 6.22 SEM images of cross-sectional structure of MCF slurry during polishing under a static magnetic field (r = 0 mm)

Fig. 6.23 displays that although the thickness of the slurry is also maximized in a

range, the range is not centred at the slurry centre during polishing under a rotary magnetic field. Therefore, the cross-sectional structure of the slurry was detailed analyzed at positions a, b, c, d, e and f. The magnetic clusters vertical to the lower end face of the slurry carrier are formed at a position (namely position d) about 4.5 mm from the slurry centre where is thought to be the magnet centre. This demonstrates that the slurry revolves around the magnet holder axis together with the magnet revolution during polishing. Similar to that during polishing under a rotary magnetic field, the abrasives are distributed along the clusters at positions a and f where are near to the edge of the magnet. Particles are in a free state at position b since magnetic field here is too weak at this moment. Maximal material removal occurs near to the position e where is farther from the spot centre than under a static magnetic field.

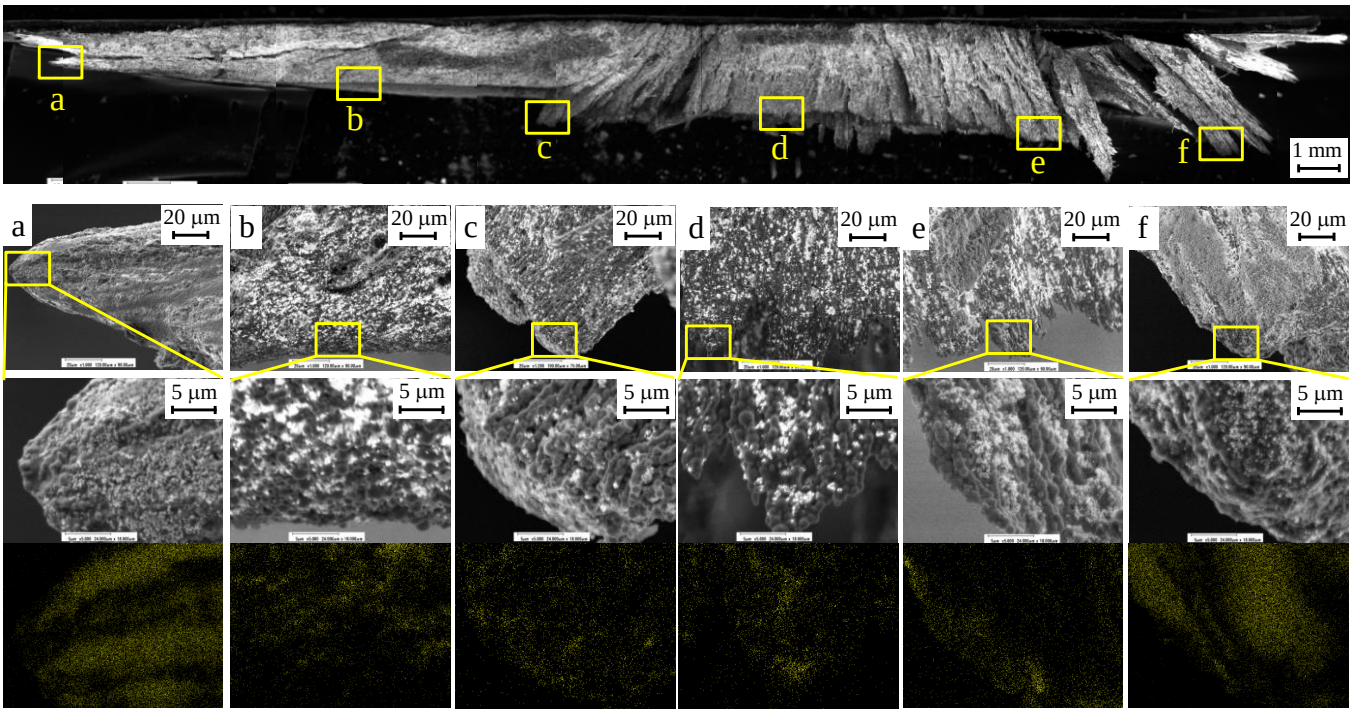

Fig. 6.23 SEM images of cross-sectional structure of MCF slurry during polishing under a rotary magnetic field (r = 4.5 mm)

6.5 Summary

In this chapter, the distributions of pressure and shear stress were measured in MCF polishing processes. The material removal rate (*MRR*) was investigated by spot polishing. The effects of the process parameters, namely the magnet revolution speed, MCF carrier rotational speed and working gap, were investigated on pressure/shear stress distributions and *MRR*. The relationship between pressure/shear stress distributions and *MRR* was researched and an *MRR* model for MCF polishing was proposed. Regarding the removal function, the effect of magnet eccentricity was also examined. In addition, the magnetic field was analysed and the structure of MCF slurry was examined to explain the characteristics of the removal function. The main conclusions are summarized below:

(1) The pressure is enhanced near the centre of the interacting area (i.e. the spot centre), and the maximum shear stress τ is generated close to the magnet centre (about 5 mm from the spot centre). Both pressure and shear stress are sensitive to the MCF slurry carrier rotational speed and to the working gap, and insensitive to magnet revolution speed. Shear stress is more sensitive to the process parameters than pressure.

(2) Cross-sectional profiles of the polishing spots are symmetric and characteristically W-shaped; material removals are minimal at the spot centre and maximal at approximately 8.2–10.2 mm from the spot centre depending on the process parameters.

(3) The *MRR* is strongly positively correlated with the MCF slurry carrier rotational speed, and negatively correlated with working gap. The *MRR* is independent of magnet revolution speed.

(4) An *MRR* model involving both the pressure and the shear stress in MCF polishing was proposed. According to the model, material removal in MCF polishing is dominated more by shear stress than by pressure.

(5) The radius of the removal function only shows relative large decrease in the increase in the working gap, a little increase with the magnet eccentricity increasing

from 0 to 4.5 mm, and a little increase when the concentration of α-cellulose increases from 0 wt.% to 3 wt.%. The position d_{max} where dRR_{max} occurs becomes largest at working gap Δ of 1 mm, is minimized at magnet eccentricity r of 3 mm and maximized at concentration of α-cellulose of 1.5 wt.% while it changes little with the variations of other process parameters. Both the depth and volume of the removal function appears insensitive to magnet revolution speed, linearly increase with the increase in the MCF slurry carrier rotational speed, linearly decrease as the working gap increases, is maximized at magnet eccentricity r of 3 mm, and maximized at concentration of α-cellulose of 3 wt.%.

(6) Magnetic clusters with the MCF slurry are formed along the magnetic lines of force. The thickness of slurry is maximized in a range during polishing. The removal function is strongly related to the magnetic field distribution and the geometry and internal structure of the slurry. The maximal material removal occurs at the position where many abrasives are collected and they possess considerable relative speed to the work surface.

References

[1] Li, Y., Hou, J., Xu, Q., Wang, J., Yang, W., Guo, Y., 2008. The characteristics of optics polished with a polyurethane pad. Opt. Express 16, 10285−10293.

[2] Tani, Y., Kawata, K., Nakayamac, K., 1984. Development of high-efficient fine finishing process using magnetic fluid. CIRP Ann. 33, 217−220.

[3] Umehara, N., Hayashi, T., Kato, K., 1995. In situ observation of the behavior of abrasives in magnetic fluid grinding. J. Magn. Magn. Mater. 149, 181−184.

[4] Prokhorov, I., Kordonski, W., 1992. New high-precision magnetorheological instruments-based method of polishing optics. OSA OF&T Workshop Digest 24, 134−136.

[5] Kordonski, W., Jacobs, S., 1996. Magnetorheological finishing. Int. J. Mod. Phys. B 10, 2837−2848.

[6] Golini, D., Kordonski, W.I., Dumas, P., Hogan, S.J., 1999. Magnetorheological finishing (MRF) in commercial precision optics manufacturing. Proc. SPIE 3782, 80−91.

[7] Shorey, A.B., Jacobs, S.D., Kordonski, W.I., Gans, R.F., 2001. Experiments and observations regarding the mechanisms of glass removal in magnetorheological finishing. Appl. Opt. 40, 20−33.

[8] Miao, C., Shafrir, S.N., Lambropoulos, J.C., Mici, J., Jacobs, S.D., 2009. Shear stress in magnetorheological finishing for glasses. Appl. Opt. 48, 2585−2594.

[9] Miao, C., Lambropoulos, J.C., Jacobs, S.D., 2010. Process parameter effects on material removal in magnetorheological finishing of borosilicate glass. Appl. Opt. 49, 1951−1963.

[10] Jha, S., Jain, V.K., 2004. Design and development of the magnetorheological abrasive flow finishing (MRAFF) process. Int. J. Mach. Tools Manuf. 44, 1019−1029.

[11] Das, M., Jain, V.K., Ghoshdastidar, P.S., 2008. Fluid flow analysis of magnetorheological abrasive flow finishing (MRAFF) process. Int. J. Mach. Tools

Manuf. 48, 415–426.

[12] Das, M., Sidpara, A., Jain, V.K., Ghoshdastidar, P.S., 2011. Parametric analysis of MR polishing fluid using statistical technique. Int. J. Precis. Technol. 2, 51–63.

[13] Cheng, H.B., Yam, Y., Wang, Y.T., 2009. Experimentation on MR fluid using a 2-axis wheel tool. J. Mater. Process. Technol. 209, 5254–5261.

[14] Dai, Y.F., Song, C., Peng, X.Q., Shi, F., 2010. Calibration and prediction of removal function in magnetorheological finishing. Appl. Opt. 49, 298–306.

[15] Sidpara, A., Jain, V.K., 2011. Experimental investigations into forces during magnetorheological fluid based finishing process. Int. J. Mach. Tools Manuf. 51, 358–362.

[16] Singh, A.K., Jha, S., Pandey, P.M., 2012. Nanofinishing of a typical 3D ferromagnetic workpiece using ball end magnetorheological finishing process. Int. J. Mach. Tools Manuf. 63, 21–31.

[17] Shimada, K., Fujita, T., Oka, H., Akagami, Y., Kamiyama, S., 2001. Hydrodynamic and magnetized characteristics of MCF (magnetic compound fluid). Trans. Jpn. Soc. Mech. Eng. B 67, 3034–3040 (in Japanese).

[18] Shimada, K., Akagami, Y., Kamiyama, S., Fujita, T., Miyazaki, T., Shibayama, A., 2002. New microscopic polishing with magnetic compound fluid (MCF). J. Intell. Mater. Syst. Struct. 13, 405–408.

[19] Shimada, K., Wu, Y., Matsuo, Y., Yamamoto, K., 2005. Float polishing technique using new tool consisting of micro magnetic clusters. J. Mater. Process. Technol. 162–163, 690–695.

[20] Furuya, T., Wu, Y., Nomura, M., Shimada, K., Yamamoto, K., 2008. Fundamental performance of magnetic compound fluid polishing liquid in contact-free polishing of metal surface. J. Mater. Process. Technol. 201, 536–541.

[21] Wu, Y., Sato, T., Lin, W., Yamamoto, K., Shimada, K., 2010. Mirror surface finishing of acrylic resin using MCF-based polishing liquid. Int. J. Abras. Technol. 3, 11–24.

[22] Sato, T., Wu, Y., Lin, W., Shimada, K., 2009. Study on magnetic compound fluid (MCF) polishing process using fluctuating magnetic field. Trans. Jpn. Soc. Mech. Eng. B 75, 1007−1012 (in Japanese).

[23] Kim, W.B., Lee, S.H., Min, B.K., 2004. Surface finishing and evaluation of three-dimensional silicon microchannel using magnetorheological fluid. J. Manuf. Sci. Eng. 126, 772−778.

[24] Sato, T., Wu, Y., Lin, W., Shimada, K., 2010. Study of three-dimensional polishing using magnetic compound fluid (MCF). J. Jpn. Soc. Abras. Technol. 54, 425−430 (in Japanese).

[25] Guo, H., Wu, Y., Li, Y., Cao, J., Fujimoto, M., Jacobs, S., 2012. Technical performance of zirconia-coated carbonyl-iron-particles based magnetic compound fluid slurry in ultrafine polishing of PMMA. Key Eng. Mater. 523−524, 161−166.

[26] Guo, H., Wu, Y., 2012. Behaviors of MCF (magnetic compound fluid) slurry and its mechanical characteristics: normal and shearing forces under a dynamic magnetic field. Jpn. Soc. Exp. Mech. 12, 369−374.

[27] Preston, F. W., 1927. The theory and design of plate glass polishing machines. J. Soc. Glass Technol. 11, 214–256.

Chapter VII
Conclusions and Future Suggestions

A magnetic compound fluid (MCF) is developed by mixing a magnetic field (MF) and a magnetorheological (MR) fluid. An MCF contains not only μm-sized iron particles but also nm-sized magnetite particles whereas there are no nm-sized magnetite particles within the MR fluid. MCFs exhibit higher magnetic pressure and apparent viscosity than MFs and a more stable distribution of particles than MR fluids under a magnetic field, while maintaining a fluid-like behaviour. An MCF slurry is generally composed of carbonyl-iron-particle (CIP), water based MF, abrasive particles and α-cellulose. In this study, a rotary magnetic field was employed. The magnetic flux density is constant but the magnetic lines of force constantly revolve around the magnet holder axis. In this thesis work, polishing with MCF slurry under a rotary magnetic field was extensively studied from the work life, dynamic behaviours, mechanical characteristics of MCF slurry, the application of MCF polishing in soft magnetic as well as non-magnetic materials, and material removal behaviours.

Work life of MCF slurry (in the absence of α-cellulose) was studied through the spot polishing tests of optical glass, namely fused silica (FS) and borosilicate glass (BK7). It is observed that MCF slurry of only a volume of 1 mL keeps stable material removal rate (*MRR*) (depth removal rate of ~0.0243 μm/min and volume removal rate of ~0.07 mm^3/min) and attains smooth surfaces inside spots ~1 nm over a relative long spot polishing period of 25 min. The removal function is depended on the compositions of MCF slurry and insensitive to the two glasses.

To clarify the behavious of MCF slurry under a rotary magnetic field, the effects of process parameters (namely magnet eccentricity r, magnet revolution speed n_m and MCF slurry supplied volume v) on the time T required for forming the slurry to its final shape, and the dimensions (namely diameter W and the maximal length H_{max}) of

the final shape were investigated. The normal and shear forces were simultaneously measured and the effects of process parameters (namely magnet revolution speed n_m, MCF slurry carrier rotational speed n_c and working gap Δ) were studied. It is noted that MCF slurry achieves a clear-cut terminal shape and the shape and dimensions of its terminal are repeated periodically with the magnet revolution at the same frequency n_m. The time T decreases with the increases in the magnet eccentricity r (significantly if $r <$ 4.5 mm) and the speed n_m, and rises up as the supplied slurry volume v increases. Both dimensions changes significantly with the variation in the magnet eccentricity r, while they are insensitive to the magnet revolution speed n_m. The W is maximized and the H_{max} is minimized both at r = 4.5 mm, and the H_{max} shows only a little increase with the increase in the supplied MCF slurry volume v. Therefore, the maximal contribution is made by magnet eccentricity on behaviours of MCF slurry, followed by MCF slurry supplied volume, whereas minimal contribution is noted by magnet revolution speed. Both forces are significantly dominated by the working gap, slightly governed by the MCF slurry carrier rotational speed and insensitive to the magnet revolution speed. More uniform distribution of abrasive particles and slurry and a better surface finish are obtained under a rotary magnetic field than under a static one.

The rotary magnetic field disperses MCF slurry uniformly during polishing, which favors nano-precision finishing. However, CIP within the MCF slurry has poor ability against corrosion in a common water based carrier. Nano-precision polishing of polymethyl methacrylate (PMMA) was performed with a novel zirconia (ZrO_2)-coated CIP based MCF slurry. Polishing performances of this kind of MCF slurry, namely surface roughness and normal force, were discussed by comparing the ZrO_2-coated CIP based MCF/MRF slurry with the HQ CIP based MCF slurry. In the presence of abrasive particles (Al_2O_3), ZrO_2-coated CIP based MCF slurry does not perform better than non-coated HQ CIP based one. In the absence of abrasive particles, the ZrO_2-coated CIP based MCF slurry behaves better than the MRF slurry; ZrO_2-coated CIP concentration should be less than a certain value (in the current work, 70 wt.%),

otherwise MCF slurry shows bad particle dispersion and is easily dried, resulting in the loss of its polishing ability.

As an extension of the application for ZrO_2-coated CIP based MCF slurry, the single crystal diamond turning (SCDT) Ni-P plating mold was polished using this kind of MCF slurry in order to eliminate SCDT-induced tool marks. By contrast, an HQ CIP based MCF slurry was used as well. Spot polishing without relative motion between the centre of the MCF carrier and workpiece was first carried out using both slurries. Scanning polishing with the MCF carrier moving along a motion path was then carried out using only the ZrO_2-coated CIP based MCF slurry. Although both slurries removed the SCDT-induced tool marks on the work surface, the MCF slurry containing relatively large Al_2O_3 abrasive particles left scratches and frequently caused CIPs to be embedded in the Ni-P plating surface, which inversely worsened the work surface roughness. In contrast, the MCF slurry that contains relatively small ZrO_2 abrasive particles resulted in a work surface roughness that was slightly improved, without scratches or the embedding of particles. The cross-sectional profile of the polishing spot manifests a characteristic symmetrical W-shape. The induced scratches display a dot-shape at the spot centre and the lengths of the scratches increase with the increase in the distance from the spot centre. In scanning polishing, the W-shaped polishing spot moves along the designed scanning path and the overlap of the instantaneous W-shaped spots occurs, which significantly improved the flatness of the Ni-P plating layer from 0.2 μm to 0.1 μm. In addition, almost all of the particles can move relative to the work surface, and the surface roughness of the Ni-P plating layer was improved without causing scratches or the embedding of particles. The preliminary results show that MCF polishing is applicable to the nano-level finishing of soft magnetic materials.

To elucidate the material removal behaviour in MCF polishing, the normal and shear forces generated in the polishing zone during polishing were measured. From these measurements, the distributions of pressure P and shear stress τ were obtained. The material removal rate (*MRR*) was investigated through spot polishing of

borosilicate glass. The *MRR* distribution was obtained and the characteristics of the removal function (namely the polishing spot), i.e. the radius *R*, maximal depth dRR_{max} and its position d_{max}, volume *VRR* of the polishing spot, were also studied. The effects of three process parameters, namely magnet revolution speed, MCF carrier rotational speed and working gap, on pressure *P*, shear stress τ and the *MRR* were first investigated. The results revealed that *P* is higher near the centre of the interacting area, (i.e. the polishing spot centre) and the point of maximum shear stress τ appears at about 5 mm from the polishing spot centre. All of *P*, τ and *MRR* are sensitive to MCF carrier rotational speed and working gap but insensitive to magnet revolution speed. Shear stress is more sensitive to these process parameters than the pressure. Cross-sectional profiles of the polishing spots exhibit a characteristic symmetric W-shape; material removals are minimal at the spot centre and maximal at approximately 8.2–10.2 mm from the spot centre depending on the process parameters. *MRR* is proportional to the MCF carrier rotational speed and is negatively correlated with working gap. An *MRR* model involving both the pressure and shear stress in MCF polishing is proposed. In the model, *MRR* is more dominated by shear stress than by pressure. Regarding the removal function, the effect of magnet eccentricity was also studied. The radius of the removal function only shows relative large decrease in the increase in the working gap, a little increase with the magnet eccentricity increasing from 0 to 4.5 mm, and a little increase when the concentration of α-cellulose increases from 0 wt.% to 3 wt.%.. The position d_{max} where dRR_{max} occurs becomes largest at working gap Δ of 1 mm, and is minimized at magnet eccentricity *r* of 3 mm and maximized at concentration of α-cellulose of 1.5 wt.% while it changes little with the variations of other process parameters. Both the depth and volume of the removal function appears insensitive to magnet revolution speed, linearly increase with the increase in the MCF slurry carrier rotational speed, linearly decrease as the working gap increases, and is maximized at magnet eccentricity *r* of 3 mm and maximized at concentration of α-cellulose of 3 wt.%.. In addition, the magnetic field was analysed and the structure of MCF slurry was

examined to explain the characteristics of the removal function. Magnetic clusters with the MCF slurry are formed along the magnetic lines of force. The thickness of slurry is maximized in a range during polishing. The removal function is strongly related to the magnetic field distribution and the geometry and internal structure of the slurry. The maximal material removal occurs at the position where many abrasives are collected and they possess considerable relative speed to the work surface.

Future work should be done in order to clarify the work life of MCF slurry. Based on the characteristic removal function, MCF polishing has a potential in finishing of free-form surfaces by designing a certain polishing path.

Accomplishments

I. 本学位論文に関するもの

著書

1. 呉勇波, 郭会茹. ”ガラス高機能化への加工技術書 第 4 章 ガラスの研削・研磨技術および表面形状評価 第 5 節 磁気混合流体(MCF)における研磨のメカニズム及び応用”, 2012 年, サイエンス & テクノロジー出版, ISBN978-4-86428-055-6 C3058.

学術論文

1. Huiru Guo, Yongbo Wu, Dong Lu, Masakazu Fujimoto, Mitsuyoshi Nomura. Effects of pressure and shear stress on material removal rate in ultra-fine polishing of optical glass with magnetic compound fluid slurry. *Journal of Materials Processing Technology*, 2014, 214(11), 2759–2769. (**IF: 2.04**)
2. Huiru Guo, Yongbo Wu, Dong Lu, Masakazu Fujimoto, Mitsuyoshi Nomura. Ultrafine Polishing of Electroless Nickel-Phosphorus Plated Mold with Magnetic Compound Fluid Slurry. *Materials and Manufacturing Processes*., 2014, 29, 1–8. (**IF: 1.48**)
3. Huiru Guo, Yongbo Wu. Behaviors of MCF (Magnetic Compound Fluid) Slurry and its Mechanical Characteristics: Normal and Shearing Forces under a Dynamic Magnetic Field. *Journal of Japan Society for Experimental Mechanics*, 2012, 12(4), 369–374.
4. Huiru Guo, Yongbo Wu, Yaguo Li, Jianguo Cao, Masakazu Fujimoto, and Stephen D. Jacobs. Technical Performance of Zirconia-coated Carbonyl-iron-particles based Magnetic Compound Fluid Slurry in Ultrafine Polishing of PMMA. *Key Engineering Materials*, 2012, 523-524, 161–166. (**Ei**)

5. Huiru Guo, Yongbo Wu, Dong Lu, Masakazu Fujimoto, Mitsuyoshi Nomura. Ultrafine polishing of optical polymer with zirconia-coated carbonyl-iron-particle-based magnetic-compound-fluid slurry. *Materials and Manufacturing Processes*. (**Under review, IF: 1.48**)

国際学術会議

1. Huiru Guo, Yongbo Wu, Masakazu Fujimoto and Mitsuyoshi Nomura. Relationship between Polishing Force Distribution and Material Removal in MCF Polishing Process. *The 7th International Conference on Leading Edge Manufacturing in 21st Century (LEM21)*, Miyagi, Japan, Nov. 7–8, 2013.
2. Huiru Guo, Yongbo Wu, Yaguo Li, Jianguo Cao, Masakazu Fujimoto and Stephen D. Jacobs. Technical Performance of Zirconia-coated Carbonyl-iron-particles based Magnetic Compound Fluid Slurry in Ultrafine Polishing of PMMA. *The 14th International Conference on Precision Engineering (ICPE 2012)*, Hyogo, Japan, Nov. 8–10, 2012.

国内学術会議

1. 郭会茹，呉勇波，藤本正和，野村光由．MCF ポリシングにおける研磨力が材料除去に及ぼす影響．2013 年度精密工学会東北支部学術講演会，秋田，2013.12.07.
2. 郭会茹，呉勇波，藤本正和，野村光由．MCF ポリシングにおける研磨力の分布と材料除去の関係．2013 年度精密工学会春季大会，東京工業大学，東京，2013.03.13–15.
3. 郭会茹，呉勇波，野村光由，藤本正和．磁気混合流体(MCF)スラリーによる Ni-P めっきの超精密研磨．第 9 回生産加工・工作機械部門講演会，秋田県立大学，秋田，2012.10.27–28.

4. 郭会茹, 呉勇波, 李亜国, 曹建国, 藤本正和, Stephen D. Jacobs. 樹脂デバイスの鏡面研磨におけるジルコニアコーテッド鉄粉ベース MCF スラリーの加工特性. 2011 年度精密工学会東北支部学術講演会, 仙台, 2011.10.21.

授賞

1. **Young Researcher Award**. *The 7th International Conference on Leading Edge Manufacturing in 21st Century*, Miyagi, Japan, Nov. 7–8, 2013.

II. その他関連業績

学術論文

1. Youliang Wang, Yongbo Wu, Huiru Guo. A new MCF (Magnetic Compound Fluid) slurry and its Performance in Magnetic Field-assisted polishing of oxygen-free copper. *Journal of Applied Physics*. (**Accept, IF: 2.210**)
2. Li Jiao, Yongbo Wu, Xibin Wang, Huiru Guo, Zhiqiang Liang. Fundamental performance of Magnetic Compound Fluid (MCF) wheel in ultra-fine surface finishing of optical glass. *International Journal of Machine Tools & Manufacture*, 2013, 75, 109–118. (**IF: 2.74)**
3. Li Jiao, Yongbo Wu, Huiru Guo. The Effect of Magnetic Field Distribution on Material Removal in Magnetic Compound Fluid Wheel Polishing. *Journal of Mechanical Engineering*, 2012, 49(17), 79–84. (**Ei**)
4. Yongbo Wu, Li Jiao, Huiru Guo, Masakazu Fujimoto and Kunio Shimada. Ultrafine Surface Finishing of Fused Silica Glass Using MCF Magnetic Compound Fluid Wheel. *Advanced Materials Research*, 2012, 565, 3–9. (**Ei**)
5. Jianguo Cao, Yongbo Wu, Huiru Guo, Yaguo Li, Masakazu Fujimoto and Akira Ohmura. Simulation investigation ultrasonically assisted grinding of SiC ceramics with single diamond abrasive grain. *Key Engineering Materials*, 2012, 523-524,

178–183. (**Ei**)

6. Yaguo Li, Yongbo Wu, Libo Zhou, Huiru Guo, Jianguo Cao, Masakazu Fujimoto, Masaaki Kemmochi. Investigation into Chemo-Mechanical Fixed Abrasive Polishing of Fused Silica with the Assistance of Ultrasonic Vibration. *Key Engineering Materials*, 2012, 523-524, 155–160. (**Ei**)
7. Dong Lu, Qiang Wang, Yongbo Wu, Jianguo Cao, Huiru Guo. Fundamental Turning Characteristics of Inconel 718 by Applying Ultrasonic Elliptical Vibration on the Base Plane. *Materials and Manufacturing Processes*. (**Under review, IF: 1.48**)

国際学術会議

1. Jianguo Cao, Yongbo Wu, Huiru Guo, Masakazu Fujimoto, Nomura Mitsuyoshi. Experimental investigation of material removal mechanism in ultrasonic assisted grinding of SiC ceramics using a single diamond tool. *The 7th International Conference on Leading Edge Manufacturing in 21st Century (LEM21)*, Miyagi, Japan, Nov. 7–8, 2013.

国内学術会議

1. 李亜国，呉勇波，曹建国，郭会茹，藤本正和，周立波．石英ガラスの超音波援用化学的機械複合研削．2012 年日本精密工学会春季大会，首都大学東京，東京，2012.03.14–16.
2. 李亜国，呉勇波，曹建国，郭会茹，藤本正和．超音波を援用した光学ガラスの化学機械複合研削．2011 年日本精密工学会東北支部講演会，仙台，2011.10.21.
3. 曹建国，呉勇波，郭会茹，李亜国，藤本正和，超音波振動を援用した SiC セラミックス内面の精密研削．2011 年度日本精密工学会東北支部学術講演会，仙

台，2011.10.21.